

**PERFORMANCE OF THE CMIP5 MODELS IN SIMULATION
OF PRESENT AND FUTURE PRECIPITATION OVER THE
LAKE VICTORIA BASIN**

ANYANGO MAUREEN WANZALA

I56/70060/2013

DEPARTMENT OF METEOROLOGY

UNIVERSITY OF NAIROBI

BOX 30197-00100,

NAIROBI, KENYA.

**A Research Project Submitted in Partial Fulfillment of the Requirements
for the Award of the Degree of Master of Science in Meteorology**

JULY 2015

DECLARATION

I certify that this research project is my original work and has not been presented for a degree
in this or any other university.

Anyango W. Maureen

Signature.....

Date.....

This dissertation has been submitted for examination with our approval as University
Supervisors:

Supervisors:

Prof. Ogallo, L.A

Signature.....

Date.....

Department of Meteorology

Dr. Opijah, F. J

Signature.....

Date.....

Department of Meteorology

Dr. Mutemi, J. N

Signature.....

Date.....

Department of Meteorology

DEDICATION

To my beloved husband Pinto and parents Mr. and Mrs. Wanzala for their wise counsel, advice, encouragement and spiritual inspiration they accorded me during the entire exercise.

ABSTRACT

The usefulness and limitations in climate information are due to uncertainty inherent in the climate system. The reduction of errors increases the reliability of the information. Therefore, for any given region to have sustainable development there is need to apply climate information into its socio-economic strategic plans.

The overall objective of the study was to assess the performance of the Coupled Model Inter-comparison Project (CMIP5) over the Lake Victoria Basin. The data used in the study included the observed point station data, gridded rainfall data from Climate Research Unit, University of East Anglia (CRU) and hindcast data from eight Coupled Model Inter-comparison Project 5 (CMIP5) for the period 1971 to 2005 for historical and 2006-2100 for model future projections. The methodology employed included trend analysis, spatial analysis, correlation analysis, Principal Component Analysis (PCA) regression analysis, and categorical statistical skill score.

The present study is a preliminary interrogation of the ability of eight CMIP5 models to characterize seasonal and annual mean precipitation cycle over LVB. Analysis of the trends in the observed rainfall records indicated an increase in rainfall variability both in space and time for all the seasons. Similarly, majority of the eight models analyzed correctly reproduce the mean seasonal and annual cycle of precipitation for the period 1971–2005 as compared to gridded satellite-derived observations. At the same time the analysis shows significant biases in individual models depending on region and season. Specifically, a modest number of models were able to capture correctly the peaks of bimodal (March - May and October - December) and June - August rainfall while a few either dragged the onset to subsequent months or displaced the locations of seasonal rainfall.

The spatial patterns of the individual models output from the models of MPI, MIROC, EC-EARTH and CNRM were closest to the observed rainfall patterns. The skill of the ensemble models was higher than those of the individual member models in terms of its ability to capture the rainfall peaks during the October - December season. Climate projections of rainfall over the region indicated that the March to May (MAM) and October to December (OND) seasonal rainfall for the period 2021–2050, 2051-2070, 2071-2100 will exhibit decreasing trends with major peaks in MAM rainfall occurring during 2041, 2083 and 2087 respectively in relation to the Representative Concentration Pathway (RCP) 4.5 scenario.

While the model was capable of reproducing the general climatological patterns over the region, it did not skillfully capture the effects of the small scale features on the region's climate. There is need for improvement in the model physics and resolution and optimization of the model domain in order to enhance the performance of the CMIP5 over the region. This study provides useful climate change and variability information for regional planning for sustainable development. The results of the study will play a crucial role in enhancing the socio-economic productivity of the region in terms of agriculture and food availability, water resources, transport, fisheries, power production, industry and health.

ACKNOWLEDGEMENT

I take this opportunity to thank God for seeing me through to the completion of this work, His grace and mercies have been immeasurable. I would also like to express my greatest appreciation to the collaboration between ICPAC and University of Nairobi that granted me the opportunity to pursue a degree in Master of Science (Meteorology) through an academic scholarship.

Special thanks go to my Supervisors, Prof. Laban Ogallo, of ICPAC, Dr. Joseph Mutemi and Dr. Franklin Opijah of the University of Nairobi for their advice, direction and support they accorded to me during the study. I am grateful to the entire staff of the department of Meteorology for their support, counsel and direction.

I acknowledge the warm relationship enjoyed during the entire Masters' program with my colleagues at ICPAC and fellow classmates at the Department of Meteorology for their academic and moral support which has been invaluable. I also acknowledge in a special way, Sabiiti Geoffrey and Jully Ouma for their guidance and motivation during the research.

Special thanks go to Prof. L. Ogallo, of ICPAC, for the academic mentorship he has provided during my entire time at ICPAC.

Table of Contents

DECLARATION	i
LIST OF FIGURES	x
LIST OF TABLES	xii
LIST OF ACRONYMS.....	xiii
CHAPTER ONE	1
1.1 Background.....	1
1.2 Problem Statement.....	2
1.3 Objectives of the Study	2
1.4 Justification of the Study.....	3
1.5 Area of Study	3
1.6 Observed Variability in the Role of the Lake Victoria Basin	4
1.7 Climatology of the Study Area.....	5
1.7.1 Lake Victoria Trough	6
1.7.2 Inter Tropical Convergence Zone.....	6
1.7.3 Subtropical Anticyclones	7
1.7.4 El Niño Southern Oscillation.....	8
1.7.5 Indian Ocean dipole	8
1.7.6 Sea Surface Temperatures	9
1.7.7 Tropical Monsoons	10
1.7.8 Jet Streams	11
CHAPTER TWO	12
2.0 LITERATURE REVIEW FOR THE STUDY.....	12
2.1 Climatology of the Lake Victoria Basin.....	12
2.1.1 Climate Extremes over the LVB	13
2.1.2 Socio-economic Activities over the LVB.....	13
2.1.3 Observations, Processes, Modeling, Prediction and Applications.....	14

2.1.4	Downscaling	16
2.1.4.1	Dynamical Downscaling	16
2.1.4.2	Statistical Downscaling	17
CHAPTER THREE		19
3.0	THE FIFTH VERSION OF THE COUPLED MODEL INTER-COMPARISON MODELS.....	19
3.1	Theoretical Framework	19
3.2	Model Physics of the Fifth Version of the Coupled Model Inter-comparison Project.....	19
3.3	Representative Concentration Pathways.....	23
CHAPTER FOUR.....		25
4.0	DATA AND METHODOLOGY	25
4.1	Data.....	25
4.1.1	In-situ Observations.....	25
4.1.2	Model Hindcast Datasets from Coupled Model Inter-comparison Project 5 Centers	28
4.2	Data Quality Control	29
4.2.1	Estimation of Missing Rainfall Data	29
4.3	Methodology	29
4.3.1	Trend Analysis.....	30
4.3.2	Standardized Anomaly Indices	30
4.3.3	Downscaling of CMIP5 Ensemble model outputs.....	30
4.3.4	Model output verification methods.....	31
4.3.4.1	Graphical Displays.....	32
4.3.4.2	Analysis of error in simulated outputs	32
4.3.4.3	Correlation Analysis	32
4.3.4.4	Multiple Linear Regression	33
4.3.5	Categorical Statistics	34
4.3.5.1	Bias Score.....	34
4.3.5.2	Probability of Detection	35

4.3.5.3 False Alarm Ratio	35
4.3.5.4 Heidke Skill Score	35
CHAPTER FIVE.....	37
5.0 RESULTS AND DISCUSSIONS	37
5.1 Result from Quality Control.....	37
5.1.1 Result from Homogeneity Test.....	37
5.1.2 Results from Evaluation of CRU datasets against station	38
5.2 Trend Analysis and the Annual Cycle	40
5.2.1 Observed and Model Annual Cycles of Rainfall.....	40
5.2.2 Observed March-May Rainfall Trends	41
5.2.3 Observed June-August Rainfall Trends	42
5.2.4 Observed October-December rainfall trends.....	43
5.3 Evaluating the Best Performing Models.....	45
5.3.1 Results from error analysis.....	46
5.3.1.1 Analysis of the Root Mean Square Errors (RMSE)	46
5.3.1.2 Root Mean Square Error for March-May Season	47
5.3.1.3 Root Mean Square Error for October-December Season	48
5.3.2 Validation of Model Outputs	48
5.3.2.1 Results from the validation of seasonal rainfall Trends	49
5.3.2.1.1 March-May Season	49
5.3.2.1.2 Ensemble Model Validation for March-May (MAM) Season.....	50
5.3.2.1.3 October–December season	50
5.3.2.1.4 Ensemble Model Validation for October-December Season.....	51
5.3.2.1.5 Regression Analysis	52
5.3.2.2 Correlation Analysis	53
5.3.3 Categorical Statistics	54
5.3.3.1 Results from the Spatial Rainfall Patterns	57

5.4	Climate Projections using Model Outputs	61
5.4.1	Projected Temporal Patterns for March-May and October- December Seasons	61
5.4.2	Projected Seasonal Spatial Rainfall Patterns for Rcp 4.5 Scenario	63
5.4.2.1	March – May and October- December Season for the Period (2021- 2050).....	63
5.4.2.2	March – May and October- December Seasons for the Period 2041- 2070.....	64
5.4.2.3	March – May and October- December Seasons for the Period 2071- 2100.....	66
CHAPTER SIX		67
6.0	SUMMARY, CONCLUSION AND RECOMMENDATIONS	67
6.1.1	Summary	67
6.1.2	Conclusion	68
6.1.3	Recommendations.....	68
References		70

LIST OF FIGURES

Figure 1: Lake Victoria Basin and its adjoining catchments.....	4
Figure 2: Homogeneous climatic zones for the March-May rainfall season over the LVB ..	26
Figure 3: Homogeneous climatic zones for the June- August rainfall season over the LVB .	26
Figure 4: Homogeneous climatic zones for the October-December rainfall season over the LVB.....	27
Figure 5: Station codes and their locations as used in the study	27
Figure 6: Mass curve to test the homogeneity of the annual observed rainfall records for the period 1961-2009.....	38
Figure 7: Inter-annual variability of rainfall output (mm) of CRU (blue shading) and station observations (red shading) over Mwanza, Kisumu and Entebbe for March-May season.....	39
Figure 8: Inter-annual variability of rainfall output (mm) of CRU (blue shading) and station observations (red shading) over Mwanza, Kisumu and Entebbe for October-December season	39
Figure 9: Rainfall annual cycle for observed (Cyan), MPI (Blue), MIROC (Red), EC-EARTH (Green) and CRNRM (Purple) models for the years 1971-2005 over the LVB.....	40
Figure 10: : Observed March-May seasonal rainfall time series (blue), trend line (purple) and 5 year moving average (red) for Kisumu for 1961-2013.	41
Figure 11: Observed March-May seasonal rainfall time series (blue), trend line (purple) and a 5 year moving average (red) for Mwanza for 1961-2009.	42
Figure 12: Observed March-May seasonal rainfall time series (red), trend line (purple) and a 5 year moving average (red) for Mbarara for 1961-2013.	42
Figure 13: Observed June-July seasonal rainfall time series (blue), trend line (purple) and a 5 year moving average (red) for Mbarara for 1961-2013	43
Figure 14: Observed June-July seasonal rainfall time series (blue), trend line (purple) and a 5 year moving average (red) for Kabale for 1961-2013.	43
Figure 15: Observed October- December seasonal rainfall time series (blue), trend line (purple) and a 5 year moving average (red) for Mwanza for 1961-2009.....	44
Figure 16: Observed October- December seasonal rainfall time series (blue), trend line (purple) and 5 year moving average (red) for Bukoba for 1961-2009.....	44
Figure 17: Sub -domains (A, B, C and D) for application of the Model simulated outputs over the LVB.	46

Figure 18: Computed RMSE for individual models for March- May season over the sub-domains A, B, C and D considered in the study for time period 1971- 2005	47
Figure 19: Computed percentage RMSE for individual models for October- December season over the sub-domains A, B, C and D for the time period 1971-2005.....	48
Figure 20: Inter- annual variability of CNRM (blue), MIROC (pink), MPI (yellow) and CRU (cyan) for March-May (MAM) for a period 1971-2005 over the sub domains A, B, C and D	49
Figure 21: Inter-annual variability of Ensemble (pink) and CRU (blue) for March-May (MAM) for the period 1971-2005 over the sub domains A, B, C and D	50
Figure 22: : Inter-annual variability of CNRM (blue), MIROC (pink), MPI (yellow) and CRU (cyan) for October-December (OND) for a period of 1971-2005 over the sub domains A, B, C and D.....	51
Figure 23: Inter-annual Variability of Ensemble (pink) and CRU (blue) for October- December (OND) for the period 1971-2005 over the sub domains A, B, C and D.....	52
Figure 24: March-May simulated spatial rainfall patterns for the period 1971-2005 as obtained from CRU, MPI, MIROC and CNRM over the LVB.....	58
Figure 25: March-May simulated spatial rainfall patterns for the period 1971-2005 as obtained from CRU and ENS over the LVB	59
Figure 26: October-December simulated spatial rainfall patterns for the period 1971-2005 as obtained from (a) CRU, (b) MIROC, (c) EC-EARTH and (d) CNRM over the LVB.	60
Figure 27: October-December simulated spatial rainfall patterns for the period 1971-2005 as obtained from (a) CRU, (b) ENS over the LVB.	61
Figure 28: Rcp 4.5 projected temporal rainfall pattern for March–May season for the period 2021-2050, 2041-2070 and 2071-2100 over the LVB.....	62
Figure 29: Rcp 4.5 projected temporal rainfall pattern for October- December season for the period 2001-2021-2050, 2041-2070 and 2071-2100 over the LVB	63
Figure 30: MIROC & MPI projected spatial rainfall patterns (2021-2050) for (a) March–May and (b) October-December following the RCP 4.5 scenario over the LVB.....	64
Figure 31: MIROC & MPI projected spatial rainfall patterns for the period 2041-2070 for (a) March–May and (b) October-December following the RCP 4.5 scenario.....	65
Figure 32: MIROC & MPI projected spatial rainfall patterns for the period 2071-2100 for (a) March–May and (b) October-December following the RCP 4.5 scenario over the LVB.....	66

LIST OF TABLES

Table 1: The Coupled Model Inter-comparison Project 5 (CMIP5) Models	23
Table 2: General overview of representative concentration pathways (RCPs) and their descriptions .	24
Table 3: Station’s latitude-longitude in (degrees), altitude (m) and their codes	28
Table 4: A 3 * 3 contingency Table	34
Table 5: Estimation of Missing Data for stations with less than 10% of missing records over the LVB	37
Table 6: Stations Considered for each season and their respective P-value	45
Table 7: Computed Root Mean Square Error (RMSE) between Model outputs and CRU seasonal rainfall records.	47
Table 8: Regression Model Equations developed for the Models output at different sub-domains with R-square value above 25% for March-May and 45% for October-December seasons respectively and their P-values	52
Table 9: Correlation Coefficients between Model output and CRU Rainfall Anomalies for March - May season over the sub domains A, B, C, D. Green and yellow shading indicates significant positive and negative correlations, respectively, while unshaded values indicate statistically insignificant correlations.....	54
Table 10: Correlation Coefficients between Model output and CRU Rainfall Anomalies for October-December season over the sub domains A, B, C, D. Green and yellow shading indicates significant positive and negative correlations respectively, while unshaded values indicate statistically insignificant correlations.....	54
Table 11: Percent correct (%), Probability of detection (POD) (%), False Alarm (FAR) (%), BIAS (%) and Heidke Skill Score (HSS) (%) for MAM Ensemble model output picked across all the four sub-domains at different Categories, Below Normal (BN), Normal (N) and Above Normal	56
Table 12: Percent correct (%), Probability of detection (POD) (%), False Alarm (FAR) (%), BIAS (%) and Heidke Skill Score (HSS) (%) for OND Ensemble model output picked across all the four sub-domains at different Categories, Below Normal (BN), Normal (N) and Above Normal.	56

LIST OF ACRONYMS

AEJ	African Easterly jet
AGCM	Atmospheric General Circulation Model
AMIP	Atmospheric Model Inter-comparison Project
AR4	Assessment Report 4
CFS	Climate Forecast System
CMIP	Coupled Model Inter-comparison Project
CRU	Climate Research Unit
DJF	December, January, February
DRC	Democratic Republic of Congo
EALLJ	East Africa Low Level Jet
ECHAM	European Centre for Hydro-Atmospheric Model
ENSO	El Niño Southern Oscillation
FAO	Food and Agricultural Organization
FAR	False Alarm Ratio
GCMs	General Circulation Models
GDPFS	Global Data Processing and Forensic System
GHA	Greater Horn of Africa
GODA	Global Ocean Data Assimilation
HSS	Heidke Skill Score
ICTP	International Centre for Theoretical Physics
ICPAC	IGAD Climate Prediction and Application Centre
IGAD	Intergovernmental Authority for Development
IOD	Indian Ocean Dipole
IPCC	Inter-governmental Panel on Climate Change
ITCZ	Inter-Tropical Convergence Zone
JJA	June, July, August
LBCs	Lateral Boundary Conditions
LEVMP	Lake Victoria Environment Management Project
LVB	Lake Victoria Basin
MAM	March, April, May
MJO	Madden Julian Oscillation
MOS	Model Output Statistics

MOM	Modular Ocean Model
MPI	Max – Plank Institute
MSL	Mean Sea Level
NCAR	National Centers for Atmospheric Research
NCEP	National Centers for Environmental Prediction
NE	North Easterly
NEMO	Nucleus for European Modeling of the Ocean
OND	October, November, December
OGCM	Oceanic General Circulation Model
PP	Perfect Prognosis
POAMA	Predictive Ocean Atmospheric Model for Australia
POD	Probability of Detection
RAMS	Regional Atmospheric Modeling System
RCMs	Regional Climate Models
RCP	Representative Concentration Pathway
SE	South Easterly
SIDA	Swedish International Development Cooperation Agency
SRES	Special Report on Emission Scenerios
SST	Sea Surface Temperature
TEJ	Tropical Easterly Jet
WHO	World Health Organization
WRMD	Water Resources and Development Department
WMO	World Meteorological Organization

CHAPTER ONE

1.0 INTRODUCTION

1.1 Background

Lake Victoria region is one of areas within East Africa with very high rate of population growth, fast growth of unplanned settlements; over use of natural resources, environmental degradation among many other socio-economic challenges (LEVMP, 2003). Lake Victoria, located at the heart of the three East African countries is the largest fresh water body in the tropical region and the second largest fresh water lake in the world after Lake Superior. The Lake and its adjoining catchments form the region known as the Lake Victoria Basin (LVB). Because of its spatial extent, Lake Victoria induces its own circulation pattern and hence influences the climate of its adjoining catchments (Anyah and Semazzi, 2005). Spatial-temporal variability in climate has resulted into extreme weather and climate events, especially the extremes that have far-reaching impacts on livelihoods of communities, particularly in developing countries such as those of East Africa (Mutai *et al.*, 1998). The weather and climate extremes of the lake region include floods, drought, lightning, hailstorm and landslides.

Due to the economic importance of the LVB and the linkage of most regional activities to weather and climate, climate studies over the region are important. Addressing climate risks of the lake region require accurate and timely climate early information.

Currently, more than 12 centers around the world have developed climate models to enhance our understanding of climate and climate change (IPCC, 2001, 2007). The use of model outputs for prediction and early warning from Global Climate Models (GCM) as well as assessment of regional climate change impacts has been inadequate and not exhaustive. This can be attributed to the coarse temporal and spatial resolution of most GCMs currently between 100 km and 300 km that makes it impossible to resolve the mesoscale forcing including orographic and other local scale drivers (such as inland water sources and convection) that play a vital role in regional climates (IPCC, 2001). Some attempts have been made to downscale GCMs output to regional level (Anyah, 2005) by scientists. Downscaling techniques help in obtaining regional projections of climatic changes ranging from smoothing and interpolation of GCM anomalies (Tabor and Williams, 2010), to neural networks, and regional climate modeling (Giorgi and Bates, 1990). Simulation of regional climates using high-resolution climate models has become a vital and an effective tool for studying regional

climate change and variability. This study focused on assessing the performance of the CMIP5 in simulation of the present and future rainfall over Lake Victoria region and downscale the model projections for future.

1.2 Problem Statement

Lake Victoria produces its own climate with distinct diurnal, seasonal and inter-annual characteristics. The social and economic importance and development of the LVB are highly dependent on rain-fed systems that are often disrupted by abrupt changes in weather and climate, which result to severe hazards such as fluctuating lake levels, frequent floods, prolonged droughts, and disease outbreak

Despite a number of studies over the region on present-day climate variability, there is still a vast present-day and future climate information gap. This is as a result of the difficulties to represent some of the unique local and regional weather and climate, together with their interaction with global systems by many dynamical models. Model simulations based on climate scenarios are some of the tools recommended for assessing the impacts of climate change-related disasters (IPCC, 2007).

The present study attempts to narrow the existing climate information gap over the LVB by assessing the performance of CMIP5 models to simulate the much needed accurate seasonal climate forecasts for early warning to reduce climate risks that affect the local livelihoods and life around the lake.

1.3 Objectives of the Study

The main objective of this study was to assess the performance of CMIP5 models in the simulation of the present and future rainfall over the Lake Victoria Basin.

The specific objectives were to:

- a) Determine the temporal variability of observed rainfall records over the LVB during the recent past over the region.
- b) Determine the accuracy and skill of the best CMIP5 ensembles in simulating the observed temporal and spatial patterns of rainfall over the study region.
- c) Downscale the CMIP5 rainfall projections for the future considering changes over various time windows (e.g., years 2006-2040, 2041-2070, 2071-2100)

1.4 Justification of the Study

Climate variability is associated with both positive and negative consequences that occur over many regions, including the Lake Victoria Basin (LVB). Thus, access to timely, accurate and detailed seasonal climate information is particularly vital in developing countries, where economic stresses are likely to increase the vulnerability to potentially damaging impacts of climate variability such as frequent floods and prolonged droughts causing famine, loss of lives and property. Information on how skillful climate models are is vital in the regional planning for sustainable development.

The highly variable customized climate over the LVB makes it almost impossible for the climate models to capture and simulate their outputs accurately. There is therefore need for comprehensive assessment of the model performance for specific regional application for optimum performance. Hence, assessing the skill of the seasonal climate models over the LVB would provide the information on climate variability required by policy makers on the mitigation and adaptation measures that are suitable for the region.

1.5 Area of Study

The study was conducted over Lake Victoria Basin (LVB). The main feature of focus in this region is the Lake Victoria. The lake is located within $0.2^{\circ}N - 3.00^{\circ}S$ and $31.5^{\circ}E - 34.5^{\circ}E$. Lake Victoria has a surface area of about 68,800 km², with a maximum depth of 79 m and a mean depth of 40 m; it is at an altitude of 1135 m (LEVMP, 2003). The LVB covers an area of 181,000 km² (LEVMP, 2003) and includes parts of Tanzania, Kenya, Uganda. The lake is shared by Kenya (6%), Uganda (45%) and Tanzania (49%). Primary inflows into the lake are the Kagera and Katonga rivers in the west and the Nzoia, Sondu and Mara rivers from the east. In all, a total of 17 perennial rivers drain the Lake Basin (Nicholson, 1996). However, the only outflow from the lake is River Nile (Victoria Nile) which leaves the lake at Jinja in Uganda and flows northward through Lake Kyoga. It is then joined by the blue Nile in Sudan to form the main river Nile that flows northward through Egypt and finally drains into the Mediterranean sea. The LVB is one of the vital natural resources on which about 33 million people in the riparian countries are mutually dependent. The LVB serves as a resource for food, energy, water, building materials, and transport in the riparian communities. Figure 1a shows Lake Victoria and its adjoining catchments.

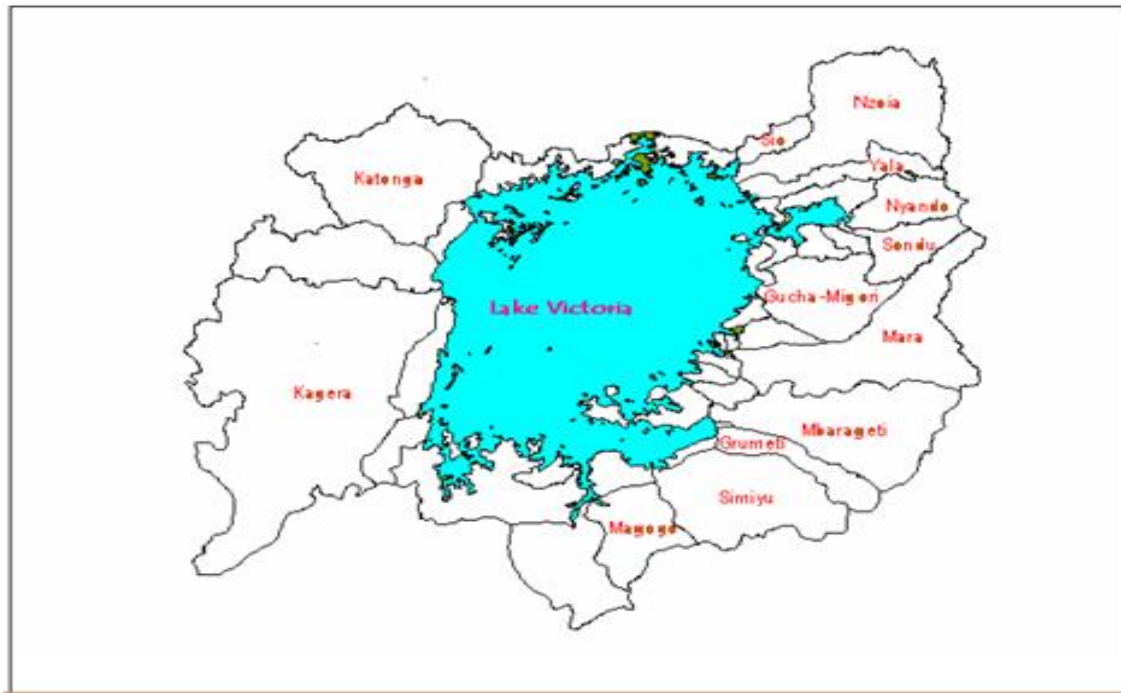


Figure 1: Lake Victoria Basin and its adjoining catchments (East Africa Secretariat report, 2006).

1.6 Observed Variability in the Role of the Lake Victoria Basin

The LVB is one of the agriculturally most productive areas in East Africa and thus a major breadbasket and major foreign exchange earner for the region (Anyah, 2005). It is also important in terms of fisheries, water transport, and generation of hydroelectric power and fresh water supplies for both domestic and industrial use, among others (Anyah and Semazzi, 2005). Moreover, Lake Victoria is the source of the Nile River, a watercourse of significant importance to many parts of Africa.

The LVB has however been exposed to wanton environmental degradation. The rapidly growing population in the region (currently over 33 million people) has exerted excessive pressure on the limited natural resources. Environmental degradation practices such as deforestation within the lake catchments, dumping of untreated industrial wastes and more recently invasion by the water hyacinth, have negatively impacted the role of the lake basin in the previous four or so decades (LEVMP, 2003). For instance, WRMD (2005) has reported significant fluctuations of the lake water levels that have greatly impacted on the regional development goals, for example, losses in terms of a fall in fish supplies, unsafe docking of lake transport vessels, and hydroelectric power crisis among others.

The physical features also play a major role in weather modification over the LVB. The topography of the region is complicated with many mountains with the Great Rift Valley running meridionally. One of the local effects of topography are the thermally-induced Katabatic winds during the early morning when the highlands are colder (due to radiational cooling) than the lowlands and water surfaces.

1.7 Climatology of the Study Area

The climate over eastern Africa in general and Lake Victoria Basin in particular is mainly characterized by the spatial and temporal distribution of rainfall. This in turn determines the settlement patterns, population density and distribution and agricultural productivity over the region. The rainfall over the LVB exhibits high space-time variability. This high variation in rainfall has been attributed to the complex topography and the existence of large inland water bodies that have a unique mesoscale forcing influence. The region generally experiences two seasonal rainfall regimes. Most parts of the region nearer to the equator experience the bimodal regime.

The first season, locally known as ‘long rains’, occurs during the months of March to May (MAM). The second season, locally known as ‘short rains’, occurs during the months of October to December (OND). These two wet seasons coincide with the passage of the Inter Tropical Convergence Zone (ITCZ) that lags behind the overhead sun by about 3 - 4 weeks (Ogallo, 1993b; Okoola, 1996; Mutemi, 2003). The intermediate periods between these two rainy seasons are relatively dry. Some parts of the region such as northern Uganda and southern Tanzania, further away from the equator experience a unimodal rainfall regime. Northern Uganda receives considerable rainfall during the months of June to July (JJA) season extending sometimes to September with a slight relaxation around June to July (Bamanya, 2007). However other parts of the region such as eastern Uganda experience three rainfall seasons exhibiting a trimodal regime, with the third peak occurring from July to August due to moisture influx from the Atlantic Ocean and Congo basin by westerly winds caused by intensification of the St. Helena anticyclone that displaces the meridional arm of the ITCZ to eastern Uganda (Bamanya, 2007).

The Climate of the region is also controlled by global and regional telecommunications, as well as synoptic and local factors. Some of the synoptic scale features that affect rainfall over the LVB are the Lake Victoria trough, ITCZ, Subtropical anticyclones, Tropical cyclones, Jet streams, westerly waves and many other global and regional systems that include El-Nino Southern Oscillation (ENSO) and Indian Ocean Dipole (IOD). The micro-scale features

interact with both the synoptic and large scale systems to produce the observed rainfall distribution over the region (Mukabana, 1992; Asnani, 1993; Ogallo, 1989). The characteristics of some of these global, regional, synoptic and local systems and their influence on the climate of East Africa and the LVB in particular are reviewed in the subsections below.

1.7.1 Lake Victoria Trough

The quasi-permanent Lake Victoria trough coupled with the complex physical features induces mesoscale circulation with a strong diurnal cycle over the region. Due to the existence of inland water bodies mainly Lake Victoria, thermal contrasts that exist between land and water surfaces usually initiate local circulations, including land-sea breeze. A good example of the local effect is observed over the Lake Victoria which has a vigorous circulation of its own (Ogallo, 1988). The lake influence is due to its large body of water, the temperature contrasts between the lake and land during the day and the night resulting in a land breeze towards the lake during the night. In general, the land-sea breeze phenomenon results in the lake basin region getting some rainfall almost throughout the year. The rainfall is however significantly enhanced during the main rainy seasons discussed above due to the passage of ITCZ.

1.7.2 Inter Tropical Convergence Zone

The Inter – tropical convergence zone (ITCZ) system is a boundary between inter-hemispheric monsoon wind systems over the region. The ITCZ is the main synoptic scale system that affects the intensity, distribution and migration of seasonal rainfall over the LVB. The onset and cessation of seasonal rainfall over the region depends on the onset and withdrawal of the ITCZ (Okoola, 1996).

Over East Africa, the ITCZ has two spatial components. These include the zonal and meridional arms. The zonal arm, which has an East-West orientation, is a zone of convergence between the northeast and southeast monsoons/trades, while the meridional arm, which has a North-South orientation, is a zone of convergence between the westerlies from the Atlantic Ocean and the Easterlies (Kiangi *et al.*, 1981; Ininda, 1995b; Okoola, 1996). The zonal component of the ITCZ migrates north and south of the equator following the seasonal migration of the sun with a time lag of about a month. The northward movement of the zonal arm of the ITCZ component is in response to the seasonal intensification (weakening) of the southeast (northeast) monsoon winds. It traverses East Africa twice a year causing the long

rains (March to May) and short rains (October to December) seasons over eastern Africa region (Ininda, 1995a; Okoola, 1996).

For instance during long rains, the zonal component of the ITCZ, which runs from west Africa through central Africa to east Africa, moves from the Southern Hemisphere towards the Northern Hemisphere passing over parts of LVB. As a result, the rains start from the southern part and spread northwards. During this period, air masses from the Indian Ocean converge over East African region bringing in moisture. This component of the ITCZ reaches the north-most position in August and there after begins to retreat southwards when the southeast (northeast) monsoons weaken (intensify) until it reaches the south-most position in January (Griffith, 1972).

The meridional component of the ITCZ oscillates from east to west and vice-versa, with the east most extent noted in July to August depending on the relative strength of the St. Helena anticyclone that is situated over the southern Atlantic Ocean. When this anticyclone intensifies, the meridional arm of the ITCZ is displaced eastwards giving rain to eastern parts of the LVB. During the season spanning from June to August the meridional arm of the ITCZ is normally located over eastern Uganda and highlands of western Kenya. This implies that much of Uganda is under the influence of moist, low-level westerly flow from the Congo Basin during this period. The effectiveness and depth of the ITCZ mainly depends on the intensity of the Subtropical anticyclones. These include the Arabian high to the northwest, the Azores high to the northeast of Africa, the Mascarene high to the southeast and the St. Helena high to the southwest. These anticyclones determine the characteristics of the monsoonal winds over East Africa. The characteristics of these subtropical anticyclones are reviewed in Section 1.7.3.

1.7.3 Subtropical Anticyclones

Subtropical Anticyclones are semi-permanent warm core, high-pressure systems centered over the subtropical latitudes, approximately $30^{\circ}S$ and $30^{\circ}N$ of the north and South Atlantic Ocean, and the Indian Ocean. Pressure differences create anticyclones between the equatorial regions and the subtropical regions necessary for driving the tropical trade winds. The anticyclones that influence the synoptic flow over East Africa are Mascarene, St Helena, Arabian, and the Azores high. These systems are most intensive during winter seasons of each hemisphere and weaken during summer. The moisture that comes into East African region depends on the location and strength of these anticyclones.

For instance, the Mascarene anticyclone over the south western Indian Ocean determines the characteristics of the moist south easterly monsoon flow over the Indian Ocean which influences rainfall over most of eastern Africa. The St. Helena anticyclone over the southeast Atlantic Ocean is responsible for the pronounced middle level westerly flow (the Congo air mass) over the region, which influences most parts of the LVB. The Azores high causes subsidence of warm dry air over the Sahara and neighboring regions while the Arabian anticyclone sends dry continental north easterly flow over most of the eastern parts of Africa (Griffith, 1972; Anyamba, 1984).

1.7.4 El Niño Southern Oscillation

The El Niño/Southern Oscillation (ENSO) phenomenon is a quasi-periodic feature of the ocean-atmosphere system (Ininda, 1995b), with extreme rainfall characteristics linked to ENSO conditions over the region (Ogallo, 1988). The ENSO have been found to play a key role in modulating climate pattern over the LVB, with ENSO alone explaining about 50% of rainfall variance (Ogallo, 1988). Rainfall variability is known to be linked to ENSO phenomena. The variability is believed to show strong link to ENSO and IOD conditions especially during the OND season (Nicholson, 2013 and Mutai and Ward, 2000).

The ENSO and IOD have been identified as a leading mode of tropical climate variability at inter-annual timescales characterized by SSTs and surface pressure anomalies over the global oceans (Ogallo, 1989). Recent study by Anyah and Otieno, (2013) over the region have demonstrated the ability of the GCM models to simulate climate scenarios especially during the ENSO and IOD episodes when downscaled. However the models still struggle to capture circulations around mountainous regions and lake breezes which call for opportunity for further research.

1.7.5 Indian Ocean dipole

The Indian Ocean Dipole (IOD) index is another mode of climate variability known to modulate rainfall over Africa region (Nicholson, 2013). The IOD is the difference between the sea surface temperature anomalies of the western and south eastern equatorial Indian Ocean. Studies by Owiti *et al.*, (2008) have shown anomalously warm sea surface temperatures are at times experienced over the western Indian Ocean and cold SSTs over the Eastern region. This condition has been found to have a great influence on the rainfall over east Africa. Mutai and Ward (2000) in his study showed that the winds from the Indian

Ocean are influenced by IOD SST anomalies especially on the amount of moisture that is pushed to the region.

The IOD is positive when western Indian Ocean is warmer than the Eastern Indian Ocean, and vice versa. The positive phase of IOD is known to be of great influence on the rainfall condition over the Equatorial and South Africa region. It activates atmospheric convection and leads to enhanced rainfall during the rainy season and wet spells during the dry season. This positive phase causes an anomalous cooling of SST in the eastern tropical Indian Ocean and brings droughts in the Indonesian and Australian region. Negative phase of IOD occurs when eastern Indian Ocean is warmer, bringing more rainfall to Australian and Indonesian region. Studies have also shown that just like ENSO, IOD may induce unusual circulation and rainfall pattern in countries beyond the proximity of Indian Ocean (Owiti and Weijun , 2012)

Owiti *et al.*, (2008) analyzed the evolution phases of IOD, and showed that it starts developing in April and reaches the peak in October or November and starts decaying in January. This therefore implies that the SST anomalies pattern experienced during IOD events have a strong signal on the regional climate system during OND rainfall season, hence indicating that some of the extreme events that have been experienced over the region have a close relationship with the negative and positive phases of IOD. Studies over the region have found strong relationships between the IOD and ENSO and the rainfall characteristics with dominant signals from easterly (westerly) wind anomalies for extremely positive (negative) IOD events (Owiti *at al.*, 2008, Bowden *et al.*, 2007 and Nichlosn, 1996).

1.7.6 Sea Surface Temperatures

Studies on SST's have pointed out their direct influence on seasonal rainfall over East Africa. The SST anomalies have been found to exert a stronger control on inter annual variability of monsoon rainfall over Africa (Pohl and Camberlin, 2006). The impact of SST anomalies is nonlinear with respect to warm and cold events. The monsoon is weakened during the warm events but changes less noticeably during the cold events. Associated with the warm SST anomalies, both the Walker circulation and local Hadley circulation diminish substantially. These changes are accompanied by reduction in total rainfall and water vapor convergence in the Asian monsoon region. Rowell, (2013) explored possible reasons for the differing characters of the long rains and short rains seasons and their respective relationships with SSTs.

Negligible correlations were found between Pacific SST's and the long rains. However, significant correlations were found with the short rains. Warmer (colder) SSTs anomalies have been associated with wet (dry) conditions over East Africa. The interactions between global atmospheric jets, Madden Jullian Oscillation(MJO), high level wind circulations amongst others modulate the rainfall characteristics of the region (Rowell, 2013, Omeny *et al.*, 2008, Pohl and Camberlin 2006, Philipon *et al.*, 2002, Mutai and Ward, 2000 and Omondi *et al.*, 2009).

1.7.7 Tropical Monsoons

Monsoons are seasonal winds, which reverse their directions depending on the temperature difference between the oceans and the continents. They are seasonal (sometimes inter-hemispheric) wind systems, which converge at the ITCZ. They are the major transporters of moisture inland for rain formation. During the short rains season (OND), the northeast monsoonal wind is advancing while the southeast monsoonal wind is receding. For the long rains season (MAM), the northeast monsoonal wind is receding while the southeast monsoonal wind is advancing. In both cases the low level monsoonal air current is topped by air due to easterly current which is generally dry.

During the Northern Hemisphere winter (DJF), most parts of East Africa are under the influence of the northeast monsoonal wind currents. These winds originate from the Arabian high and are generally dry since they are of continental origin and their trajectory is largely over the land (Anyamba, 1984; Okoola, 1996). They enter East Africa in a north easterly direction and bifurcate into two air streams over northern Kenyan. One stream flows southward along the east African coast and over the mainland Tanzania while the other flows westward into Uganda, southern Sudan and eastern Democratic Republic of Congo (DRC).

The southeast/southwest monsoonal wind currents are experienced during the Southern Hemisphere winter (June-September). These winds are cool and moist, and originate from the Mascarene Anticyclone in the southern Indian Ocean. They are transported by the east African low level jet stream that is fully developed in July. They branch into two air streams over the coastal plains of Tanzania and eastern Kenya. These monsoonal currents are shallow, being confined to the lowest three kilometers above sea level (Findlater, 1969; 1971; Okoola, 1996). Their inversion hinders cloud development, rendering them shallow and therefore unable to precipitate. Much of the equatorial eastern Africa is cold and dry during the inversion of these Southeast/Southwest monsoonal currents. However, eastern Uganda and western Kenya receive considerable amounts of rainfall due to the interaction between

the southeast monsoonal wind currents, the Congo air mass and the Lake Victoria thermally-induced mesoscale circulation (Kiangi *et al.*, 1981; Mukabana and Pielke, 1996).

The intensity of the southeast monsoonal air currents is stronger in a narrow zone which is confined to the east Africa highlands. The peak wind speed is found near 850 mb level. This maximum in the southeast monsoonal current constitutes the east African low level jet (Findlater, 1971). The influence of this jet stream together with other global jet streams on the LVB weather is reviewed in section 1.7.8.

1.7.8 Jet Streams

A jet stream is a current of fast moving air found in both the upper and the lower levels of the atmosphere. Jet streams are usually found somewhere between 10-15 km (6-9 miles) above the earth's surface. The jet streams that have been observed to influence weather over eastern Africa are the Subtropical Jet, Tropical Easterly Jet (TEJ) at about 650 mb, African Easterly Jet (AEJ), Turkana Jet (Kinuthia and Asnani, 1982) and East African Low Level Jet (EALLJ). Several authors have discussed the effect of these jet streams on the climate of East Africa. These include Findlater (1969); Okoola (1996); Mukabana (1992) and Asnani (1993). Jet streams are associated with the formation of the waves in some regions (Krishnamurti and Bhalme, 1976).

CHAPTER TWO

2.0 LITERATURE REVIEW FOR THE STUDY

2.1 Climatology of the Lake Victoria Basin

The general climate of the basin is highly variable ranging from equatorial type, modified with rainfall occurrences all year round, particularly over the lake surface, to semi arid type characterized by intermittent droughts over regions near the shores (Anyah, 2005). However, the seasonal rainfall is also characterized by a bimodal cycle, just like most areas of East Africa.

While this seasonal cycle of rainfall is mainly controlled by the north-south migration of ITCZ, studies have shown the existence of a quasi-permanent trough that occurs over Lake Victoria (Asnani, 1993) due to locally induced convection, orographic influence and land-lake thermal contrast modulates rainfall pattern over the lake and hinterlands. The existence of this quasi-permanent trough over the lake favors convection over the basin throughout the year.

It has been established that the estimates of the mean annual rainfall distribution over the Lake Basin based on the measurements taken from lakeshore rain gauge stations vary between 800mm and 3000 mm (Ogallo 1981, Nicholson 1996, Asnani, 1993). The large-scale precipitation over the lake is mainly initiated from the easterly/southeasterly (Indian Ocean) monsoon flow that transports maritime moisture into the interior of East Africa. The humid Congo air mass has also been linked to significant rainfall amounts received over the western and northwestern parts of the lake (Asnani, 1993).

Large-scale winds over the Lake Basin are mainly easterly trades most of the year. Superimposed on this basic flow regime are the south-easterly (SE) or north-easterly (NE) monsoons that are mostly driven towards, and often converge over, the ITCZ location. The strength of the monsoons also depends on the sub-tropical anticyclones over the Arabian Sea (Arabian high pressure cell) and southwestern Indian Ocean (Macarene high pressure cell).

The distribution of solar radiation over the lake is also partly related to the season, altitude and latitude. Thus, since the lake lies astride the equator, the lake basin is characterized by intense insolation throughout the year. Lake water temperatures also usually follow the magnitude of solar radiation input but with some lag (Bugenyi and Magumba, 1996). Thus, based on sample measurements over a number of points over the lake surface, the mean

monthly solar radiation is estimated at 240-270W/m ranges between 24 and 28 and the surface water temperatures (Ochumba, 1996; Bugenyi and Magumba, 1996).

2.1.1 Climate Extremes over the LVB

The inter-annual variability of the Lake Basin is closely linked to the SST anomalies over the global ocean basins. The inter-annual variability of the LVB climate is characterized by periodic episodes of anomalously wet/dry conditions. Some of the most recent events include the 1961/62 and 1997/98 floods that left behind a huge trail of damage to property and infrastructure (Anyah, 2005). The 1961/62 floods were associated with a strong zonal SST gradient over the equatorial Indian Ocean and mid-troposphere westerly flow from Tropical Atlantic (Anyamba, 1984; Anyah and Semazzi, 2005).

On the other hand, the 1997/98 floods coincided with one of the warmest ENSO episodes (strongest El Niño) of the last century as well as very strong Indian Ocean dipole mode. These floods resulted to the displacement of communities, and destruction of the infrastructure and crops as well as outbreak of diseases. Droughts on the other hand affect food production, availability of water, and generation of hydroelectric power for industrial and domestic consumption and outbreak of some unique diseases including those related to water scarcity and contamination. The majority of short falls in food supply recorded in 1928, 1933-34, 1937, 1939, 1942-44, 1947, 1951, 1952-55, 1957-58m 1984/85 and 1999-2000 over the region could be easily associated with rainfall deficits experienced in the respective years (Odada *et al.*, 2006).

2.1.2 Socio-economic Activities over the LVB

There are several socioeconomic activities which the people of the LVB are involved in and these include: fishing, farming, bee keeping, trading activities, quarrying and sand mining and mining of gold and other minerals (Odada *et al.* 2006).

Fishing is undertaken for both subsistence and commercial goals. Most of the fisher folk have been fishing over the years as a source of their livelihood. In the past decade fishing became increasingly commercialized threatening even the nutrition source for the LVB inhabitants. Most fish and particularly Nile Perch is sold to fish processing plants or other agents as a result increased prices that are out of reach of most poor to average households. Fish frames from the processing plants are now common sources of nutrition to these households (LEVMP, 2003). Fish catch is also declining due to increased fishing effort and illegal fishing methods.

Agriculture by far is the main stay of the LVB inhabitants. Farming of food and cash crops is practiced in the LVB. Food crops include maize, bananas, cassava, sorghum, millet, rice, sweet potatoes and an assortment of vegetables and fruits. Main cash crops include coffee, cotton and sugar cane. Livestock in the LVB is significant particularly in the Tanzania, Uganda, Rwanda and Burundi sides. The traditional way of livestock keeping is still practiced. This has some environmental implications, cultural traits and economic significance. However, with the declining open spaces for grazing and pressure for land, there is a need for adapting cattle rearing to new realities. In the natural resources utilization area, the LVB inhabitants also indulge in beekeeping for livelihood and commerce. Tourism is based on mainly wildlife. In this basin, the Serengeti, Maasai Mara, Owen falls and the source of the Nile at Jinja among others represent the wealth of tourist attractions of the LVB (Odada *et al.*, 2006).

Mining is another natural resource-based activity in the LVB. Gold mining, quarrying and sand mining are some of the major mining activities. On the Tanzania side, gold mining is quite a big industry. This, however, poses a threat to the Lake and its flora and fauna if it is not carried out in a responsible manner. Mercury, which is mainly used by small-scale miners for processing of gold, is a heavy metal which accumulates in the food chain and may be dangerous once the amounts accumulated are high and widespread. Odada *et al.*, 2006 found evidence of low mercury concentrations in fish and human hair, lower than the WHO reference value, in Mgusu gold mine and the Nungwe Bay of the Lake Victoria goldfields of Tanzania. Living organisms in the water like fish may take it in small proportions from the contaminated water flowing from mining sites or riverbanks; human beings eat the fish and the metal accumulates in their bodies.

2.1.3 Observations, Processes, Modeling, Prediction and Applications

In terms of climate, the lake produces its own climate with distinct diurnal, seasonal and inter-annual characteristics. Kinuthia and Asnani, (1979) reported that meso-scale circulation (lake/land breeze) generated by land/sea interactions and orographic forcing, for instance, around Lake Victoria, have a great impact on the climate of the surrounding regions. The high ground to the east and north east of Lake Victoria experiences a phenomenal level of hailstorms occurrences annually. Temporal variation of rainfall over the LVB occurs on various time scales, which include diurnal time scales (Kinuthia and Asnani, 1979; Asnani, 1993; and Barring, 1987), quasi-biweekly time scales (Okoola, 1993), intra-

seasonal/monthly time scales (Tomsett, 1969, Mutai, 2000), seasonal time scales (Ogallo, 1988) and annual time scales (Ogallo, 1984).

Kizza *et al.*, (2009) studied the temporally variability of rainfall over the LVB. They established a positive trend in the Oct-Dec rainfall. The extreme rains in 1961 and 1997 were studied by Conway (2002) who showed that the two events were associated with a dipole-like reversal of Indian Ocean sea surface temperatures. In addition, 1997 was a strong El Niño year. The 1961 and 1997 events were, similar in spatial and temporal characteristics and occurred mainly in the short rains period (October–December). The two events had far reaching hydrological impacts in the regions (including record river flows and flooding) with large socio-economic consequences (Conway *et al.* 2005). Other years with extreme rainfall include 1937, 1941, 1947, 1951, 1961, 1963, 1977, 1989, 1997 and 2001.

It has been reported that the current state of prediction over the monsoon region is not much better than the prediction of long-term mean climate and there is almost no skill in the prediction of seasonal anomalies (Palmer *et al.*, 2000). The use of an ensemble mean of seasonal forecasts, generated from adjacent start dates, also appeared to perform very close to a climatological forecast, thus showing almost no skill for the prediction of seasonal anomalies (Palmer *et al.*, 2004). Fowler and Ekstrom, (2009) examined the performance of seasonal climate prediction using atmospheric GCMs in the context of the Atmospheric Model Inter-comparison Project (AMIP) data sets. The examination of the performance of monthly and seasonal forecasts from a number of research and operational atmospheric GCMs showed very low skill for the prediction of precipitation.

In an attempt to solve the problem of uncertainty and sensitivity to parameterization and initial conditions that are characterized in most GCMs, the concept of multimodal ensemble prediction has been developed and tested for forecasting purposes, Palmer *et al.*, (2000). The use of an ensemble prediction from one model systematically provides better results than the standard deterministic forecasting with only one run which improves the accuracy and forecasts reliability to the consumers. This in the past has been studied by researchers including (Krishnamurti *et al.*, 2000 and Hagedorn *et al.*, 2005).

Using numerical simulation, Ininda (1998) showed that the rainfall over most regions in East Africa is influenced by the SST through modification of the east-west (Walker's) circulation and the local north-south (Hadley) circulation. Mutemi (2003) applied an updated version of ECHAM AGCM (ECHAM4.5) to study the variability of East Africa climate. The model

reproduced the climatological mean pattern such as the bimodal seasonality of rainfall associated with the north-south migration of the ITCZ and monsoonal flow, except the correct amplitudes of the inter-annual variability linked to extreme El-Niño episodes such as the 1982 and 1997 were not well reproduced.

Otieno (2013) analyzed GPC model performance over the Greater Horn of Africa using the twelve GPC models. He found that the forecast skill is much better over the equatorial region and the models perform poorly in the northern and southern sectors.

2.1.4 Downscaling

Despite notable development, GCMs do not provide perfect simulations of reality and cannot provide the details on very small spatial scales due to incomplete scientific understanding and limitations of available observations (Jolley and Wheeler, 1996). For bridging the gap between the scale of GCMs and required resolution for practical applications, downscaling provides climate change information at a suitable spatial and temporal scale from the GCM data. Statistical and dynamical downscaling are two broad main types.

2.1.4.1 Dynamical Downscaling

Dynamical downscaling is usually based on the use of regional climate models (RCMs), which generate finer resolution output based on atmospheric physics over a region using GCM fields as boundary conditions (Giorgi and Mearns, 1991 and 1999). The physical consistency between

GCMs and RCMs are controlled by the agreement of their large-scale circulations (Von Storch *et al.*, 2000). The individual choice of domain size controls the divergence between the RCMs and their driving GCMs (Jones *et al.*, 1997).

As a consequence of the higher spatial resolution output, RCMs provide a better description of topographic phenomena such as orographic effects (Christensen, 2007). Moreover, the finer dynamical processes in RCMs produce more realistic mesoscale circulation patterns (Buonomo *et al.*, 2007). However, RCMs are not expected to capture the observed spatial precipitation extremes at a fine cell scale (Fowler and Ekstrom, 2009). A study by Rauscher *et al.*, (2009) has found that the skill improvement of RCM depends not only on the RCM resolution but also on the region and the season. Although RCMs may give feedback to their driving GCMs, many dynamic downscaling approaches are based on a one-way nesting approach and have no feedback from the RCM to the driving GCM (Maraun *et al.*, 2010).

The main problem with RCMs is that significant biases in the simulation of mean precipitation on large scales can be inherited from the driving GCM (Durman *et al.*, 2004). Frei *et al.* (2006) noted that inter-model differences are related to model biases. Moreover, Christensen *et al.* (2008) suggest that GCM biases may not be linear and biases may not be cancelled out by simply taking differences between the control and future scenarios, which many studies have adopted (Jenkins *et al.*, 2009).

Despite their rapid development, RCMs are still ridden with problems related to parameterization schemes due to the fact that physical processes are modeled at a scale on which they cannot be explicitly resolved (Maraun *et al.*, 2010). The RCM precipitation outputs are still found to be sensitive to the numerical scheme and parameters (Fowler and Ekstrom, 2009; Bachner *et al.*, 2008; Murphy *et al.*, 2009).

2.1.4.2 Statistical Downscaling

Based on particular statistical relationships between the coarse GCMs and fine observed data, statistical downscaling is a straightforward means of obtaining high resolution climate projections (Wilby *et al.*, 2004). Taking the relationship with RCMs into consideration, Maraun *et al.*, (2010) divided statistical downscaling approaches into perfect prognosis (PP), model output statistics (MOS) and weather generators. In PP, the statistical downscaling relationships are established by observations. In MOS, gridded RCM simulations and observations are used together to develop downscaling relationship. Using PP, MOS or both of them, weather generators are hybrid downscaling methods.

With respect to types of statistical methods, downscaling can be categorical, continuous-valued or hybrid (Wilby and Wigley, 1997). In categorical downscaling, classifications and clustering are the common statistical techniques to relate data to different groups according to large-scale circulation patterns and data attributes (Fowler and Ekstrom, 2009). For continuous-valued downscaling, regression relationships are widely used to map large scale predictors onto local-scale predictands (Chandler and Wheeler, 2002). In hybrid downscaling, different statistical approaches are combined (Wilby *et al.*, 2002) and they are sometimes referred to as weather generators, based on algorithms of conceptual processes (Chandler, 2006; Kilsby *et al.*, 2007).

Although statistical downscaling can be a computationally efficient alternative to dynamic downscaling, the validity of statistical downscaling is based on an assumption that the empirical relationship identified for the current climate will hold for future climate scenarios

(Wilby *et al.*, 2004). It also assumes that the employed large-scale predictor variables are adequately modeled by the GCM for the resultant scenarios to be valid. Busuioc *et al.* (1998), in their verification of the validity of empirical downscaling techniques, found that in the case considered, GCMs were reliable at the regional scale with respect to precipitation in their study area and that the assumptions of validity of predictor-predictand relationship held up under changed climate conditions.

Von Storch *et al.* (1993) suggested that if statistical downscaling is to be useful, the relationship between predictor and predictand should explain a large part of the observed variability and that the expected changes in the mean climate should lie within the range of its natural variability. This is generally true for temperature. However, for precipitation the influence of 'local' factors on occurrence and amounts can often be considerable. As a result of these site-specific considerations the relationship between the large-scale predictors and local outputs often reflects a smaller part of the actual observed variability (Sweeney and Fearl, 2003).

CHAPTER THREE

3.0 THE FIFTH VERSION OF THE COUPLED MODEL INTER-COMPARISON MODELS

3.1 Theoretical Framework

The key tool in this research was the fifth version of the Coupled Model Inter-comparison Project (CMIP5) model output. An attempt was made in this section to provide detailed information on the CMIP5. The CMIP5 project comprises 29 modeling centers with each centre giving outputs from their models on monthly and seasonal basis. Some of the CMIP5 models being used worldwide for predictions and climate projections and adopted in this study are the Australian, Beijing, Institute of Space Research model, Canadian, Ec- Earth Consortium, NOAA, Korean, Japan, Max-Planck, and Norwegian models.

Over the last 15 years, a number of international climate centers have developed operational capabilities for global long-range prediction, typically for 3 months mean climate anomalies and to 6 months ahead, using ensemble integrations of dynamical models. Working through Expert Teams, WMO has fostered coordination between these centers, leading to the establishment of new infrastructure within the Global Data Processing and Forecasting System (GDPFS) that improves both access to the forecast information and the usefulness of this information for generating climate services.

3.2 Model Physics of the Fifth Version of the Coupled Model Inter-comparison Project

EC-EARTH is an Earth System Model (ESM) that is developed by a consortium of European Weather Services and university groups. It is based on the seasonal prediction system of European Centre for Medium-Range Weather Forecasts (ECMWF) and currently consists of an atmosphere and an ocean model that communicate with each other through the Oasis coupler (Rotstayn, 1998).

In EC-EARTH it is possible to modify the external climate forcing, for example by imposing different concentrations of greenhouse gases, resulting in changes in the atmospheric and ocean circulation at global and regional scales. One can also produce several simulations with a specific forcing but slightly different initial conditions to explore the uncertainty of future climate projections. The ensembles of ESM simulations can thereafter be downscaled to

study the impact of a changed climate at regional and local scales, as is planned in Mistra-SWECIA.

The atmospheric component of EC-EARTH is the ECMWF IFS (Integrated Forecast System) model version 31r1. There are 62 levels in the vertical, with a model top at 5hPa (~37 km). The dynamical part of the model uses a spectral transform approach, with a present horizontal resolution of TL159. The physical parameterization schemes of the model (including clouds, rain, turbulence and land surface processes) are all calculated on a reduced N80 Gaussian grid, which corresponds to a 1.125 degrees spacing (125 km).

The ocean component is NEMO (Nucleus for European Modelling of the Ocean), a primitive equation model adapted to regional and global ocean circulation problems. Prognostic variables are the three-dimensional velocity field, a linear or non-linear sea surface height, temperature and salinity. In the horizontal direction, the model uses a curvilinear orthogonal grid with the North Pole shifted to Greenland. The nominal horizontal resolution is 2 degrees with refinement at the equator. In the vertical direction, a full or partial step z-coordinate, or s-coordinate, or a mixture of the two can be used. There are 31 levels in the vertical. The grid is based on a three dimensional Arakawa C-grid. Various physical choices are available to describe ocean physics. NEMO includes the sea-ice model LIM2(LouvainIceModelversion2) (Rotstayn, 1998).

CNRM-ESM was developed by the European Centre of Meteorology in order to contribute to phase 5 of the Coupled Model Inter-comparison Project (CMIP5). CNRM includes the atmospheric model ARPEGE-Climat ,the ocean model NEMO, the land surface scheme ISBA and the sea ice model GELATO coupled through the OASIS system (Zhang and McFarlane, 1995). Horizontal resolution has been increased both in the atmosphere (from 2.8_ to 1.4_) and in the ocean (from 2_ to 1_). The dynamical core of the atmospheric component has been revised. A new radiation scheme has been introduced and the treatments of tropospheric and stratospheric aerosols have been improved.

The global spectral ARPEGE-Climat atmospheric model is derived from the ARPEGE/IFS (Integrated Forecast System) numerical weather prediction model developed jointly by Meteo-France and European Center for Medium-range Weather Forecast (ECMWF). This is a spectral model that operates on a T127 triangular truncation within CNRM-ESM. All the physics and the calculations of the nonlinear terms require spectral transforms onto a reduced Gaussian grid (Hortal and Simmons, 1991) equivalent to a spatial resolution of about 1.4 in

both longitude and latitude. CNRM-ESM is run in a “low-top” configuration with 31 vertical levels, following a progressive hybrid r-pressure discretization.

The ocean component of CNRM-ESM.1 is based on the ocean part of the “Nucleus for European Modelling of the Ocean” (NEMO, version v3.2). refinement of $1/3_{\Delta}$ is added in the tropics. In the vertical, 42 levels are used (from 10 m at the surface, to 25 at 100 m, 130 at 600 m, and 300 at 5,000 m) and a partial step formulation (Barnier *et al.*, 2006; Penduff *et al.*, 2007) is applied to the thickness of the bottom layer. At the surface, the model has a linear free surface (Roullet and Madec, 2000). Advection of temperature and salinity is done using a total variance dissipation scheme (Levy *et al.*, 2001 and Cravatte *et al.*, 2007), a second-order, two-step monotonic scheme with moderate numerical diffusion.

MIROC-ESM is based on a global climate model MIROC (Model for Interdisciplinary Research on Climate) which has been cooperatively developed by the University of Tokyo, NIES, and JAMSTEC (K-1 model developers, 2004; Nozawa *et al.*, 2007). A comprehensive atmospheric general circulation model (MIROC-AGCM 2010) including an on-line aerosol component (SPRINTARS 5.00), an ocean GCM with sea-ice component (COCO 3.4), and a land surface model (MATSIRO) are interactively coupled in MIROC. These atmosphere, ocean, and land surface components, as well as a river routing scheme, are coupled by a flux coupler (K-1 model developers, 2004).

The MIROC-AGCM has a spectral dynamical core, and uses a flux-form semi-Lagrangian scheme for the tracer advection. The horizontal triangular truncation at a total horizontal wave number of 42 (T42; equivalent grid interval is approximately 2.8125 degrees in latitude and longitude) is used.

An aerosol module in MIROC, SPRINTARS, predicts mass mixing ratios of the main tropospheric aerosols: carbonaceous (BC and organic matter; OM), sulfate, soil dust, and sea salt, and the precursor gases of sulfate, i.e. sulfur dioxide (SO_2) and DMS. The aerosol transport processes include emission, advection, diffusion, sulfur chemistry, wet deposition, dry deposition, and gravitational settling. Emissions of soil dust, sea salt, and DMS are calculated using the internal parameters of the model, and external emission inventories are used for the other aerosol sources. SPRINTARS is coupled with the radiation and cloud/precipitation schemes for calculating the direct, semi-direct, and indirect effects of aerosols.

The MPI-ESM was developed by the Max-Planck Institute of Meteorology. MPI-ESM couples the atmosphere, ocean and land surface through the exchange of energy, momentum, water and important trace gases such as carbon dioxide. Compared to the previous version ECHAM5/MPIOM, the MPI-ESM was extended by numerous developments. It is based on the components of ECHAM6 for atmosphere and MPIOM for ocean as well as JSBACH for terrestrial biosphere and HAMOCC for the ocean's biogeochemistry. The coupling of atmosphere and land on the one hand and ocean and biogeochemistry on the other hand is made possible by the separate coupling program OASIS3. Energy, momentum, water and CO₂ are exchanged with the help of this coupling.

The atmospheric component focuses on the coupling between diabatic processes and large-scale circulations, both of which are ultimately driven by radiative forcing. It consists of a dry spectral-transform dynamical core, a transport model for scalar quantities other than temperature and surface pressure, a suite of physical parameterizations for the representation of diabatic processes, as well as boundary data sets for externalized parameters, such as trace gas and aerosol distributions, tabulations of gas absorption optical properties, temporal variations in spectral solar irradiance, land-surface properties

Table 1 summarizes the main characteristics of the eight CMIP5 models, including the resolution of the models and hindcast period of each Center model as well as the convective schemes employed in each of the models.

Table 1: The Coupled Model Inter-comparison Project 5 (CMIP5) Models

Model Name	Center	Convective Scheme	Horizontal Resolution	Hindcast period
CCCMA	Canadian Centre for Climate Modelling and Analysis	Zhang and McFarlane scheme (Zhang and McFarlane, 1995)	2.8125* 2.79062	1951–2005
EC-EARTH	EC-EARTH consortium	Prognostic Arakawa-Shubert based Rotstayn, (1998)	1.125 * 1.12148	1951–2005
GFDL-ESM	NOAA Geophysical Fluid Dynamics Laboratory Center	Brethron scheme (Bretherton <i>et al.</i> , 2004)	0.625 * 0.5	1951–2005
MIROC-ESM	Japan Agency for Marine-Earth Science and Technology, (The University of Tokyo)	Arakawa and Shubert (Arakawa and Shubert, 1974)	1.4 * 1.4	1951–2005
MPI-ESM	Max Planck Institute for Meteorology)	Bulk mass flux scheme (Tiedtke, 1989) with modification for deep convection according to Nordeng (1994)	1.875 * 1.85	1951–2005
NorESM	Norwegian Climate Centre	Zhang and McFarlane scheme (Zhang and McFarlane, 1995)	2.5 * 1.895	1951–2005
HadGEM2	Korea Meteorological Administration	Bulk mas flux scheme (Del Genio and Yao, 1993)	1.25 * 2	1951–2005
CNRM	European Centre of Meteorology	Zhang and McFarlane scheme (Zhang and McFarlane, 1995)	2.8125* 2.79062	1951-2005

3.3 Representative Concentration Pathways

Socio-economic and emission scenarios are used in climate research to provide plausible descriptions of how the future may evolve with respect to a range of variables including socio-economic change, technological change, energy and land use, and emissions of greenhouse gases and air pollutants. They are used as input for climate model runs and as a basis for assessment of possible climate impacts and mitigation options and associated costs. In the past, several sets of scenarios have performed such a role, including the IS92 scenarios (Leggett *et al.*, 1992) and, more recently, the scenarios from the Special Report on Emission

Scenarios (SRES) (Nakicenovic *et al.*, 2000). A literature review revealed that scenarios can be found with a year 2100 radiative forcing from as low as 2.5 W/m² to between 8 and 9 W/m² and higher (Fisher *et al.*, 2007). The RCP set, thus, should cover this range, but also include intermediate scenarios as the majority of the scenarios in the literature lead to intermediate forcing levels.

The Representative Concentration Pathways (RCPs) are named according to radiative forcing target level for 2100. The radiative forcing estimates are based on the forcing of greenhouse gases and other forcing agents. The four selected RCPs were considered to be representative of the literature, and included one mitigation scenario leading to a very low forcing level (RCP2.6), two medium stabilization scenarios (RCP4.5/RCP6) and one very high baseline emission scenarios (RCP8.5) (Moss *et al.*, 2008). The first scenario (RCP2.6) has also been referred to as RCP3PD, a name that emphasizes the radiative forcing trajectory (first going to a peak forcing level of 3 W/m² followed by a decline (PD = Peak–Decline). The Fourth Assessment Report (AR4) identified only 6 scenarios that lead to forcing levels below 3 W/m², but by now more than 20 scenarios in the literature lead to similar forcing levels as RCP2.6. RCP4.5 corresponds to the ‘category IV’ scenarios in AR4 (containing the far majority of the scenarios assessed in AR4, i.e. 118). The number of mitigation scenarios leading to 6 W/m² in the literature is relatively low (around 10)—but at the same time many baseline scenarios (no climate policy) correspond to this forcing level. Finally, RCP8.5 leads to a forcing level near the 90th percentile for the baseline scenarios, but a recent literature review was still able to identify around 40 scenarios with a similar forcing level.

Table 2 summarizes the general overview of representative concentration pathways (RCPs) and their descriptions.

Table 2: General overview of representative concentration pathways (RCPs) and their descriptions

Scenario	Description
RCP8.5	Rising radiative forcing pathway leading to 8.5 W/m ² (~1370 ppm CO ₂ eq) by 2100.
RCP6	Stabilization without overshoot pathway to 6 W/m ² (~850 ppm CO ₂ eq) at stabilization after 2100
RCP4.5	Stabilization without overshoot pathway to 4.5 W/m ² (~650 ppm CO ₂ eq) at stabilization after 2100
RCP2.6	Peak in radiative forcing at ~3 W/m ² (~490 ppm CO ₂ eq) before 2100 and then decline (the selected pathway declines to 2.6 W/m ² by 2100).

CHAPTER FOUR

4.0 DATA AND METHODOLOGY

This section presents a discussion of the data and methodology that were used in the study.

4.1 Data

The data used in the study included observed point stations datasets consisting of the monthly rainfall archives used for GHA/ East Africa climate operations at the IGAD Climate Prediction and Application Centre (ICPAC), Individual model hindcasts from the CMIP5 website and Climate Research Unit (CRU) monthly datasets. The observed point station datasets cover Kenya, Uganda and Tanzania all making a total of 14 stations considered in the study within the Lake Victoria basin. All the datasets were spanning from 1971 to 2005 (35years) for historical records and 2006- 2100 for future projections.

4.1.1 In-situ Observations

The in-situ data including observed monthly station rainfall datasets for various National Meteorological Services of regional institutions were obtained from the respective meteorological headquarters and were picked based on the rainfall homogenous zones. The climatic homogeneous zones adopted in the study were developed by the IGAD Climate Prediction and Applications Centre (ICPAC), (Mutua *et al.*, 1999).

Figures 2- 4 indicate the stations and homogeneous zones used for March to May (MAM), June to August (JJA) and October to December (OND) respectively. Figure 5 shows the distribution of the selected stations over the area of study. Table 3 shows the latitude-longitude locations and altitude of the various stations that were considered in the study.

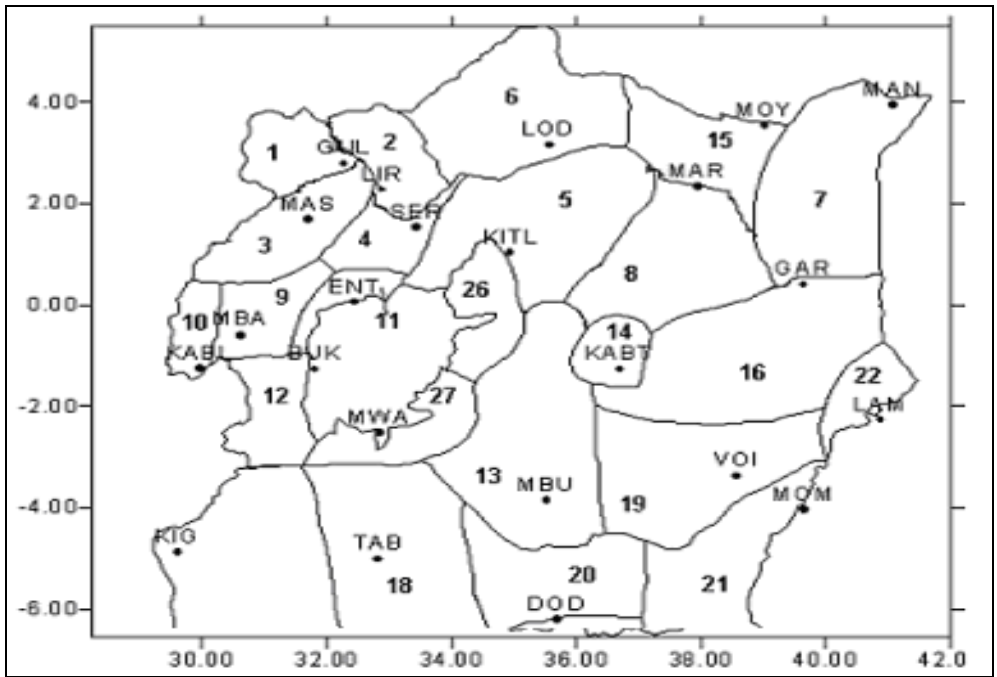


Figure 2: Homogeneous climatic zones for the March-May rainfall season over the LVB (Mutua et al., 1999.)

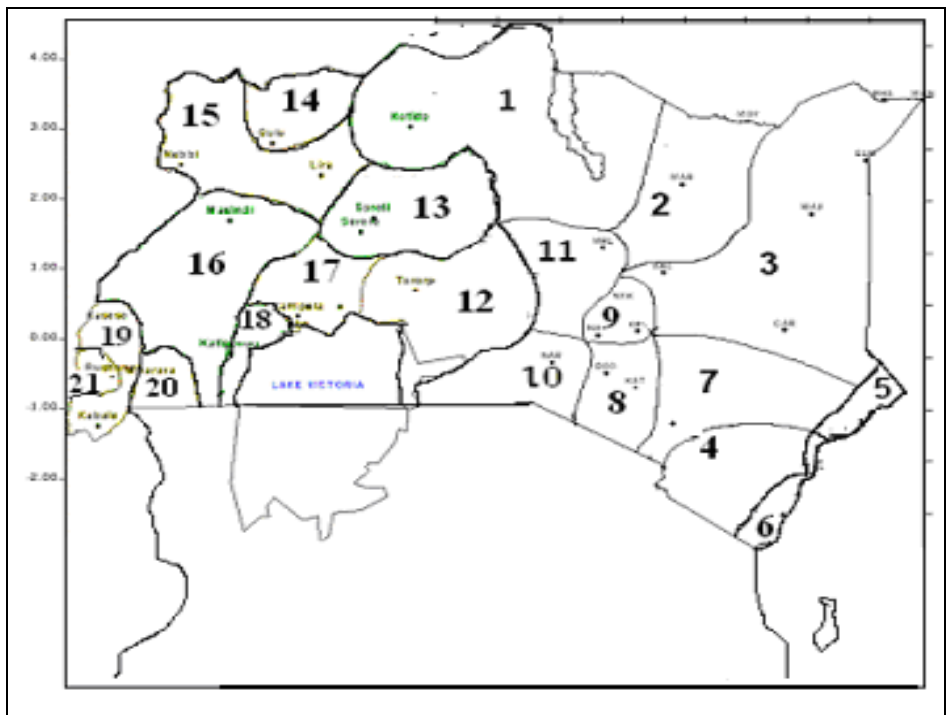


Figure 3: Homogeneous climatic zones for the June- August rainfall season over the LVB (Mutua et al., 1999.)

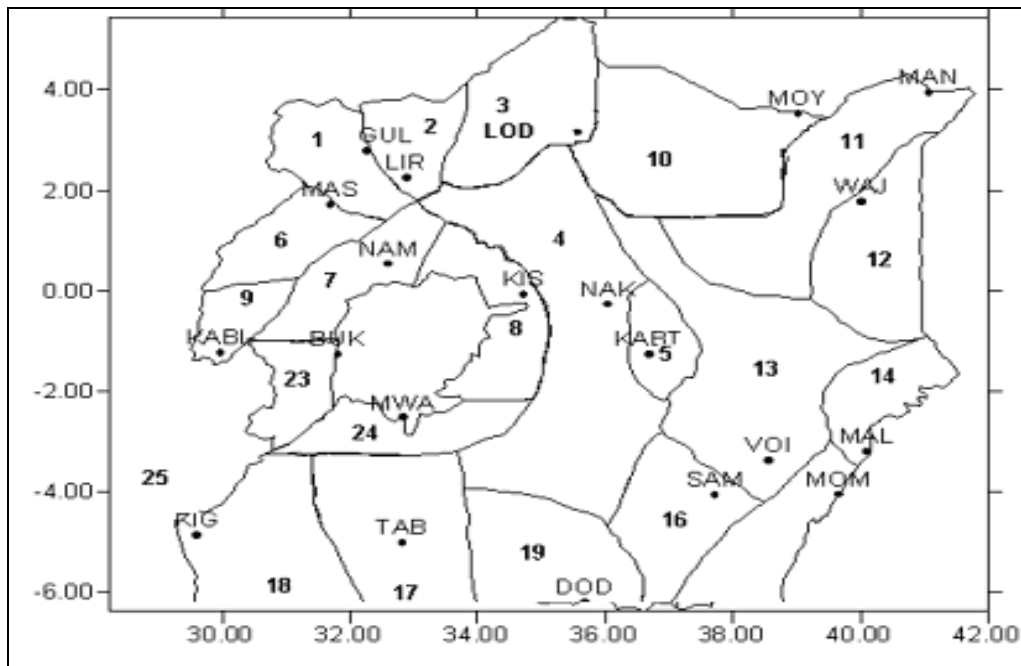


Figure 4: Homogeneous climatic zones for the October-December rainfall season over the LVB (Mutua et al., 1999.)

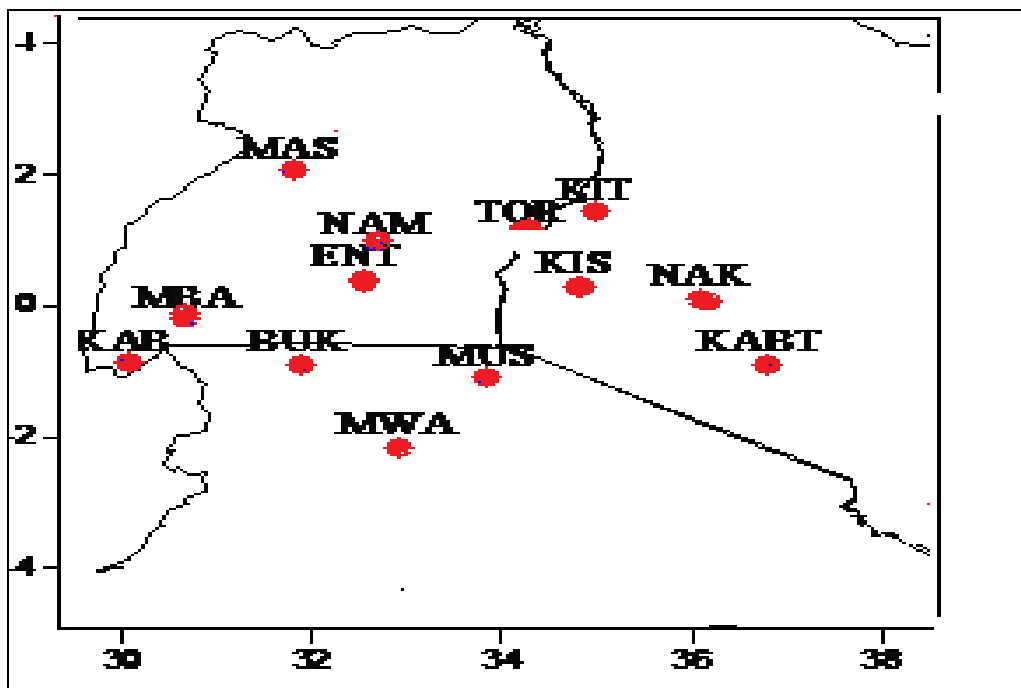


Figure 5: Station codes and their locations as used in the study (Sabiiti, 2008)

Table 3: Station's latitude-longitude in (degrees), altitude (m) and their codes

STATION	CODE	LONGITUDE	LATITUDE	ALTITUDE (M) ABOVE MSL
BUKOBA	BUK	31.82	-1.27	1150
ENTEbbe	ENT	32.45	0.05	1200
KABETE	KABT	36.7	-1.27	1180
KABALE	KAB	29.98	-1.25	1870
KISUMU	KIS	34.73	-0.07	1200
KITALE	KIT	34.95	1.03	1900
MASINDI	MAS	32.9	2.25	1140
MBARARA	MBA	30.63	-0.6	1399
MUSOMA	MUS	33.8	-1.5	1148
MWANZA	MWA	32.85	-2.53	1144
NAKURU	NAK	36.05	-0.27	1848
NAMULONGE	NAM	32.62	0.53	1167
SOROTI	SOR	33.62	1.72	1073
TORORO	TOR	34.17	0.72	1171

4.1.2 Model Hindcast Datasets from Coupled Model Inter-comparison Project 5 Centers

The model hindcast rainfall datasets will be obtained from individual CMIP5 centers. The datasets are at a horizontal resolution of 50 km. For the part of historical assessment, the datasets were spanning from 1970 to 2005 for historical and 2006-2100 for the future scenarios considering RCP 4.5 and RCP 8.5.

4.2 Data Quality Control

In order to make valid inference from the analysis of the observed data, it is necessary to ascertain its quality. Errors in the datasets arise from instrumentation errors, station conditions, observational and recording procedures, transmission, coding and decoding, and during data processing. Data quality control refers to careful scrutiny of the completeness and consistency of the climate data records over an area. Therefore, the data quality was examined before being used in the analysis in order to remove any errors inherent in the data. The method of estimation of missing rainfall data and temporal consistency check described Section 4.2.1 was used.

4.2.1 Estimation of Missing Rainfall Data

Several methods are available in literature for estimating missing data. These include simple long-term average, correlation, isopleths or Thiessen polygon methods.

In this study missing data values were estimated using long-term average and correlation methods based on the cross-correlation between the nearest rainfall stations to the one with missing value and the ratio of the climatological values of rainfall over the stations. The missing records in station data were estimated using the relation given by the WMO (1986) in Equation (1).

$$X_m = \frac{X_n - \bar{X}_m}{\bar{X}_n} \dots\dots\dots (1)$$

In Equation (1) X_m is the estimated rainfall for the month at a station, X_n is the observed rainfall for the month at the neighboring station, \bar{X}_n is the average rainfall of the neighboring station, \bar{X}_m is the average rainfall of the station with missing data which is highly correlated with the station, m and n are the length of the records for the station with missing data and the neighboring station. To fill in the missing data, a station with the highest cross-correlation to the one with missing data was used.

Under the temporal consistency check, the mass curve analysis techniques were used. Under this technique, the observed values were compared to the preceding ones. The method was also used to detect omissions in sequential records.

4.3 Methodology

This section presents methods that were used to achieve various specific objectives listed above.

4.3.1 Trend Analysis

Analysis of trends of data in time series will be carried out using several methods. These will include graphical and statistical methods (Ogallo 1980, 1981). The Graphical method involves plotting of smoothed and unsmoothed times series. The time series will be smoothed using 5 running average filter. Under statistical method a linear polynomial function was fitted and significance of slope tested using the Equation 2 of the form

$$y_t = a + b_i x_t \dots\dots\dots (2)$$

Trend is significant when b is significant based on T- test.

4.3.2 Standardized Anomaly Indices

The amount of rainfall varies significantly from one location to another. It is therefore necessary to standardize rainfall values at the specific location before any comparisons can be made between the two locations. Many methods have been used to standardize time series observations. The two most common parameters that have been used in normalizing time series observations are the mean and the variance.

Various indices have been used to assess rainfall anomaly in East Africa. Studies in the region that have used such indices include the standardized rainfall anomaly index (Ogallo and Nassib, 1984) and weighted rainfall anomaly index (Ininda, 1995 a). The standardized rainfall anomaly was adopted in this study for fair comparison of model simulated and observed records. The standardized anomaly, z, was computed using Equation (3)

$$z = \frac{X - \bar{X}}{S_x} \dots\dots\dots(3)$$

In Equation 3, X is the observed data, \bar{X} is the mean of the data and S_x is the standard deviation of the data set. The value of z provides immediate information about the significance of a particular deviation from the mean (Nyenzi, 1988).

4.3.3 Downscaling of CMIP5 Ensemble model outputs

In this study, the primary downscaling technique considered for downscaling CMIP5 outputs was empirical statistical downscaling technique-

Empirical statistical downscaling is based on the development of mathematical transfer functions or relationships between observed large-scale precipitation and the observed surface precipitation. The transfer function is generally regression-based and is derived between a set of atmospheric grid scale predictors, output from both reanalysis projects and CMIP5, and a single predictand. However, the use of statistical downscaling requires a

number of assumptions, the most fundamental of which is that the derived relationships between the observed predictor and predictand will remain constant under conditions of climate change and that the relationships are 'time-invariant' (Maraun *et al.*, 2010).

This was determined in terms of multivariate linear regression of the form given by Equation (4)

$$y_i = a_o + \sum_{i=1}^n b_i x_i + e_i \dots\dots\dots (4)$$

In Equation 4, a_o and b_i are the intercept and regression coefficients for the predictors x_i applied in the Equation and e_i is the multivariate error term. In this study, the predictors were the model outputs.

Principal Components Regression (PCR) was employed with gridded predictors, to recalibrates large-scale CMIP5 fields to the observed smaller spatial scale observed precipitation using regression analyses in which the predictand was observed rainfall over a region (P). PCR does not only relates large-scale climatic information to the smaller spatial scale variable of interest, but also eliminates systematic errors and biases in CMIP5 fields by regressing with the predictand fields. Expressing PCR in Equation 5

$$\ln(P_t) = \beta_0 + \sum_{k=1}^k \beta_k + PC_{k,t} \dots\dots\dots (5)$$

In Equation 5, P_t is the seasonal rainfall in year 't', $PC_{k,t}$ is the k^{th} Principal Components (PCs) from the retained k PCs of precipitation forecast, β denote the regression coefficients obtained by minimizing the sum of squares of error. We considered the logarithm of the rainfall as predictand to eliminate the possibility of estimating negative flows. To select 'K' PCs from the predictor set (gridded precipitation forecasts). Step-wise regression was employed since it maximizes the correlation between the observed rainfall and predicted rainfall for the chosen validation scheme.

4.3.4 Model output verification methods

Determination of the skill of the downscaled model outputs during the climatological period were investigated through the verification of model outputs using simple correlation analysis, analysis of errors, linear regression analysis and graphical displays.

4.3.4.1 Graphical Displays

The method of graphical display is the simplest way of comparing the relationship between variables. This method was used to provide visual comparison between the trends of CRU and model outputs. Such a method however is subjective and provides only qualitative comparison, and may be biased by the scales of the various datasets used and needs to be supplemented by other methods described in respective Sections.

4.3.4.2 Analysis of error in simulated outputs

Error analysis was used to determine the Root Mean Square Error (RMSE) in the simulated model outputs. The Root Mean Square Error (RMSE) was computed as in Equation 6

$$RMSE = \sqrt{\frac{\sum_{i=1}^N (M_i - O_i)^2}{N}} \dots\dots\dots (6)$$

In Equation 6, M_i and O_i are the model simulated and observed values respectively. N is the length of the records.

4.3.4.3 Correlation Analysis

Correlation analysis was done between the CRU rainfall data and the model data to determine stations that strongly correlate with the CMIP5 outputs. The correlation coefficient (r) between a model output variable (f_i) and the corresponding observation (O_i) is given by Equation 7

$$r = \frac{\frac{1}{N} \sum_{i=1}^N (M_i - \bar{M})(o_i - \bar{o})}{\left[\frac{1}{N} \sum_{i=1}^N (M_i - \bar{M})^2 \cdot \frac{1}{N} \sum_{i=1}^N (o_i - \bar{o})^2 \right]^{1/2}} \dots\dots\dots (7)$$

In Equation 7, N is the total number of years used for analysis, \bar{f} is the mean of the model output and \bar{O} is the mean observation of the observed variable. The correlation ranges from -1 to 1 where a value of 1 denotes perfect linear relationship and -1 denotes a perfect inverse linear relationship.

The computed value of correlation coefficient between observed and model output was tested using the student t-test. The test significance level considered was 95% level of significance. If the computed value of t is greater than the tabulated value, then the correlation coefficient was significant. The t-test for correlation coefficient is given by Equation 8:

$$t_{n-2} = r \sqrt{\frac{(n-2)}{1-r^2}} \dots\dots\dots (8)$$

In Equation 8, n is the total number of years used in the study; $n - 2$ is the degrees of freedom, t_{n-2} is the value of the confidence level computed from the correlation coefficient and r is the correlation coefficient. If the computed value of t is greater than the tabulated value of t_{n-2} , then the correlation coefficient is significant.

4.3.4.4 Multiple Linear Regression

Once the correlation between variables is established, it is usually important to determine the nature of the relationship between the correlating variables. Regression analysis helps determine linear relationships between variables. In this study regression analysis was done using Equation 9.

$$y_i = a_o + \sum_{i=1}^n b_i x_i + e_i \dots\dots\dots (9)$$

In Equation 9, a_o and b_i are the intercept and regression coefficients for the predictors x_i applied in the Equation. In this study, the predictors were the model outputs. The variance of the error term e_i , in this case is given by Equation 10.

$$S^2 = \frac{SSE}{n - (k + 1)} \dots\dots\dots (10)$$

In Equation 10, SSE is the sum of the square of errors, n is the period of time considered for the study.

The test of the adequacy of the model was done by computing R^2 (the multiple coefficient of determination) given by Equation 11.

$$R^2 = 1 - \frac{SSE}{\sum_{i=1}^n (y_i - \bar{y})^2} \dots\dots\dots (11)$$

In Equation 11, y_i is the model output and \bar{y} is the mean of the model output. For a perfect model the value of R^2 should be 100%. For $R^2 = 0$, it implies lack of fit, while $R^2 = 1$ implies perfect fit. Regression analysis in this study was used to determine the linear relationship between the model outputs and seasonal rainfall anomalies for the 14 rainfall stations used in

the study. The stepwise regression technique was used as a means of picking the best individual predictor into the regression model equation.

4.3.5 Categorical Statistics

Categorical statistics was used to analyze the relationship of model output and the observed rainfall values. A 3 x 3 contingency table was used to display the data.

Table 3 gives the basic structure and entries from categorical analysis from which some skill score was evaluated. The letters in the Table were used to calculate the various scores. Below Normal (BN), Normal (N) and Above Normal (AN) categories were used to indicate the rainfall that was observed and predicted. Letters A-I denote the values obtained at different categories for the predicted and observed events. Letters J-O show the totals of the events observed at different categories, and letter T is the total number of events carried out.

Table 4: A 3 * 3 contingency Table

	FORECAST			TOTAL	
OBSERVED		BELOW NORMAL	NORMAL	ABOVE NORMAL	
	BELOW NORMAL	A	B	C	M
	NORMAL	D	E	F	N
	ABOVE NORMAL	G	H	I	O
TOTAL		J	K	L	T

4.3.5.1 Bias Score

The bias score measures the ratio of the frequency of forecast rainfall events to the frequency of observed rainfall events. It indicates whether the forecast system has a tendency to under forecast (Bias<1) or over forecast (Bias>1) rainfall events. It ranges from 0 to ∞ the perfect score is 1 (100%). The Bias score will be calculated using Equation 12 generated from Table 4.

$$Bias = \left\{ \begin{array}{l} \frac{J}{M} \quad BN \\ \frac{L}{O} \quad AN \\ \frac{K}{N} \quad N \end{array} \right\} \dots\dots\dots (12)$$

4.3.5.2 Probability of Detection

The Probability of Detection (PoD) gives a simple measure of proportion of rainfall events successfully forecasted by the model. It is calculated by dividing the total number of correct forecasts by total number of events observed. PoD ranges from 0 to 1 where a perfect score is 1 (100%). Equation 5, gives the formula for computing the PoD for below normal, normal and above normal categories with the letters have their meanings as defined in Subsection 4.3.5.

$$PoD = \left\{ \begin{array}{l} 100 * \frac{A}{M} \quad BN \\ 100 * \frac{I}{O} \quad AN \\ 100 * \frac{E}{N} \quad N \end{array} \right\} \dots\dots\dots (13)$$

4.3.5.3 False Alarm Ratio

The FAR gives a simple proportional measure of the model’s tendency to forecast above normal rainfall where the rainfall is below normal. The score ranges from 0 to 1 (100%), the perfect score is 0. The FAR for the below and above normal categories will be given by Equation 14 with the letters having their meanings defined Subsection 4.3.5.

$$FAR = \left\{ \begin{array}{l} 100 - 100 * \frac{A}{J} \quad BN \\ 100 - 100 * \frac{I}{L} \quad AN \end{array} \right\} \dots\dots\dots (14)$$

4.3.5.4 Heidke Skill Score

The Heidke Skill Score (HSS) measures the fraction of correct forecasts after eliminating those forecasts which would be correct due to purely random chance. The numerator is the number of correct forecasts, and the reference forecast in this case is the rainfall events experienced by a given geographical location (Climatology). The score ranges from $-\infty$ to 1,

the perfect score is 1 (100%). Any score less than zero means the model is worse off than climatology. The HSS for this study will be computed using Equation 15. The meanings of the letters in Equation 15 are defined in Subsection 4.3.5.

$$\text{HSS} = \frac{A + E + I - \frac{JM + KN + LO}{T}}{T - \frac{JM + KN + LO}{T}} \dots\dots\dots (15)$$

CHAPTER FIVE

5.0 RESULTS AND DISCUSSIONS

5.1 Result from Quality Control

The missing data of stations with less than 10% of records missing were estimated, while those which had more than 10% of missing records were omitted from the study. The rainfall data that were estimated in the study are summarized in Table 5

Table 5: Estimation of Missing Data for stations with less than 10% of missing records over the LVB

Station	Years with Missing Data	Months with Missing Data
Mbarara	1973, 1974, 1985	Jan, Feb, Mar
	1990	Aug, Dec
	1992	Dec
	1994	Dec
Kabale	1973, 1974, 1985	Jul, Aug, Sept, Nov, Dec
	1990	Aug, Sept, Oct, Nov, Dec
Namulonge	2003	Sept, Oct, Nov, Dec
	2004	Nov
Kitale	1994	May
	2004	Dec
Musoma	2004	Dec

5.1.1 Result from Homogeneity Test

The single mass curve homogeneity test was applied to the data. The Figure 6 shows some of the examples of results obtained from the homogeneity test for the observed rainfall. All the

mass curves were almost linear, signifying that the rainfall records were homogeneous. The data was therefore considered homogeneous and hence suitable for use in the study.

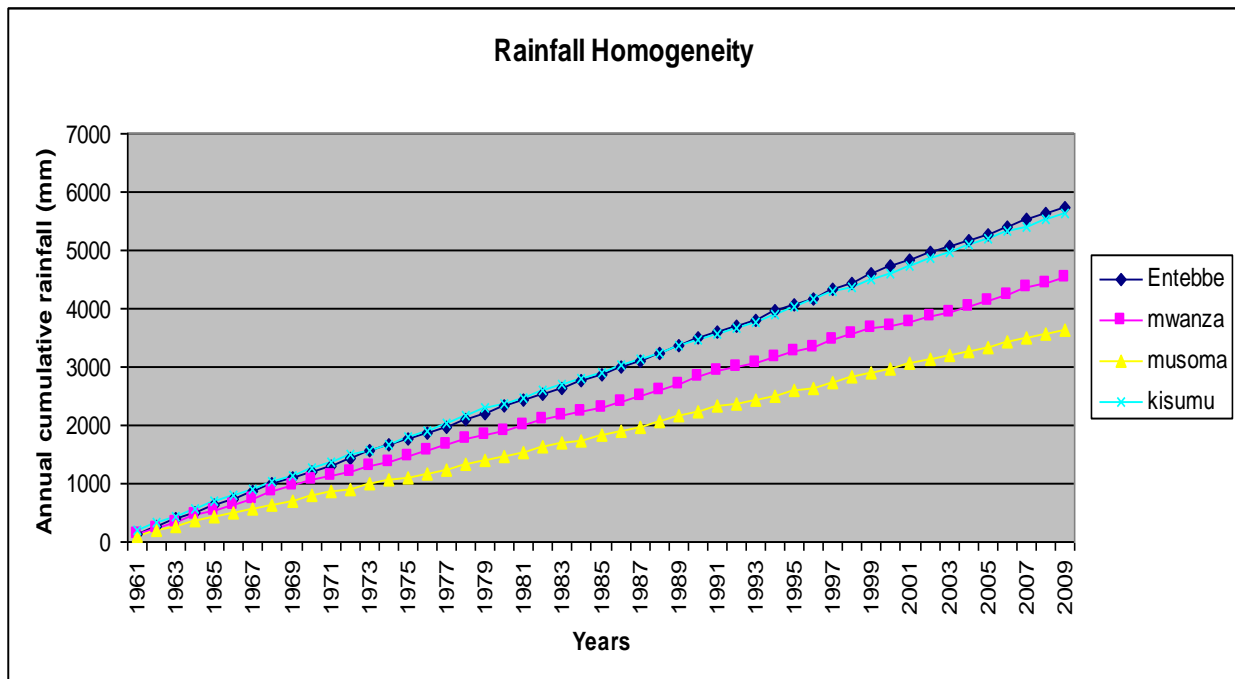


Figure 6: Mass curve to test the homogeneity of the annual observed rainfall records for the period 1961-2009

5.1.2 Results from Evaluation of CRU datasets against station

The choice of CRU datasets for this study was based on the fact that CRU data strongly correlates with the observed rainfall station data during the MAM and OND seasons over the LVB. Figures 7 and 8 show the inter-annual variability of CRU and observed rainfall datasets for representative stations of the LVB, i.e., Mwanza, Kisumu and Entebbe stations. From Figure 7 it can be noticed that CRU datasets picked most of the station extremes with significant correlations of 0.82, 0.44 and 0.30 respectively and from Figure 8, the significant correlations of 0.61, 0.74 and -0.30 respectively. However the highest correlation explained only 51% and less in accuracy of the datasets over these stations, hence subsequent results in the study used CRU for the analyses.

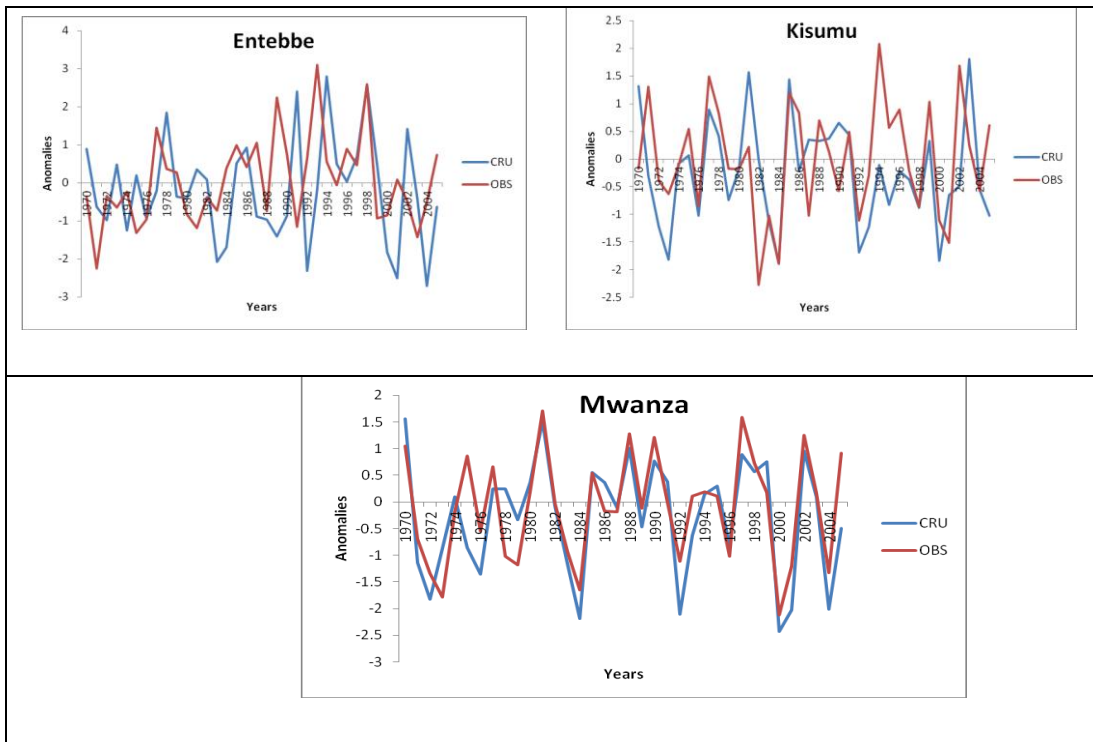


Figure 7: Inter-annual variability of rainfall output (mm) of CRU (blue shading) and station observations (red shading) over Mwanza, Kisumu and Entebbe for March-May season.

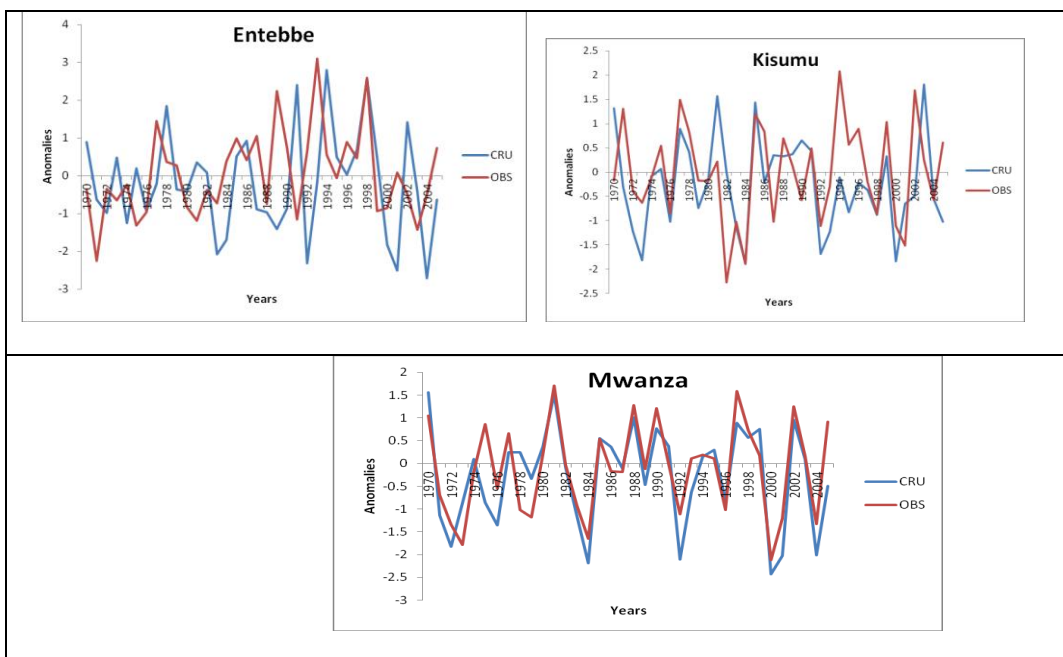


Figure 8: Inter-annual variability of rainfall output (mm) of CRU (blue shading) and station observations (red shading) over Mwanza, Kisumu and Entebbe for October-December season

5.2 Trend Analysis and the Annual Cycle

The trends in rainfall showing the temporal patterns are presented. To examine rainfall trends over the area of study, climatic homogeneous zones over the region were used. Each of the two main rain seasons was considered using the representative stations for each of the rainfall homogeneous zones. The observed annual cycle of rainfall as well as the seasonal trends of the three seasons: MAM, JJA and OND were plotted and the results are in the respective Subsections 5.2.1, 5.2.2, 5.2.3 and 5.2.4 respectively.

5.2.1 Observed and Model Annual Cycles of Rainfall

Figure 9 represents the plotted rainfall cycle for observed rainfall and MPI, CNRM, MIROC and EC-EARTH models over the area of study. It can be seen that over the LVB, there are two major rainfall seasons occurring between March–May (MAM) with its peak in April and October–December (OND) with a peak occurring in November

The months of June–August (JJA) are relatively dry. The observed rainfall pattern over this region can be alluded to the systems discussed earlier in Section 1.7. The models were able to simulate the observed annual cycle of bimodal rainfall with peaks in April and November respectively. However, during the March-May season, the MPI, CNRM and EC-EARTH had their peaks in May except for the MIROC model which had a peak in April. During the OND season, the entire represented model had a peak rainfall in the in October except for the MIROC model whose peak was in September.

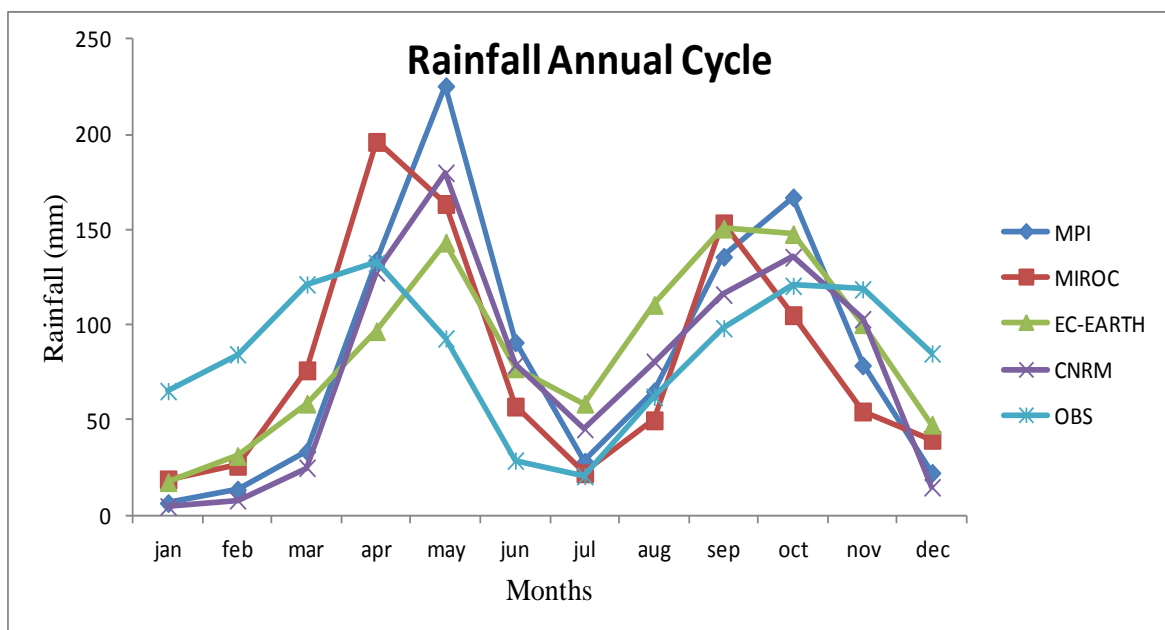


Figure 9: Rainfall annual cycle for observed (Cyan), MPI (Blue), MIROC (Red), EC-EARTH (Green) and CRNRM (Purple) models for the years 1971-2005 over the LVB

5.2.2 Observed March-May Rainfall Trends

Figures 10, 11 and 12 show observed March-May rainfall trends over Kisumu, Mwanza and Mbarara. Following the March–May (MAM) homogeneous climatic zones over the area of study, outlined in Figure 2, seasonal rainfall from Kisumu, Mwanza and Mbarara was used to examine the trends in MAM season rainfall over the LVB. The results for three stations in Figures 10, 11 and 12 indicated, Mwanza in the northern part of Tanzania, and Kisumu in the southwestern part of Kenya, are experiencing decreasing rainfall trends. The results in Figure 12 show an increasing rainfall trend over Mbarara station. However, the test for the significance of the trend indicated that Kisumu and Mwanza had insignificant decreasing trend whereas, Mbarara had an insignificantly increasing trend as shown in Table 6.

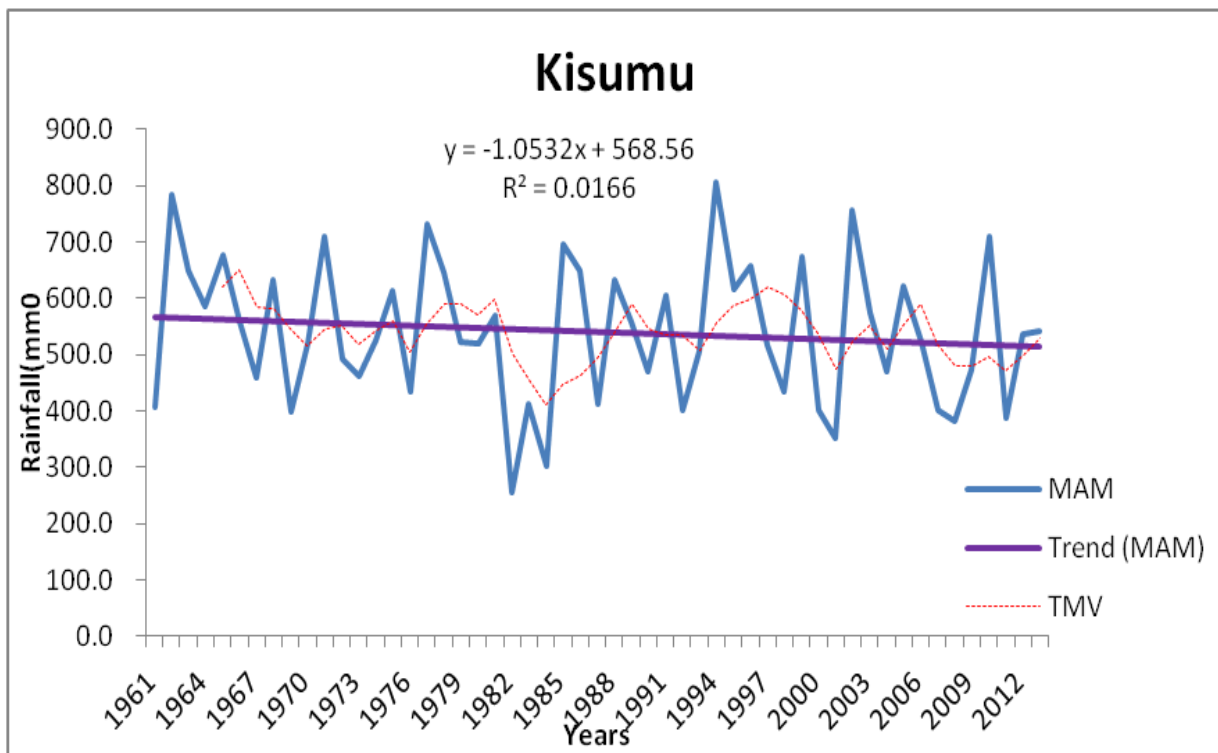


Figure 10: : Observed March-May seasonal rainfall time series (blue), trend line (purple) and 5 year moving average (red) for Kisumu for 1961-2013.

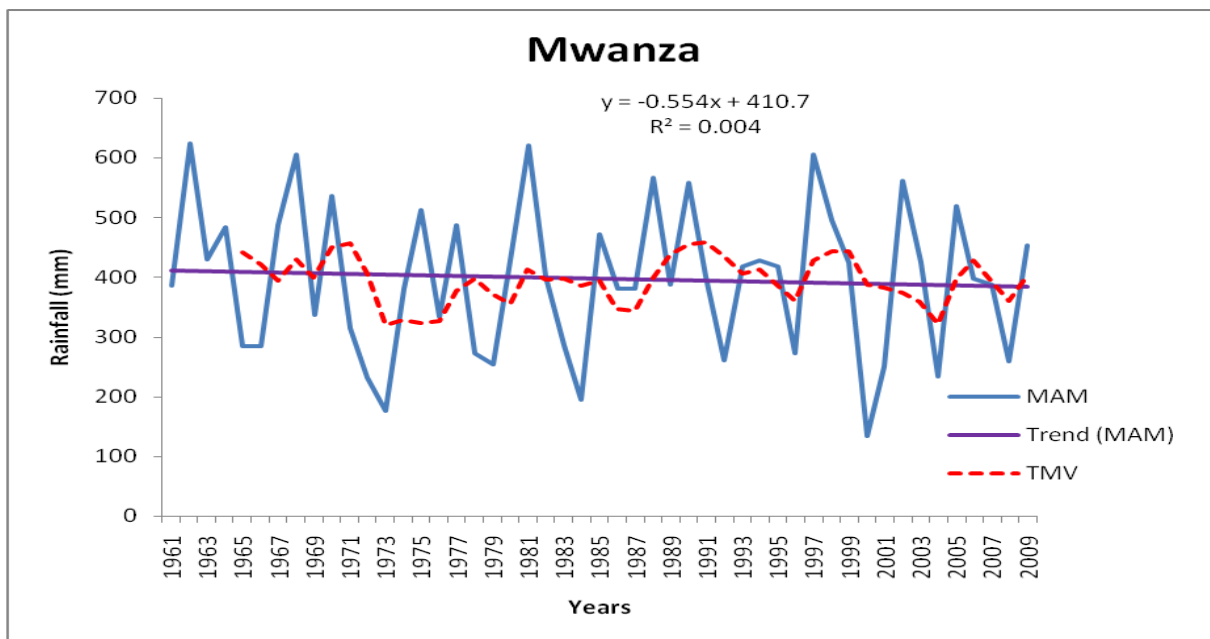


Figure 11: Observed March-May seasonal rainfall time series (blue), trend line (purple) and a 5 year moving average (red) for Mwanza for 1961-2009.

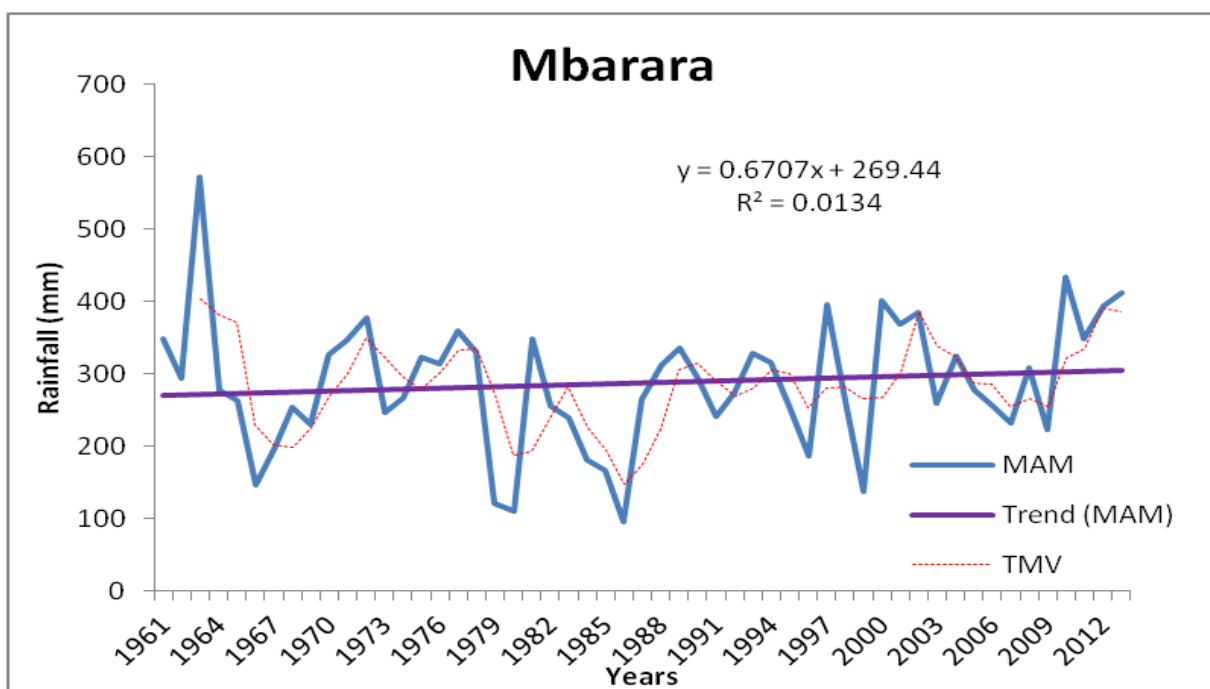


Figure 12: Observed March-May seasonal rainfall time series (red), trend line (purple) and a 5 year moving average (red) for Mbarara for 1961-2013.

5.2.3 Observed June-August Rainfall Trends

The trends in June-August rainfall are presented in Figures 13-14. The results for Mbarara indicate increasing trend while Kabale indicate decreasing trend in rainfall during this season. Mbarara, which is situated North-South of the LVB had a significant increasing slope while Kabale had an insignificant decreasing slope.

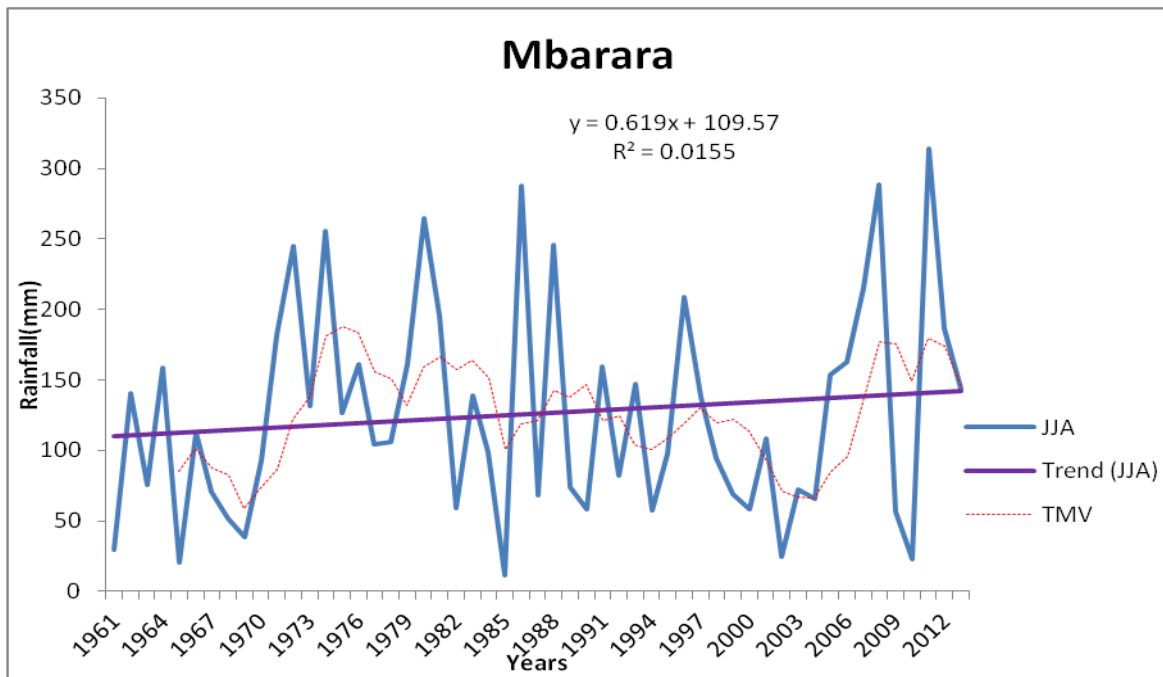


Figure 13: Observed June-July seasonal rainfall time series (blue), trend line (purple) and a 5 year moving average (red) for Mbarara for 1961-2013

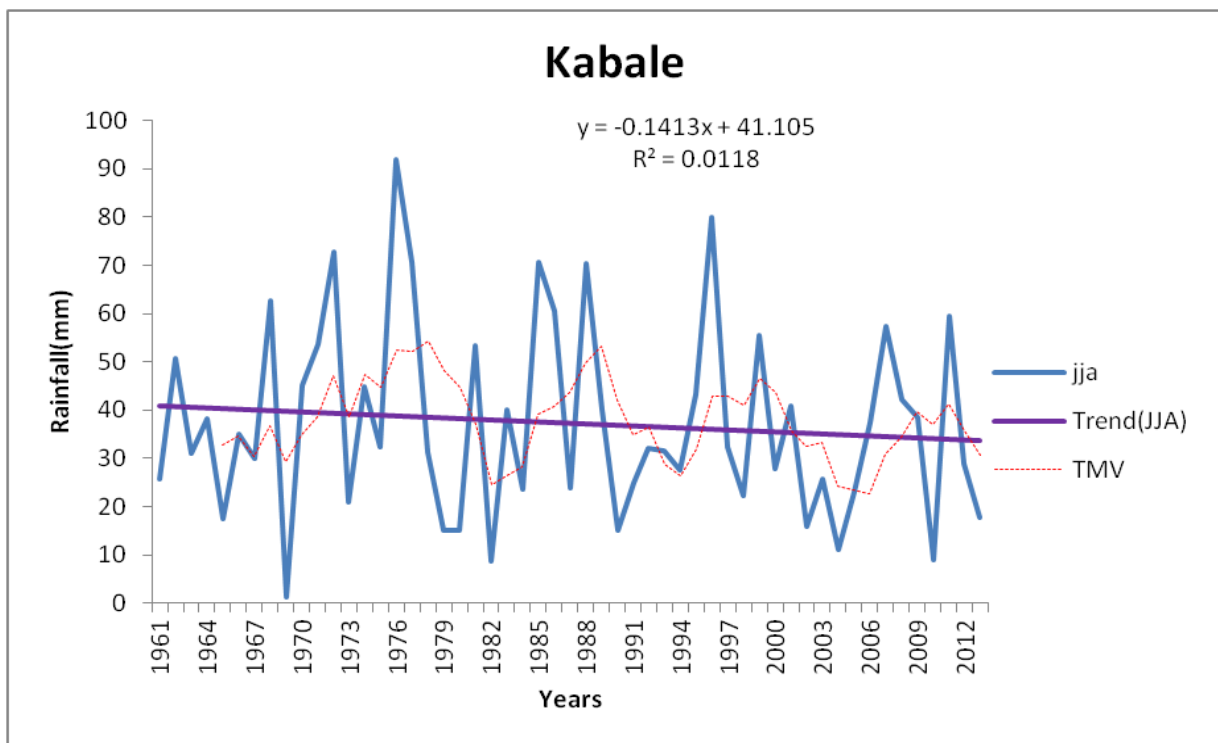


Figure 14: Observed June-July seasonal rainfall time series (blue), trend line (purple) and a 5 year moving average (red) for Kabale for 1961-2013.

5.2.4 Observed October-December rainfall trends

Figures 15 and 16 show the rainfall trends in the October–December (OND) season over the area of study basing on the representative stations from OND homogeneous climatic zones

(Figure 4) were used. The stations considered here included Bukoba and Mwanza. The seasonal rainfall trends for Mwanza (Figure 15) and Bukoba (Figure 16) were analyzed. The results for Bukoba and Mwanza show insignificantly decreasing trends during the OND season. This implies some evidence of rainfall variability over the region of study.

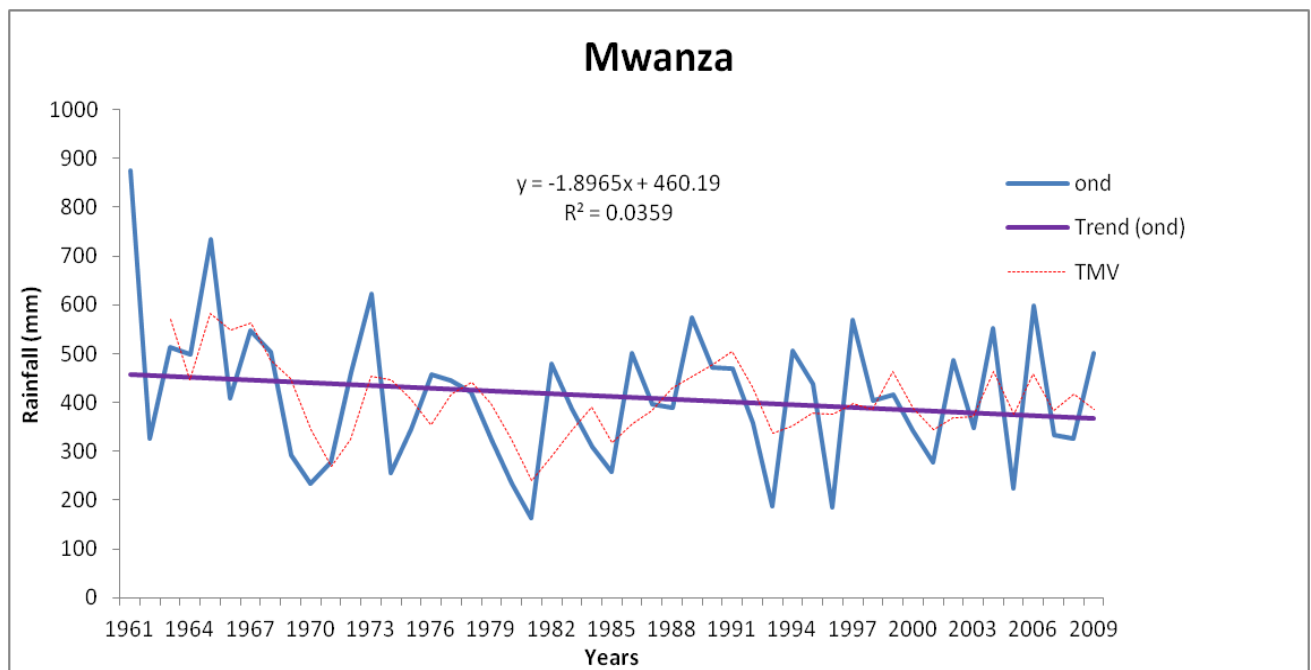


Figure 15: Observed October- December seasonal rainfall time series (blue), trend line (purple) and a 5 year moving average (red) for Mwanza for 1961-2009

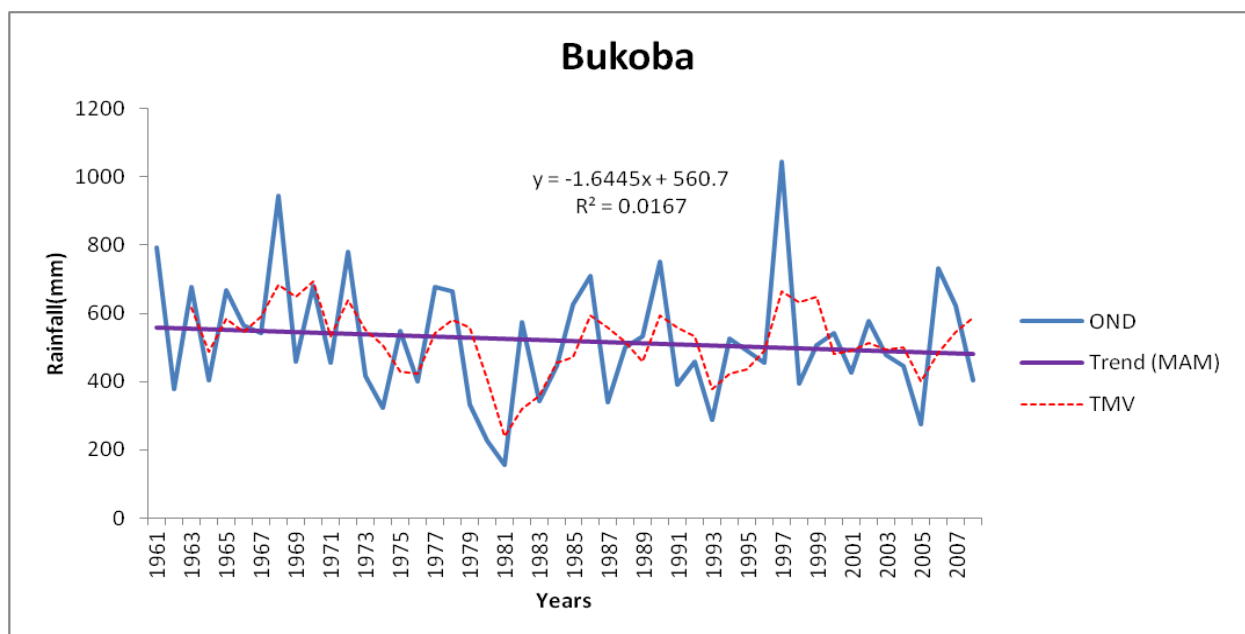


Figure 16: Observed October- December seasonal rainfall time series (blue), trend line (purple) and 5 year moving average (red) for Bukoba for 1961-2009

The Table 6 summarizes the stations considered for each season and their respective p-value.

Table 6: Stations Considered for each season and their respective P-value

March-May Season	
Station	P-value
Kisumu	0.066
Mwanza	0.38
Mbarara	0.32
July-August Season	
Mbarara	0.042
Kabale	0.057
October-December Season	
Mwanza	0.073
Bukoba	0.061

5.3 Evaluating the Best Performing Models

In order to select the models that were performing better in terms of skill over the LVB, error analysis, correlation analysis and categorical statistics were carried out. These are discussed in the Subsections 5.3.1, .5.3.2 and 5.3.3.

Figure 17 shows the sub-domains that were considered in the study for ease of application of model simulated outputs.

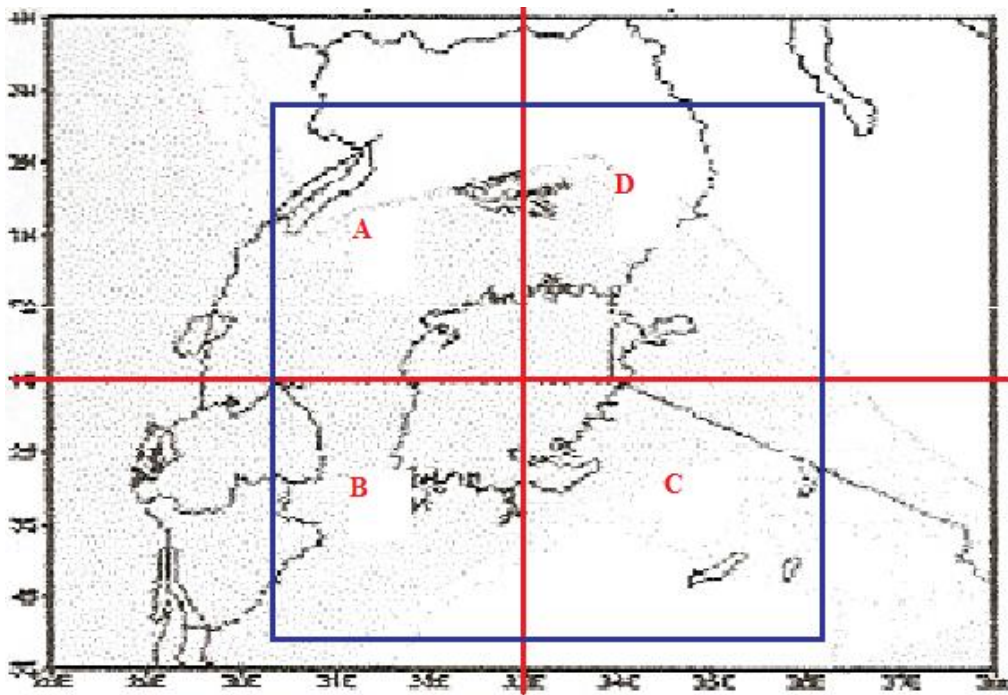


Figure 17: Sub -domains (A, B, C and D) for application of the Model simulated outputs over the LVB.

5.3.1 Results from error analysis

The study examined the errors between the seasonal model outputs and the CRU seasonal rainfall for the seasons within the year. The Root Mean Square Errors (RMSE) shown in Table 7 were analyzed for the sub-domains representative stations shown in Figure 17. The results from error analysis indicated that most of the models had larger errors during the MAM season and decrease during the OND season. This implies that the model performances in simulating the observations are fairly better over some parts of the region during the OND season as compared to the MAM season.

5.3.1.1 Analysis of the Root Mean Square Errors (RMSE)

The results in Table 7 show the values of the root mean square errors computed using Equation (6) in Section 4.2.4.2 over the sub-domains A, B, C and D indicated in Figure 17. The results show that the models had larger errors during the MAM season and they decrease during the OND season. Shaded values show cases where the errors were fairly large by more than 0.2. The larger errors during MAM season are attributed to poor simulation of the observations during this season. The improvement of the model performance in simulating the observations results to lesser errors during the OND season.

Table 7: Computed Root Mean Square Error (RMSE) between Model outputs and CRU seasonal rainfall records.

Sub-Domain/ season	MAM								OND							
	CCCMA	CNRM	EC-EARTH	GFDL	HadGEM	MIROC	MPI	NorESM	CCCMA	CNRM	EC-EARTH	GFDL	HadGEM	MIROC	MPI	NorESM
A	0.28	0.17	0.22	0.2	0.23	0.18	0.18	0.20	0.19	0.12	0.12	0.18	0.14	0.10	0.14	0.15
B	0.21	0.18	0.41	0.27	0.34	0.11	0.18	0.27	0.32	0.14	0.20	0.23	0.16	0.10	0.15	0.17
C	0.19	0.15	0.18	0.26	0.31	0.12	0.16	0.32	0.19	0.15	0.14	0.26	0.16	0.12	0.14	0.16
D	0.22	0.19	0.34	0.26	0.33	0.15	0.20	0.28	0.21	0.17	0.14	0.27	0.17	0.12	0.16	0.19

5.3.1.2 Root Mean Square Error for March-May Season

Figure 18 shows bar graphs representing the RMSE computed for the individual models over the sub-domains A, B, C and D for March-May season. Across the four sub-domains, EC-EARTH and HadGEM models had the highest RMSE of approximately 0.41 and 0.35 respectively, whereas, MIROC, MPI and CNRM had the lowest RMSE of 0.11, 0.12 and 0.14 respectively, for the period 1971- 2005. However, the errors committed by the individual models during this season were fairly larger by 0.17 and this may be attributed to the poor simulation of the observed rainfall by the global models.

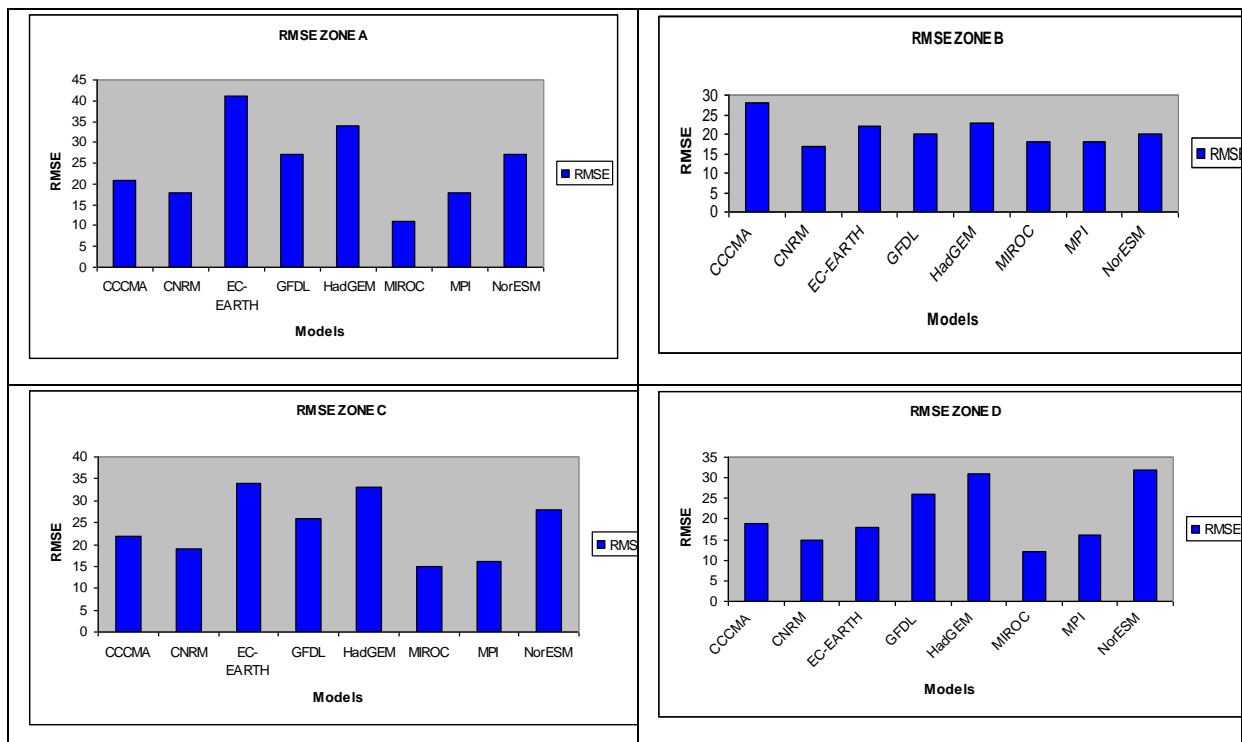


Figure 18: Computed RMSE for individual models for March- May season over the sub-domains A, B, C and D considered in the study for time period 1971- 2005

5.3.1.3 Root Mean Square Error for October-December Season

Figure 19 shows the RMSE computed for the individual models over the sub-domains A, B, C and D for the October-December season. Across the four sub-domains, CCCMA, GFDL and NorESM models had the highest RMSE of 0.31, 0.24 and 0.21 respectively, whereas, MIROC, EC-EARTH and CNRM had the lowest RMSE of 0.11, 0.12 and 0.14 respectively for the time period 1971- 2005. However, during this season the errors were fairly lower than the March-May season by 0.07 and this may be attributed to the improvement in the simulation of the observed rainfall by the global models

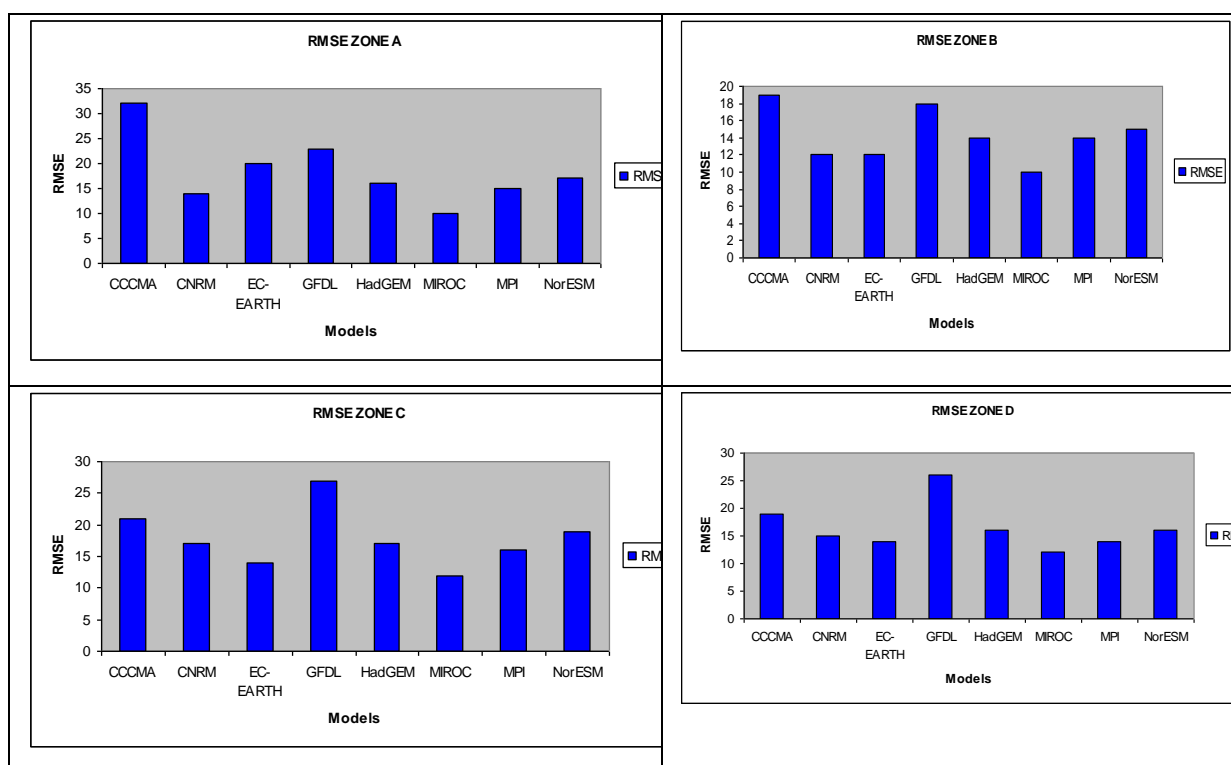


Figure 19: Computed percentage RMSE for individual models for October- December season over the sub-domains A, B, C and D for the time period 1971-2005.

5.3.2 Validation of Model Outputs

The study validated the rainfall outputs from the best models basing on the RMSE as an objective to evaluate model performance over the region. The results from the validation of the model would provide the reliability (confidence) that would be attached to the climate change projection obtained by the CMIP5 Representative Concentration Pathways (RCPs) system over the region.

Model performance was evaluated on the basis of its ability to simulate the annual cycle and the observed temporal patterns of rainfall over the region of study. CRU rainfall data records

at a spatial resolution of $1.5^{\circ} \times 1.2^{\circ}$ were used to aid the comparison of model gridded data with observations over the area of study.

5.3.2.1 Results from the validation of seasonal rainfall Trends

The study evaluated the skill of the CMIP5 models in simulating the observed trends in seasonal rainfall over the region of study. Model-simulated seasonal rainfall outputs were compared with CRU datasets. Some results for the various seasons are presented for the sub-domains over the area of study in the Subsections 5.3.2.1.1 and 5.3.2.1.2.

5.3.2.1.1 March-May Season

Figure 20 shows the graphical display of March-May (MAM) seasonal rainfall as simulated by the some of the individual CMIP5 models obtained from CRU for the period 1970–2005 over the sub-domains A, B, C and D shown in Figure 17. The results indicate that although some of the models underestimate rainfall during this season the observed year to year rainfall trends for the months of March-May are fairly well simulated by the model over sub-domains in the area of study.

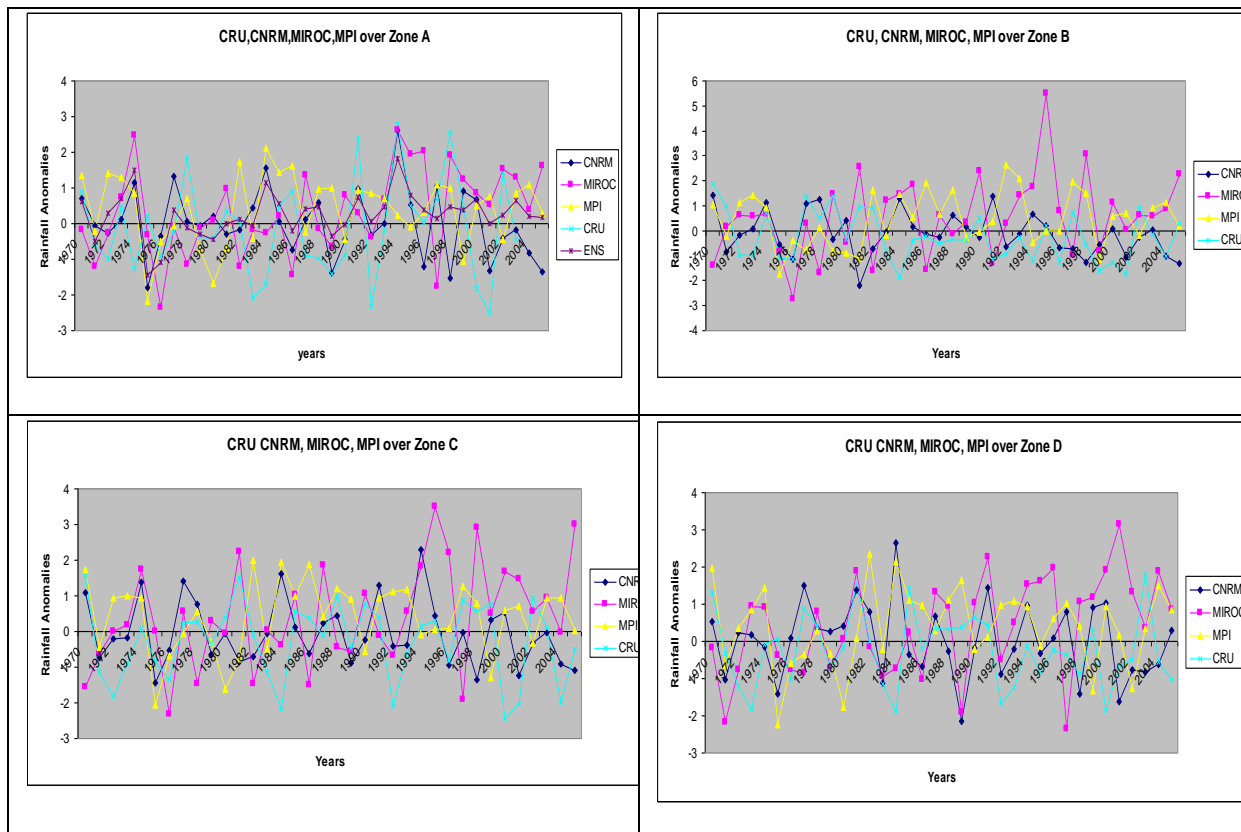


Figure 20: Inter- annual variability of CNRM (blue), MIROC (pink), MPI (yellow) and CRU (cyan) for March-May (MAM) for a period 1971-2005 over the sub domains A, B, C and D

5.3.2.1.2 Ensemble Model Validation for March-May (MAM) Season

Figure 21 shows the graphical display of March-May (MAM) seasonal rainfall as simulated by the ensembles of the best three models, CNRM, MIROC and MPI models based on the RMSE in Table 6, compared with CRU for the period 1970–2005 over the sub-domains A, B, C and D shown in Figure 17. The results indicate that the observed year to year rainfall trends for the months of March-May are fairly well simulated by the model over sub-domains in the area of study as compared to the individual models in Figure 21. An ensemble model output minimizes the errors observed in the individual models (Otieno, 2013). In addition, the model ensemble picked the direction but still underestimated the observed variability.

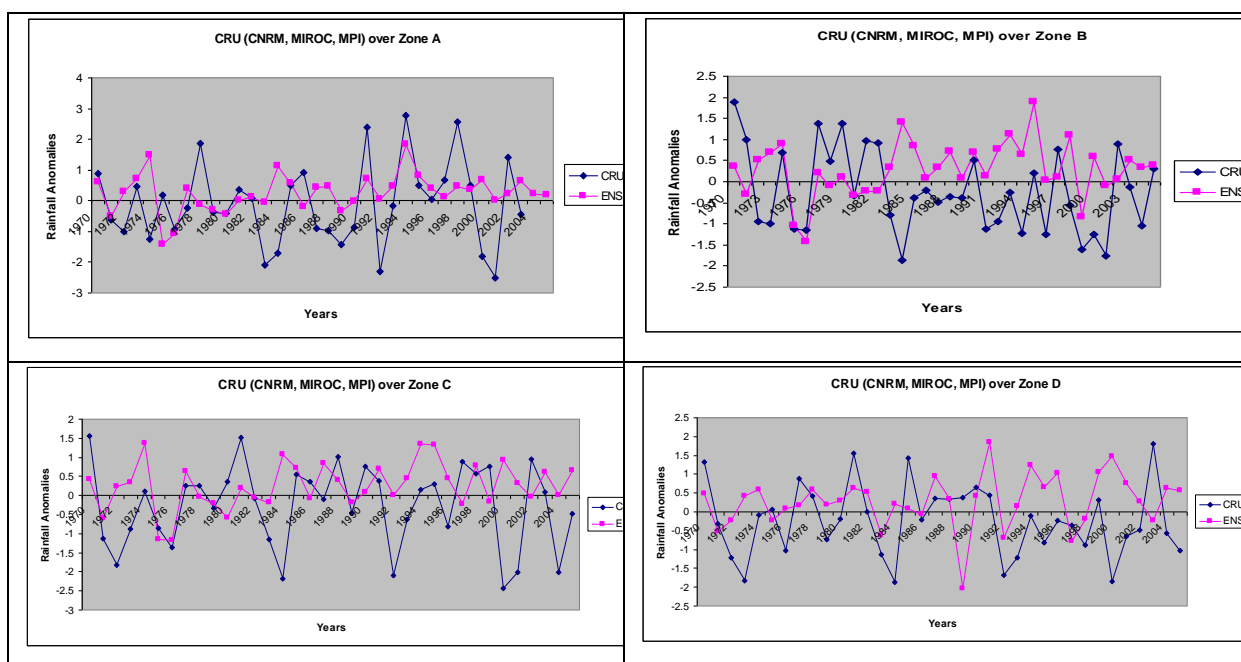


Figure 21: Inter-annual variability of Ensemble (pink) and CRU (blue) for March-May (MAM) for the period 1971-2005 over the sub domains A, B, C and D

5.3.2.1.3 October–December season

Figure 22 graphical display of October- December (OND) seasonal rainfall as simulated by the some of the individual CMIP5 models as compared to CRU for the period 1970–2005 over the sub-domains A, B, C and D shown in Figure 17. The results show individual models fairly simulates rainfall during this season. The year to year rainfall trends for MIROC, CNRM, EC-EARTH and CRU rainfall exhibit reasonable harmony over sub-domain A, B, C, and D in the area of study.

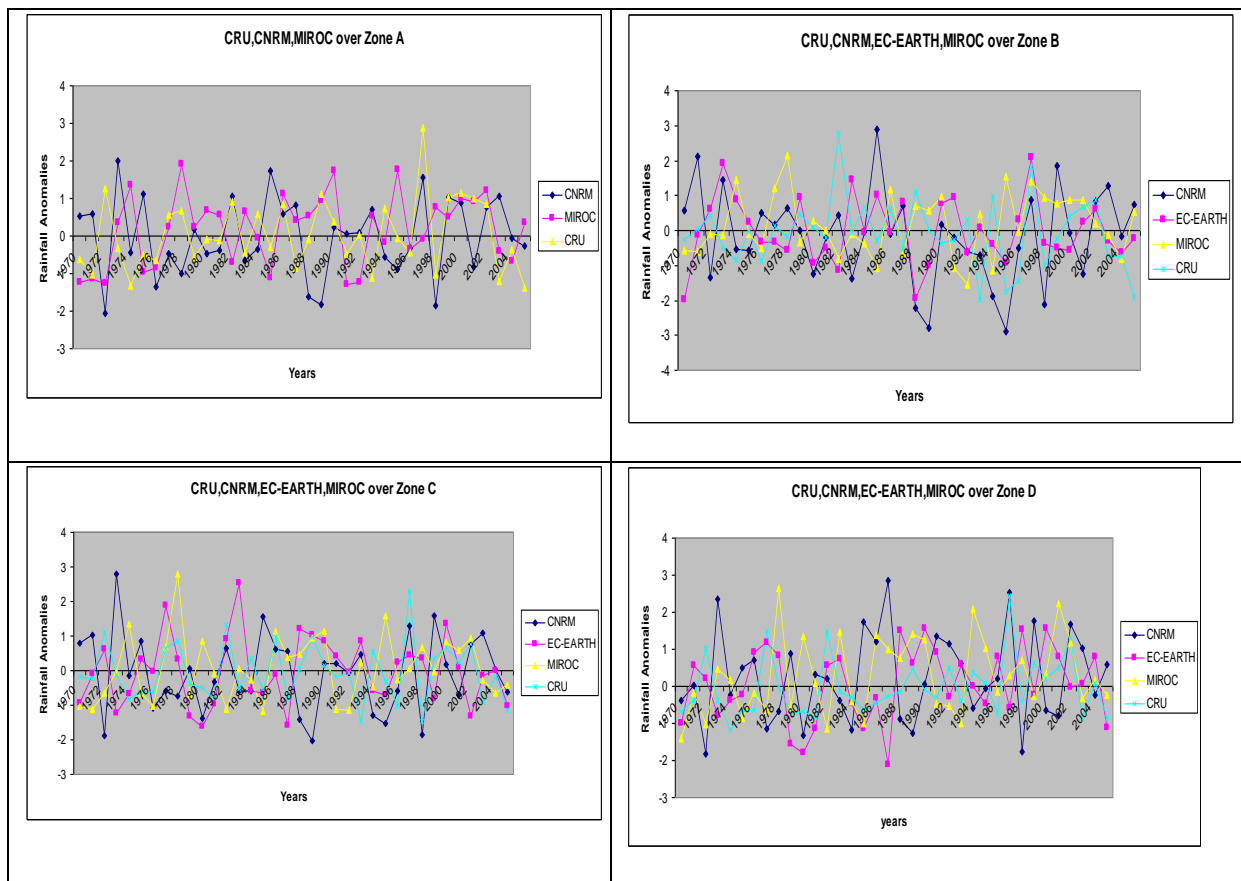


Figure 22: : Inter-annual variability of CNRM (blue), MIROC (pink), MPI (yellow) and CRU (cyan) for October-December (OND) for a period of 1971-2005 over the sub domains A, B, C and D

5.3.2.1.4 Ensemble Model Validation for October-December Season

Figure 23 shows the graphical display of October- December (OND) seasonal rainfall as simulated by the ensembles of the best three models based on the RMSE in Table 6, these models were CNRM, MIROC and EC-EARTH, compared with CRU for the period 1970–2005 over the sub-domains A, B, C and D shown in Figure 17. The results indicate that the observed year to year rainfall trends for the months of October-December are well simulated by the model over sub-domains in the area of study as compared to the individual models in Figure 23. From this it is noted that an ensemble model output minimizes the errors observed in the individual models.

The peaks during the OND season associated with ENSO events were fairly well replicated by the ensemble of these three models i.e., MIROC, EC-EARTH and CNRM over the four sub-domains in the study area. These peaks could be associated with some global tele-connection like ENSO phenomenon which is the main driver during the OND season (Muhati *et al.*, 2007). However a few peaks of the observed rainfall pattern were missed in sub-domain D and this could be due to weak linkage with ENSO conditions in these region.

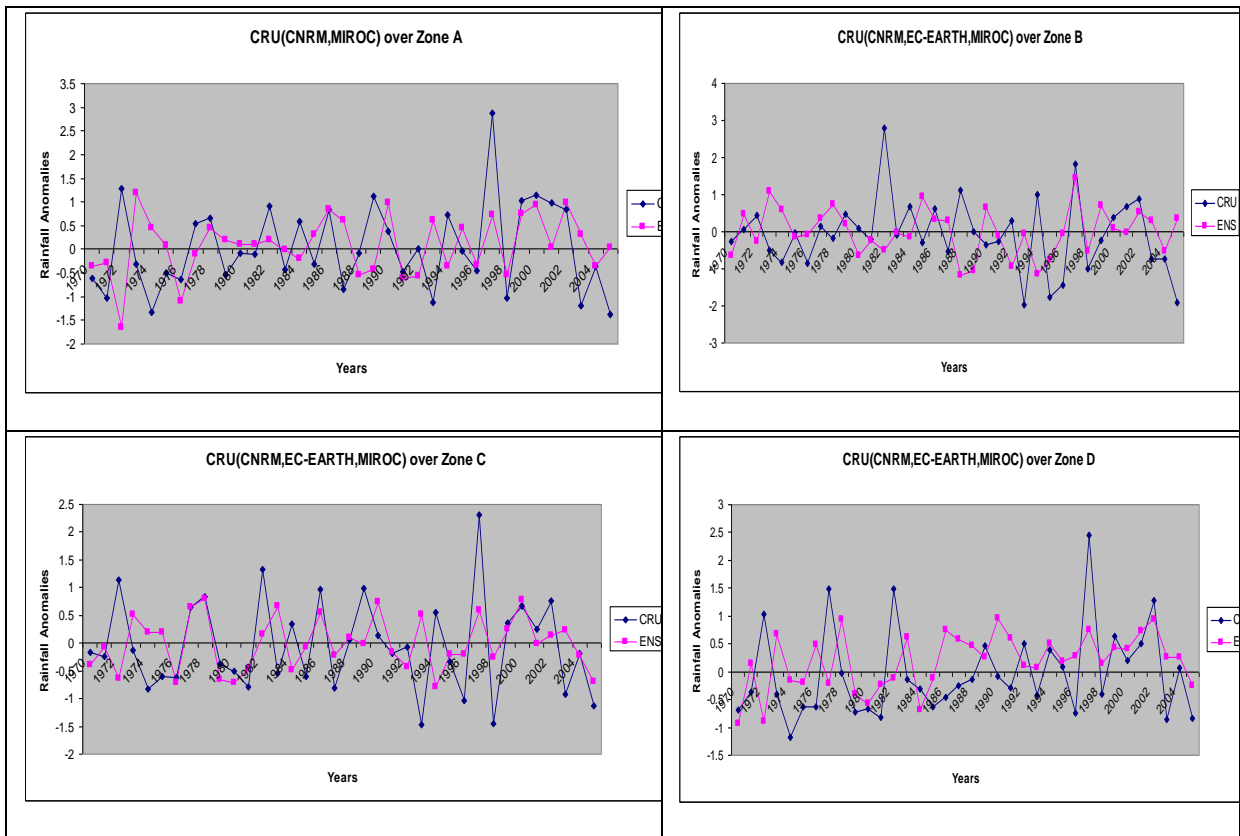


Figure 23: Inter-annual Variability of Ensemble (pink) and CRU (blue) for October-December (OND) for the period 1971-2005 over the sub domains A, B, C and D

5.3.2.1.5 Regression Analysis

Table 8 shows the performance of the individual models output based on their coefficient of determination and P-values from the regression analysis. The regression equation developed for each zone shows the models output that were picked at 95% confidence level. High R-square values and low P-values is an indication of good performance of the model output across the zones. Most zones had values of R-square below 45% and P-values below 0.002. These results could be an indication that the models have low skill around these zones during the MAM season.

Regression analysis helped to determine linear relationships between model output and CRU. The stepwise regression analysis was used as a mean of picking the best individual predictors (model output) into the regression model equation. The sub domains showed higher skill during the OND season than the MAM season as indicated by a high R-square value of 50% and a low P-value of 0.001.

Table 8: Regression Model Equations developed for the Models output at different sub-domains with R-square value above 25% for March-May and 45% for October-December seasons respectively and their P-values

March-May Season			
Sub-domains	Regression Equation	R-Square	P-Value
A	$A_{25} = -0.555 * CCMA - 0.305 * CNRM - 0.332 * MIROC$	25	0.064
B	$B_{26} = -0.495 * CNRM + 0.583 * MPI$	26	0.022
C	$C_{27} = -0.538 * CNRM + 0.465 * ECEARTH + 0.189 * MPI$	27	0.046
D	$D_{49} = 0.314 * MIROC + 0.371 * MPI + 0.289 * CNRM$	49	0.012
October-December Season			
Sub-domains	Regression Equation	R-square	P-Value
A	$A_{50} = -0.201 * CNRM + 0.185 * EC-EARTH - 0.104 * NorESM$	50	0.007
B	$B_{51} = -0.295 * CCMA - 1.175 * EC-EARTH + 0.152 * MIROC$	51	0.006
C	$C_{59} = 0.292 * EC-EARTH + 0.15 * MIROC - 0.164 * MPI$	59	0.002
D	$D_{53} = -0.360 * CNRM + 0.434 * EC-EARTH$	53	0.026

5.3.2.2 Correlation Analysis

Tables 9 and 10 show the negative and positive correlation values obtained between the model output and the CRU rainfall for MAM and OND seasons respectively. The analysis was done and the significance of each correlation coefficient tested using the student T-test at 95% confidence level. Any correlation value equal or greater than 0.30 was statistically significant. This however explained less than 8% of the total variance.

From Table 9, it can be noted that the significant correlations between the model outputs and the CRU rainfall anomalies were from three models CNRM, MIROC and MPI whereas the other models showed relatively low correlations. The three models with significant correlations across the four representative sub domains also had relatively low RMSE values as shown in Table 6. This shows that these models can simulate the observed rainfall patterns relatively well compared to the rest during this season.

Table 10 shows correlation coefficients between model outputs and CRU rainfall anomalies for the October- December season. Most of the significant correlations were obtained between CNRM, EC-EARTH and MIROC models and the CRU anomalies. During this season, the correlation coefficients were relatively higher than those obtained during the MAM season, an indication of the models ability to simulate the observed pattern during this season.

Table 9: Correlation Coefficients between Model output and CRU Rainfall Anomalies for March - May season over the sub domains A, B, C, D. Green and yellow shading indicates significant positive and negative correlations, respectively, while unshaded values indicate statistically insignificant correlations.

CRU/ sub-somain	CCMA	CNRM	EC- EARTH	GFDL	HadGEM	MIROC	MPI	NorESM
A	-0.20	0.31	0.16	0.27	-0.15	-0.36	0.39	0.18
B	0.17	-0.32	-0.33	-0.19	0.12	0.32	0.40	-0.20
C	0.19	0.30	0.10	0.19	0.13	0.33	0.31	0.10
D	-0.23	-0.40	0.19	0.26	0.26	0.37	-0.43	0.17

Table 10: Correlation Coefficients between Model output and CRU Rainfall Anomalies for October-December season over the sub domains A, B, C, D. Green and yellow shading indicates significant positive and negative correlations respectively, while unshaded values indicate statistically insignificant correlations.

CRU/ Sub- domain	CCMA	CNRM	EC- EARTH	GFDL	HadGEM	MIROC	MPI	NorESM
A	0.26	0.32	0.39	0.23	0.29	0.36	-0.29	-0.22
B	-0.22	-0.44	-0.32	0.36	-0.14	-0.33	-0.21	-0.38
C	0.16	-0.35	0.35	0.21	0.26	0.35	-0.31	-0.22
D	0.22	0.34	-0.42	0.14	0.24	0.44	-0.25	-0.24

5.3.3 Categorical Statistics

Tables 11 and 12 show the various scores that were used to assess the skill and accuracy of the ensemble model output at various sub-domains. A regression analysis was done to establish the best individual model output at 95% confidence level. Only the model output in the regression equation that had high R-square and low P-values were picked at sub-domains. The results for Percent correct, Probability of Detection, Heidke Skill Score, the False Alarm Ratio and bias for MAM and OND seasons were calculated from the 3 by 3 contingency table.

From the analysis of the Percent correct in Table 11, sub-domains A and B recorded a 50 percent correct while sub domains C and D recorded less than 50 percent correct. These results show that the skill of the models is much lower during the March-April-May season over the LVB.

From the analysis of the Heidke skill score (HSS); none of the model outputs had values close to a perfect score of 100%. The score were especially higher for all the sub-domains considered in the study.

The analyses from the Bias score show that the perfect score of 100% was not achieved in any of the instances for the model output presented. The cases of forecasting nearing almost perfect were achieved in no instances. The cases of over-forecasting were more than those under-forecasted especially for most stations over the LVB.

From the analysis of FAR, for the normal category, two sub- domains C and D predicted above 50%; for the above normal category, and all the sub domains predicted below 50% for below normal category. PoD gives the proportion of rainfall events successfully forecasted by the model. For a good forecast the PoD is 100%. Most of the sub domains had a score of more than 50% in the three categories. This indicates that the model successfully forecasts more than half of the rainfall events in region.

Table 12 shows the skill scores of the ensemble model output during the OND season. During this season all the sub domains got a score of more that 50% correct as compared to the March-May season. The skills were generally better than those obtained during March-May season an indication that there is a remarkable improvement in the way in which the models simulate the observed pattern in October- December season.

Table 11: Percent correct (%), Probability of detection (POD) (%), False Alarm (FAR) (%), BIAS (%) and Heidke Skill Score (HSS) (%) for MAM Ensemble model output picked across all the four sub-domains at different Categories, Below Normal (BN), Normal (N) and Above Normal

Sub-domains	Model Output	Percent Correct	POD			FAR		BIAS			HSS
			BN	N	AN	BN	AN	BN	N	AN	
A	CNRM,MIROC, MPI	50	33	58	61	22	33	43	161	109	0.262
B	CNRM,MIROC, MPI	53	40	64	60	25	44	51	118	90	0.317
C	CNRM,MIROC, MPI	46	29	52	57	28	50	38	161	114	0.196
D	CNRM,MIROC, MPI	44	28	51	57	22	53	36	160	122	0.184

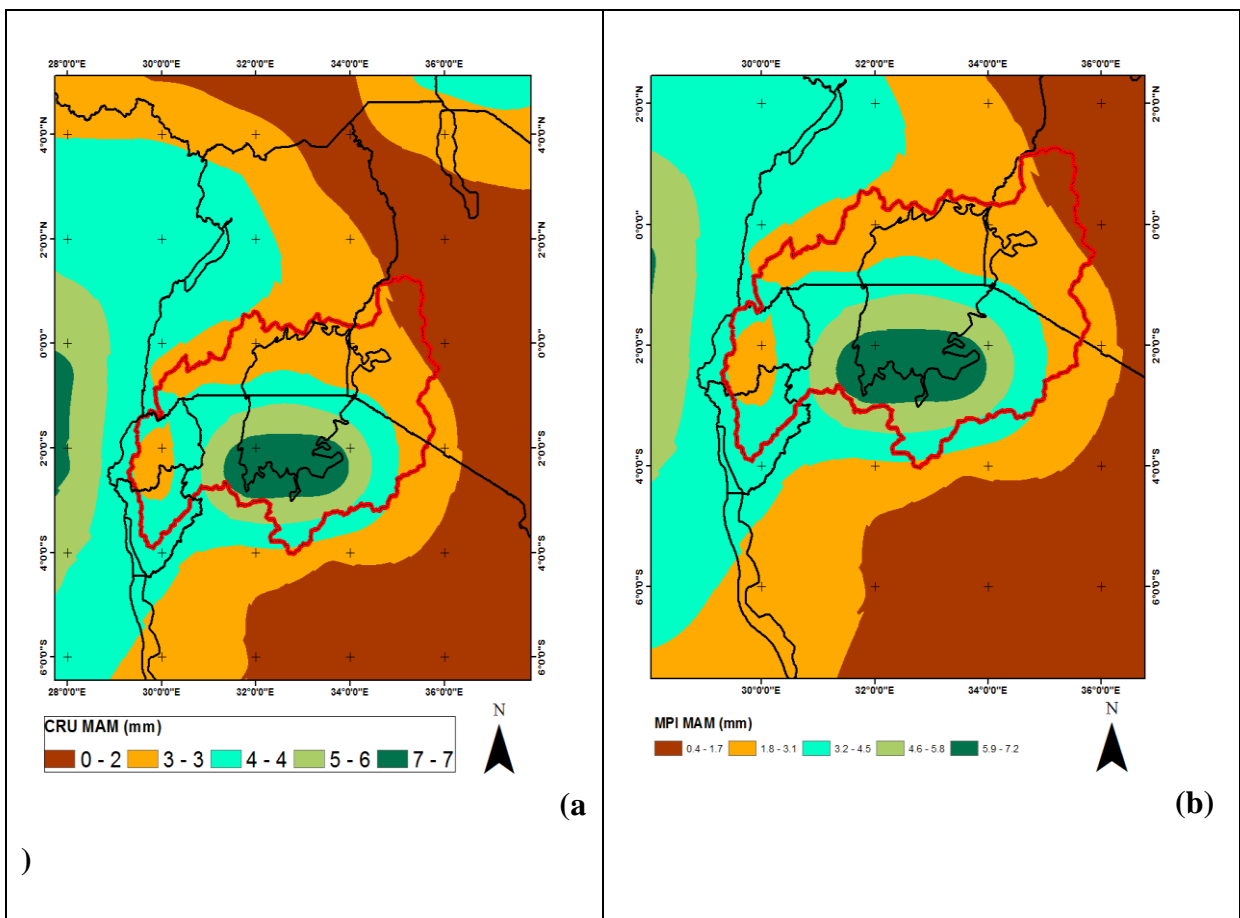
Table 12: Percent correct (%), Probability of detection (POD) (%), False Alarm (FAR) (%), BIAS (%) and Heidke Skill Score (HSS) (%) for OND Ensemble model output picked across all the four sub-domains at different Categories, Below Normal (BN), Normal (N) and Above Normal.

Sub-domains	Model Output	Percent Correct	POD			FAR		BIAS			HSS
			BN	N	AN	BN	AN	BN	N	AN	
A	CNRM,MIROC,EC-EARTH	53	27	51	56	30	53	38	158	117	0.168
B	CNRM,MIROC,EC-EARTH	61	27	49	53	38	55	44	158	117	0.182
C	CNRM,MIROC,EC-EARTH	58	26	52	52	41	54	44	160	112	0.178

D	CNRM,MIROC,EC-EARTH	51	25	47	57	43	52	43	151	119	157
---	---------------------	----	----	----	----	----	----	----	-----	-----	-----

5.3.3.1 Results from the Spatial Rainfall Patterns

Figure 24 shows the simulated spatial patterns of rainfall in hundreds of millimeters per day as obtained from (a) the CRU (b) MPI (c) MIROC (d) CNRM. The figure shows rainfall distribution during March-May season. The results indicate that rainfall decreases towards the eastern part of the region. Over the western part, there are markedly similar patterns in almost all the four plots during this season. The MPI model was able to capture the effect of orographic features and inland water bodies as indicated by the extreme over the water body. From all the spatial plots, it was noted that the models were able to capture two extremes both on land and over the water body.



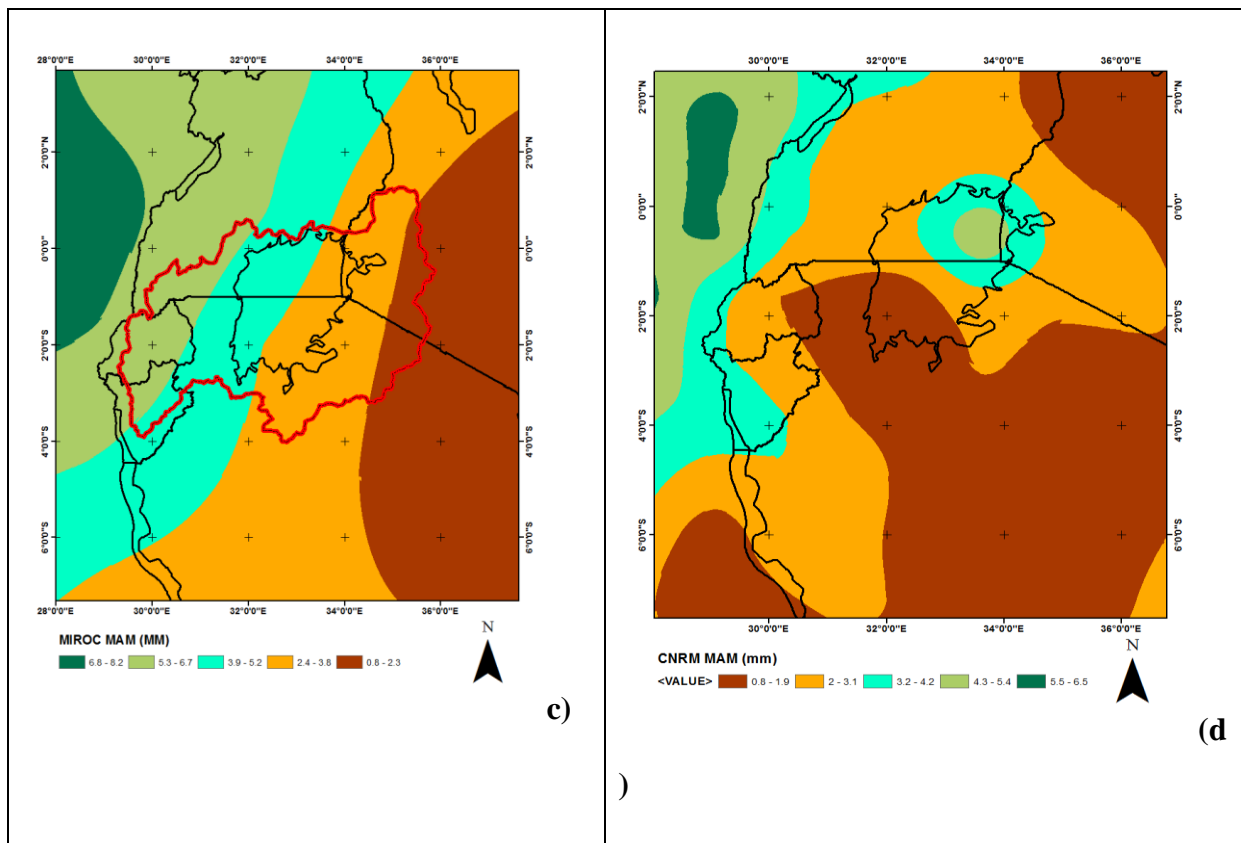


Figure 24: March-May simulated spatial rainfall patterns for the period 1971-2005 as obtained from CRU, MPI, MIROC and CNRM over the LVB

Figure 25 shows the simulated spatial patterns of rainfall in hundreds of millimeters per day obtained from (a) CRU and (b) model ensemble for the March- May season of the three models in Figure 25 over the Lake Victoria Basin. The ensemble model output was able to capture and replicate a spatial pattern as depicted by the CRU rainfall pattern. There was a marked extreme over the water body and depressed rainfall on the eastern side of the study region.

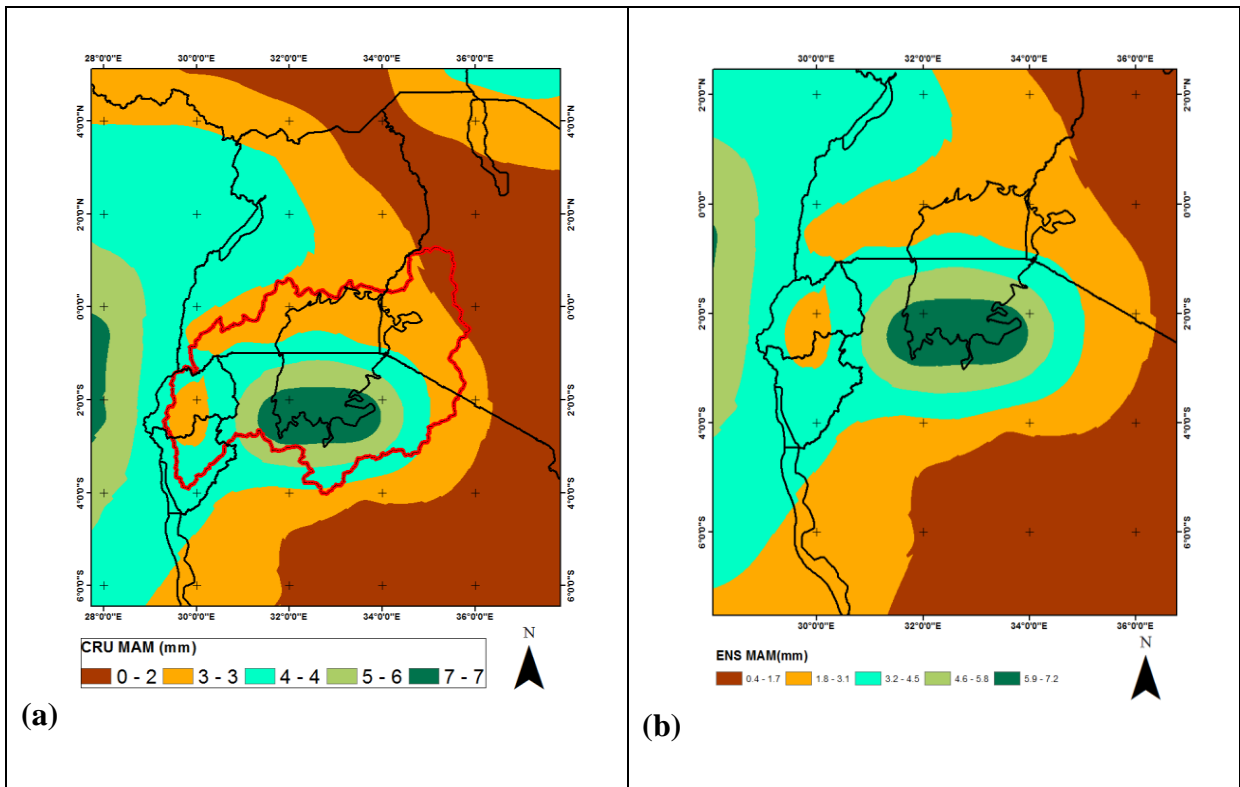


Figure 25: March-May simulated spatial rainfall patterns for the period 1971-2005 as obtained from CRU and ENS over the LVB

Figure 26 shows the simulated spatial patterns of rainfall in hundreds of millimeters per day as obtained from (a) the CRU (b) MIROC (c) EC-EARTH (d) CNRM. The figure shows rainfall distribution during October- December season (the scale is in hundreds of milliliters). The results show that nearly all the three models EC-earth, CNRM and MIROC simulate the OND season fairly well and indicate that most of the rainfall is influenced by increased ENSO events and the eastward shift the Congo rainfall belt during this season. This implies that the climate model used captures the effect of such features like the ITCZ and the influence of the Lake effect.

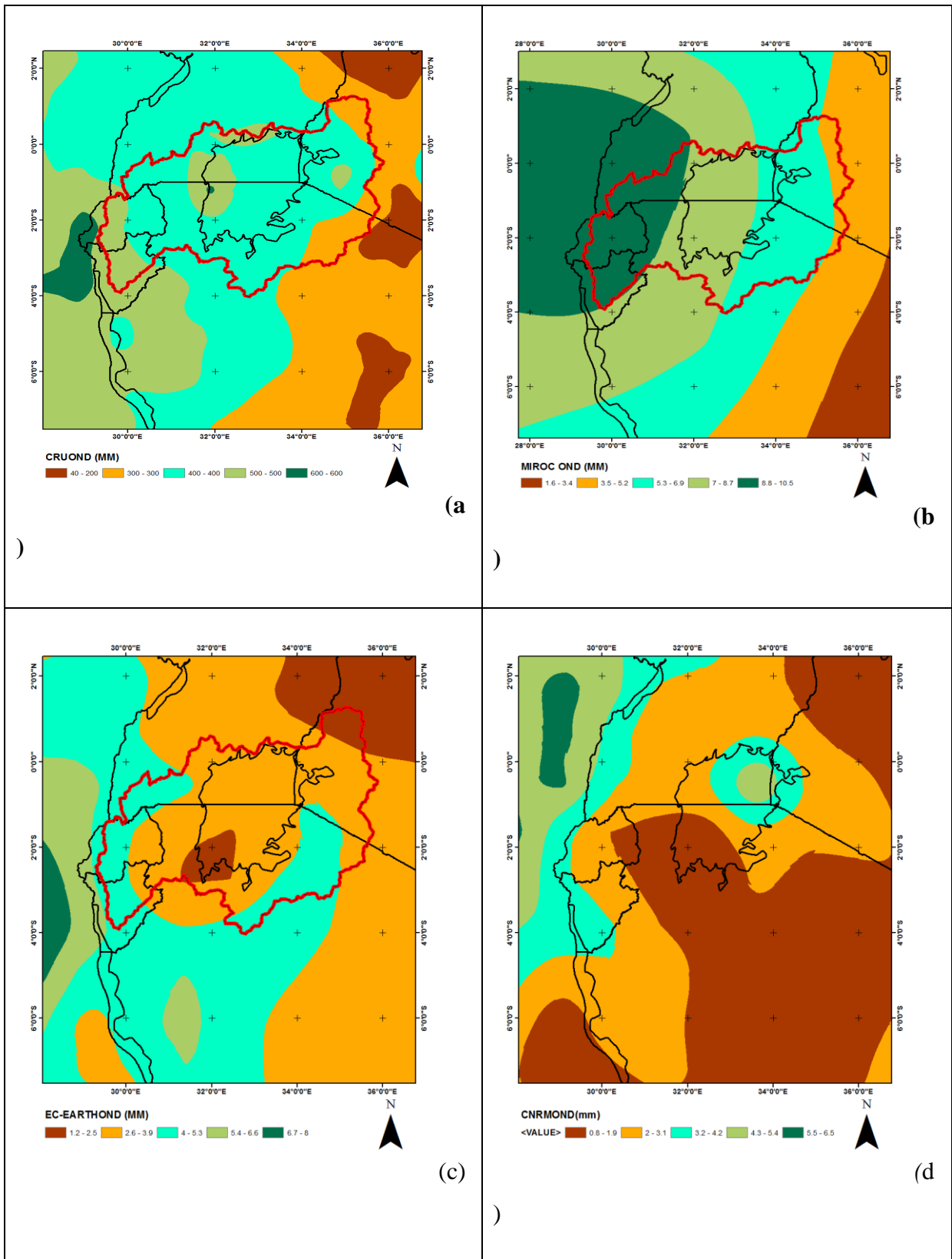


Figure 26: October-December simulated spatial rainfall patterns for the period 1971-2005 as obtained from (a) CRU, (b) MIROC, (c) EC-EARTH and (d) CNRM over the LVB.

Figure 27 represents simulated spatial rainfall pattern in hundreds of millimeters per day for ENS and CRU of the three models in Figure 26 over the LVB. The results indicate enhanced rainfall on the western side of the study region and an extreme event over the land on the

same side. The eastern side experiences depressed rainfall as in the earlier case. However, the ensemble output replicates the rainfall pattern better than the individual models.

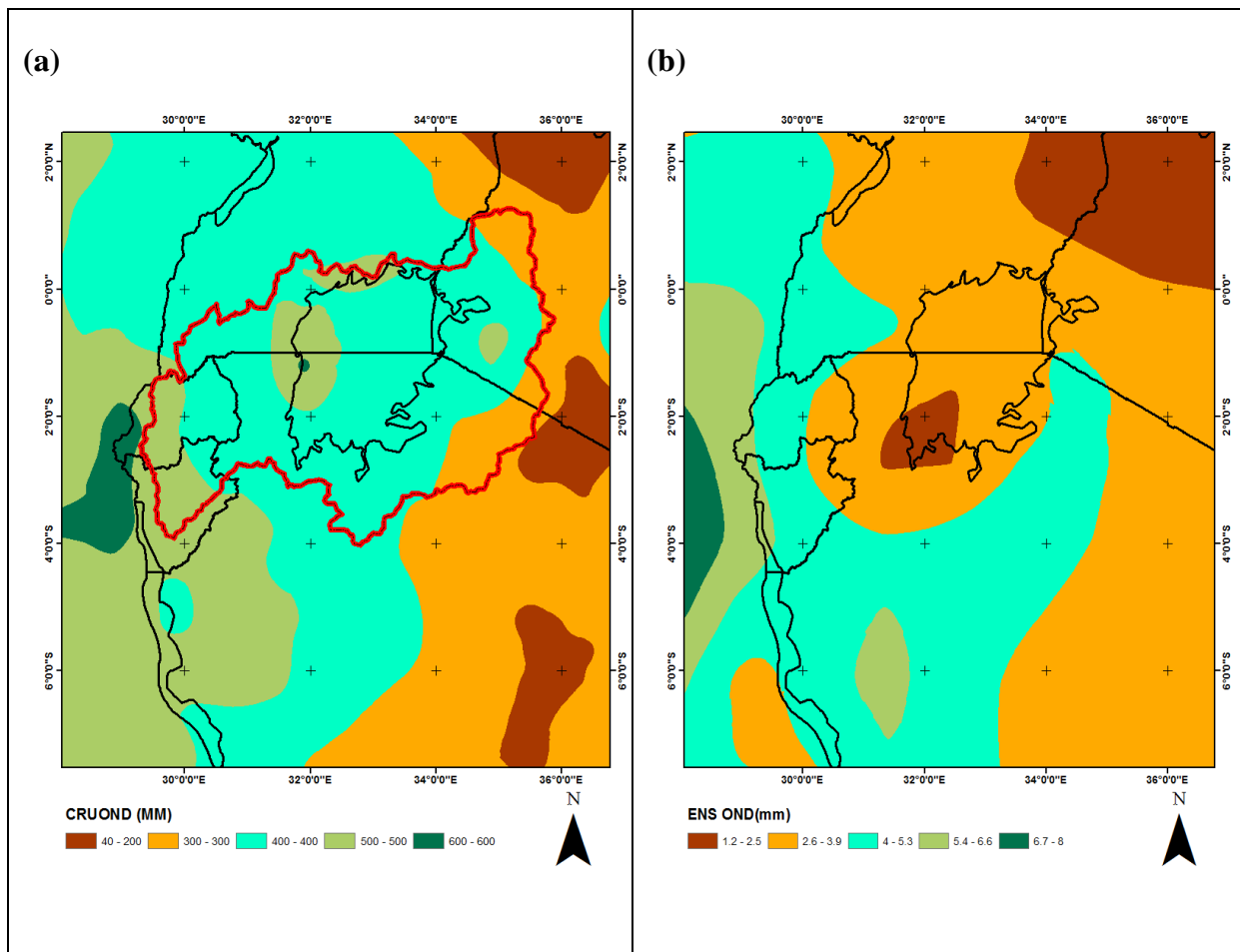


Figure 27: October-December simulated spatial rainfall patterns for the period 1971-2005 as obtained from (a) CRU, (b) ENS over the LVB.

5.4 Climate Projections using Model Outputs

The results from the Subsection 5.3.3.1 indicated that, when averaged over a large area, the present-day simulated model rainfall is fairly accurate compared to the observed datasets over the LVB. The study examined the model-projected climate for RCP 4.5 scenario over the LVB for the downscaled outputs. The downscaling process was done following the procedure outlined in Section 4.2.3.1. The results of the downscaled projected temporal and spatial model patterns are presented.

5.4.1 Projected Temporal Patterns for March-May and October- December Seasons

Figures 28 and 29 represent the projected temporal rainfall patterns for the seasons of March-May, and October-December over the study area. The results presented in each case are for RCP 4.5 scenario for the period 2001-2030, 2041-2070 and 2071-2100.

The results from time series analysis for March- May season indicate that there shall be no significant trend in the rainfall in the near future. However, during the period ranging from 2041-2070, MAM rainfall is projected to decrease as indicated by a decreasing trend. The highest rainfall is projected in 2047 while lowest rainfall is projected in 2041. The figure also shows that rainfall is not likely to stabilize towards the mean rainfall for the MAM season in the projected time windows 2001-2030, 2041-2070 and 2071-2100.

Figure 29 shows the trend analysis for October- December season for the time period 2021-2050, 2041-2070 and 2071-2100. From the plots, there is unlikelihood of a significant trend in the near future in the entire three time window. However, the highest rainfall is projected in 2041 and 2081 while the lowest rainfall is projected in 2085. The figure also shows that rainfall is not likely to stabilize towards the mean rainfall for the season in the year 2030.

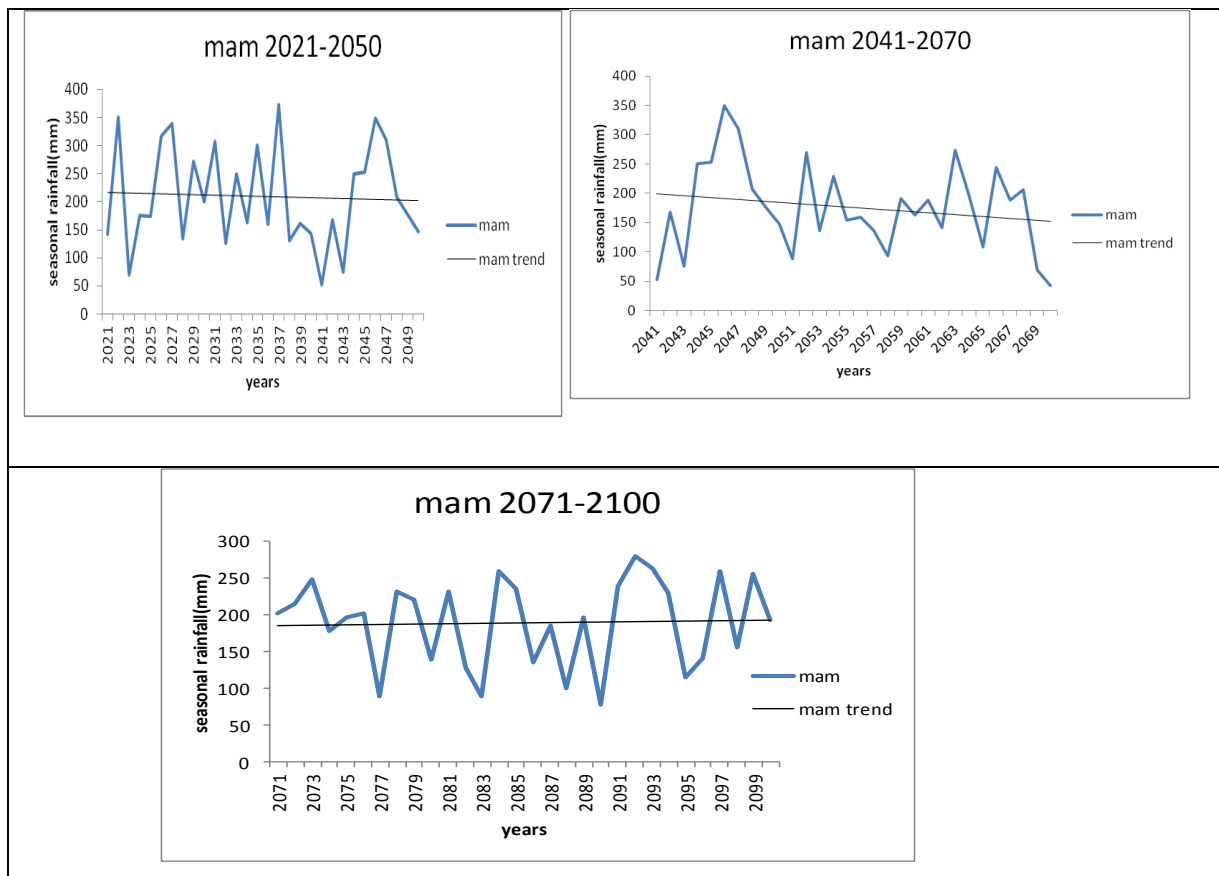


Figure 28: Rcp 4.5 projected temporal rainfall pattern for March–May season for the period 2021-2050, 2041-2070 and 2071-2100 over the LVB

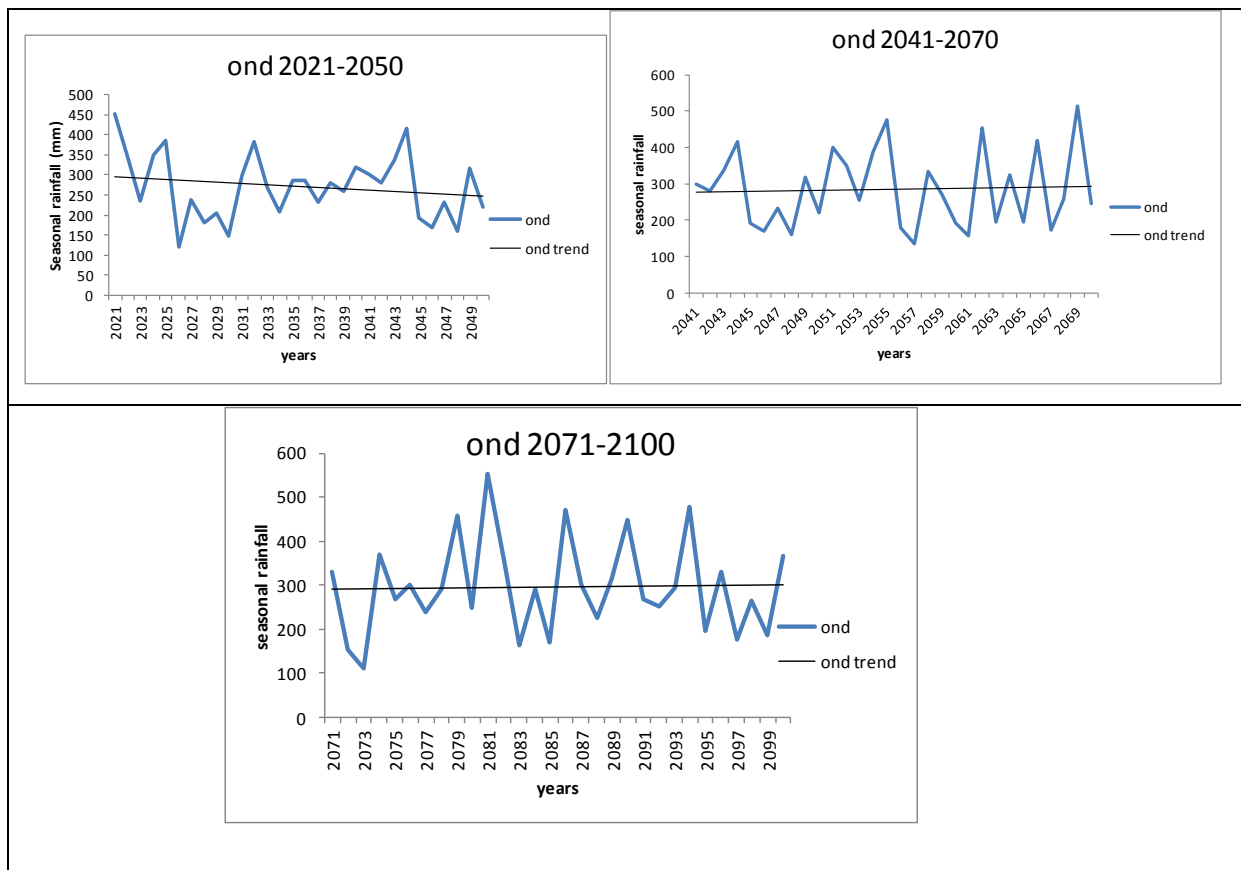


Figure 29: Rcp 4.5 projected temporal rainfall pattern for October- December season for the period 2001-2021-2050, 2041-2070 and 2071-2100 over the LVB

5.4.2 Projected Seasonal Spatial Rainfall Patterns for Rcp 4.5 Scenario

This section presents the spatial rainfall patterns for model projections for the time windows 2021-2050, 2041-2070 and 2071-2100 for MAM and OND seasons following RCP 4.5 scenario over the LVB.

5.4.2.1 March – May and October- December Season for the Period (2021- 2050)

Figures 30-32 represent the projected spatial patterns of rainfall in millimeters per day over the LVB using the MPI and MIROC models for time windows 2021-2050, for RCP 4.5 scenario. The results in Figure 31 show rainfall spatial patterns during March-May for MPI and MIROC models and October- December following the RCP 4.5 scenario for the period 2021-2050.

The results indicate drier conditions for the time period 2021-2050 during MAM over towards the eastern part of the study region and an extreme over the water body and towards the western side of the study region. However, during the OND season, the MIROC model projects enhanced rainfall on the western part with an extreme over land and water, while MPI model projects depressed rainfall with an extreme over the lake only.

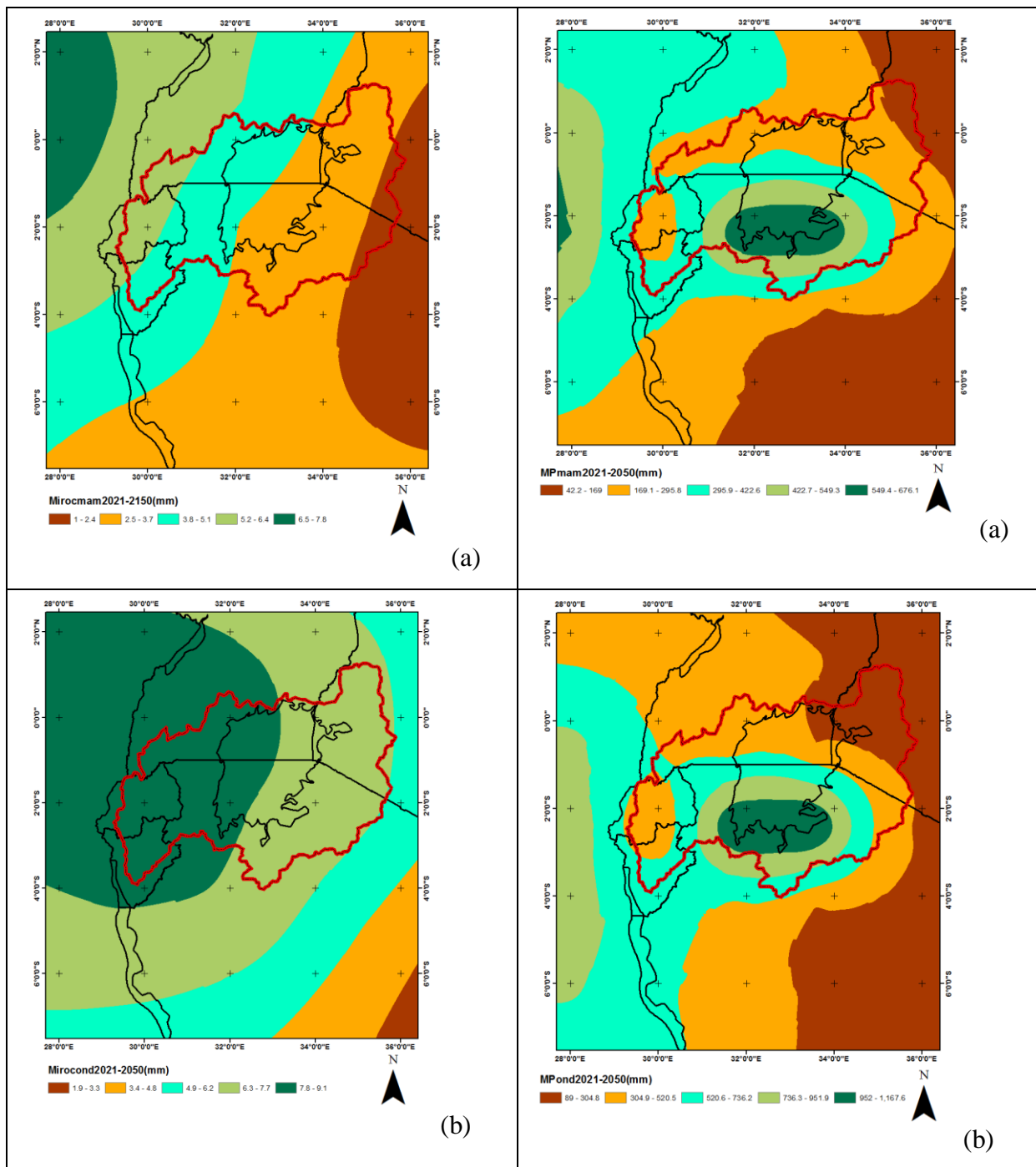


Figure 30: MIROC & MPI projected spatial rainfall patterns (2021-2050) for (a) March–May and (b) October–December following the RCP 4.5 scenario over the LVB

5.4.2.2 March – May and October- December Seasons for the Period 2041- 2070

Figure 31 shows rainfall spatial patterns during March-May for MPI and MIROC models and October- December for RCP 4.5 scenario for the period 2041-2070.

The results indicate drier conditions for the time period 2041-2070 during MAM over towards the eastern part of the study region and an extreme over the water body and the western side of the study region. However, during the OND season, the MIROC model

projects enhanced rainfall on the western part with an extreme over land and water, while MPI model projects depressed rainfall with an extreme over the lake only.

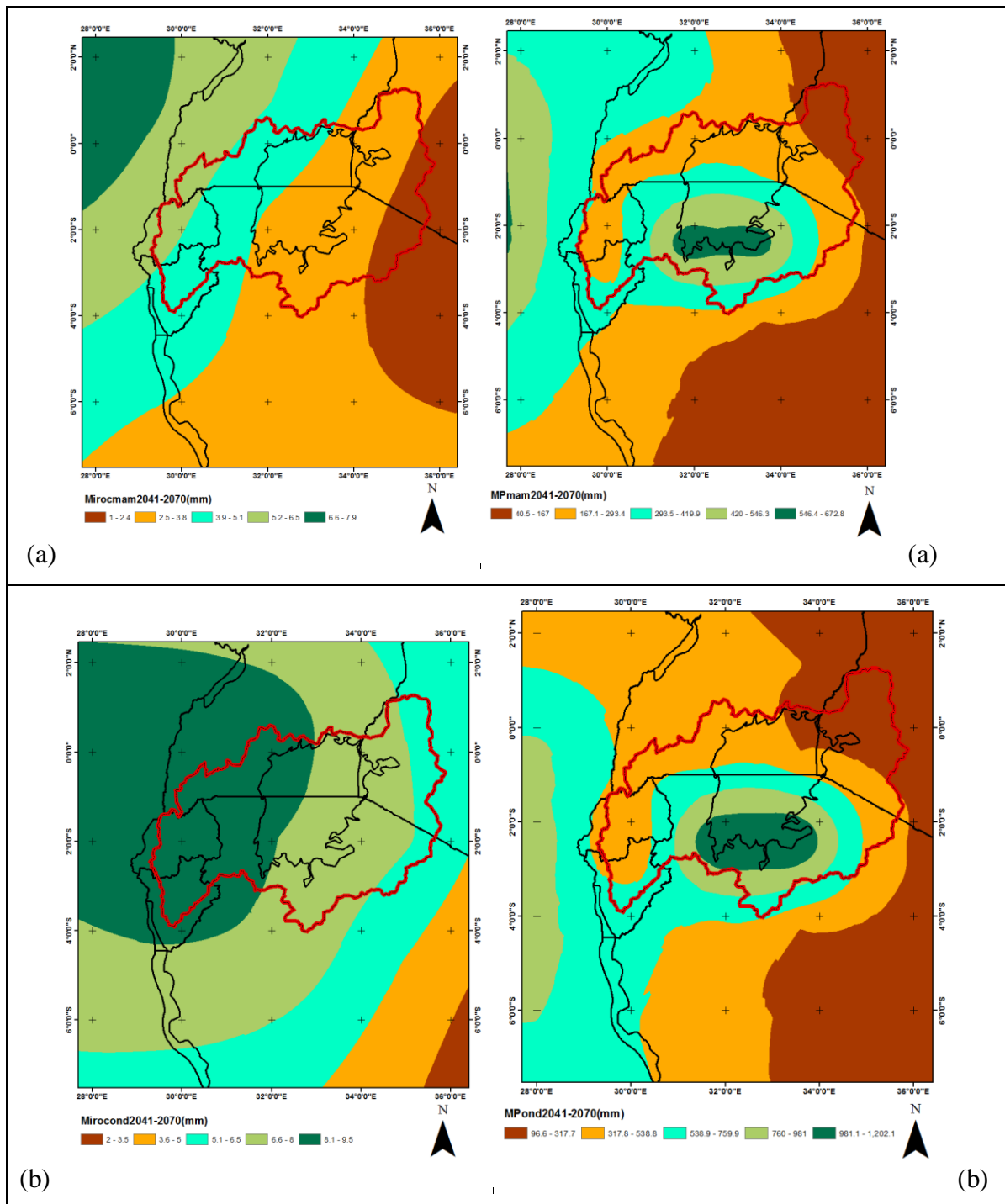


Figure 31: MIROC & MPI projected spatial rainfall patterns for the period 2041-2070 for (a) March–May and (b) October–December following the RCP 4.5 scenario.

5.4.2.3 March – May and October- December Seasons for the Period 2071- 2100

Figure 32 shows rainfall spatial patterns during March-May for MPI and MIROC models and October- December for RCP 4.5 scenario for the period 2071-2100.. The results in both cases indicate that MAM is likely to experience depressed rainfall except for an extreme event over the Lake Victoria whereas the highest rainfall will be experienced around Lake Victoria during mainly OND and significant amount of rainfall expected to the western part of the region. Enhanced rainfall during OND is likely to be caused by increased ENSO events and the eastward shift the Congo rainfall belt during this season. The lowest rainfall is expected on the eastern side of the region of study.

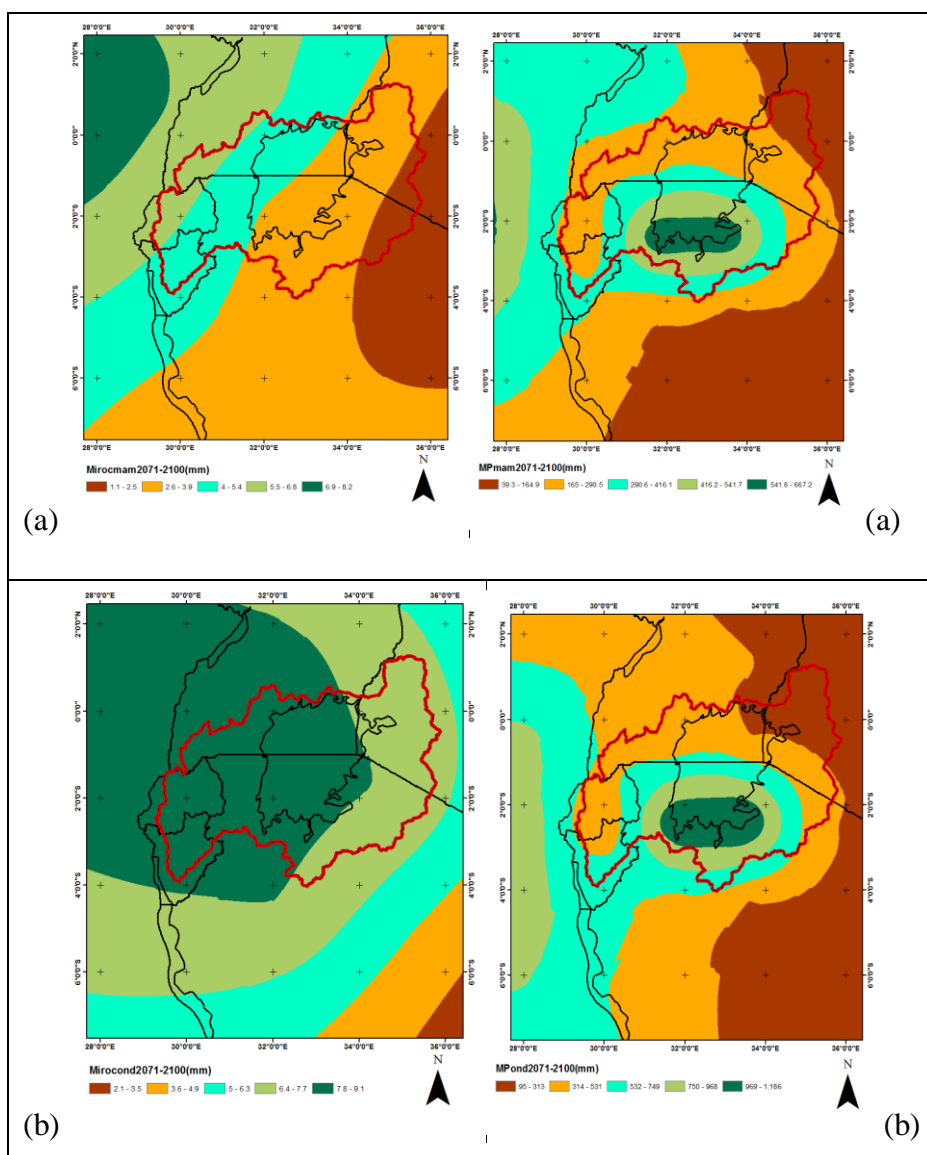


Figure 32: MIROC & MPI projected spatial rainfall patterns for the period 2071-2100 for (a) March–May and (b) October-December following the RCP 4.5 scenario over the LVB.

CHAPTER SIX

6.0 SUMMARY, CONCLUSION AND RECOMMENDATIONS

This chapter provides a summary of the results obtained from the various methods used to achieve the objectives of the study. The chapter also provides the conclusions drawn and the recommendations made.

6.1.1 Summary

The overall objective of the study was to assess the performance of the Coupled Model Inter-comparison Project (CMIP5) over the Lake Victoria Basin. The data used in the study included the observed point station data, gridded rainfall data from Climate Research Unit, University of East Anglia (CRU) and hindcast data from eight Coupled Model Inter-comparison Project 5 (CMIP5) for the period 1971 to 2005 for historical and 2006-2100 for model future projections. The methodology employed included trend analysis spatial analysis, correlation analysis, Principal Component Analysis (PCA) regression analysis, and categorical statistical skill score.

Majority of the eight models analyzed correctly reproduce the mean seasonal and annual cycle of precipitation for the period 1971–2005 as compared to gridded satellite-derived observations. There were no significant trends in the observed rainfall over the study region for MAM and OND seasons. However, for OND all the representative stations used had increasing rainfall trends which signify the possibility of wetter conditions in future. The spatial patterns of the individual model output from MPI, MIROC and CNRM were closest to the observed rainfall pattern for OND season than MAM season, with two extremes on land and over the water body.

The analysis for the correlation coefficients showed relatively higher coefficients for the ensemble model output than for the individual models. Categorical statistics score showed higher skill for the ensemble models than for the individual models output. The skill and accuracy of the forecasts was enhanced especially during OND season. Model projection trends showed decreasing trends for MAM and increasing trends for OND season. The spatial patterns for future projections indicates enhanced rainfall pattern in the eastern side of the study region with the enhanced two rainfall extremes over the land and water body.

6.1.2 Conclusion

This study has indicated some evidence of increasing trends in observed rainfall patterns over some areas in the region of study and decreasing trends in others. The trends indicate that climate change and its impacts will affect the different regions differently depending on the micro climate and season of the year.

CMIP5 models considered in the present study were able to capture the main features of seasonal mean rainfall distribution and its annual cycle, albeit significant biases in individual models depending on region and season. For instance, MPI, MIROC and CNRM were able to replicate the observed annual and seasonal patterns whereas GFDL was not able to capture the center of JJA seasonal rainfall, while EC-EARTH delayed the onset of the same season. NorESM pushed the center of MAM, JJA and OND seasonal rainfall further north.

The spatial pattern of rainfall modes identified important features over the LVB region. Two centers of enhanced precipitation were identified over land and Lake areas in the first rainfall mode. The center over the Lake Victoria seemed to be enhanced than the center over land which might be a pointer to increasing sea surface temperatures. However, the models seemed to be struggling to capture the observed patterns since for LVB, rainfall events are controlled by the mesoscale systems.

6.1.3 Recommendations

The results of the study will be useful to climate model research scientists, policy makers, National Meteorological and Hydrological Services (NMHS), and other professionals in all sectors that are affected by the climatic information. Such sectors include Meteorology, Hydrology, agriculture, industry, energy and researchers, among others.

Further research using all the 19 CMIP 5 models needs to be done to assess the improvement performance skill. There is need for a similar research with 12 global models for JJA season to contrast and compare with the performance of the model output for the OND and MAM seasons. In addition, further analyses of the future climate projections should be considered for the rcp 8.5 to compare and contrast with the rcp 4.5 considered in the present study.

As multi-model ensembles have been suggested as one of the methods to reduce model uncertainty; it is important that the performance of the individual member is assessed for its

reliability. A model that struggles to represent climate system properly would surely not add any value to the ensemble, and while refining parameterization by either including additional parameters might be one of the ways of enriching the model performance, there are new parameters to amplify biases and more uncertain model parameters to constrain as is the case in the CMIP5 models, thus, uncertainty assessment as a precursor in climate change studies remain valid in the current CMIP generation.

References

- Anyah, R. O (2005): Modeling the variability of the climate system over Lake Victoria Basin: *PhD. Thesis*, Department of Marine, Earth and Atmospheric Sciences, North Carolina University, USA.
- Anyah, R.O., and F. H. M. Semazzi (2005): Simulation of the response of Lake Victoria Basin climate to lake surface temperatures. *Theor. Appl. Climatol*, **79**, 55-69.
- Anyah, R. O., and Otieno, V., (2013).CMIP5 simulated climate conditions of the Greater Horn of Africa (GHA). Part 1: contemporary climate. *Climate Dynamics* , **41**, 2081-2097.
- Anyah, R., and Otieno, V., (2012): CMIP5 simulated climate conditions of the Greater Horn of Africa (GHA). Part 1: contemporary climate. *J. Climate Dynamics* **41**, 2081-2097
- Anyamba, E. K (1984): On the monthly mean lower tropospheric circulation and anomalous circulation during the 1961/62 floods in East Africa: *MSc. Thesis*, Department of Meteorology, University of Nairobi.
- Arakawa A, Shubert WH (1974): Interaction of a cumulus cloud ensemble with the large-scale environment, Part 1. *J Atmos Sci* **31**, 674–701
- Asnani G. C (1993): Tropical Meteorology Vol. 1 and Vol. 2 Second Edition. Indian Institute of Tropical Meteorology, Pashan.
- Bachner, S., Kapala, A. & Simmer, C. (2008): Evaluation of daily precipitation characteristics in the CLM and their sensitivity to parameterizations. *Meteorologische Zeitschrift*, **17** (4), 407-420.
- Bamanya, D (2007): Intraseasonal characteristics of daily rainfall over Uganda during wet seasons: *MSc. Thesis*, Department of Meteorology; University of Nairobi.
- Barring, L (1987): Spatial patterns of daily rainfall in Central Kenya: Applications of Principal Component Analysis, Common Factor Analysis. *J. Clim.*, **7**, 7-287.
- Barnier B, Madec G, Penduff T, Molines J-M, Treguier A-M, Le Sommer J, Beckmann A, Biastoch A, Boning C, Dengg J, Derval C, Durand E, Gulev S, Remy E, Talandier C, Theetten S, Maltrud M, McClean J, De Cuevas B (2006) Impact of partial steps and momentum advection schemes in a global ocean circulation model at eddy-permitting resolution. *Ocean Dyn* **56**:543–567

- Bowden, Jared H., Fredrick H. M. Semazzi, (2007): Empirical Analysis of Intraseasonal Climate Variability over the Greater Horn of Africa. *J. Climate*, **20**, 5715–5731. doi: <http://dx.doi.org/10.1175/2007JCLI1587.1>
- Bretherton CS, McCaa JR, Grenier H (2004): A new parameterization for shallow cumulus convection and its application to marine subtropical cloud-topped boundary layers. Part I: description and 1-D results. *Mon Weather Rev* 132:864–882
- Bugenyi, F.W.B. and Magumba, K.M., (1996): The present physicochemical ecology of Lake Victoria, Uganda. In *The Limnology, Climatology and Paleoclimatology of the East African Lakes* (T.C. Johnson and E.O. Odada, eds.). Gordon and Breach Publ, Amsterdam, p. 141-154.
- Buonomo, E., Jones, R., Huntingford, C. & Hannaford, J. (2007): On the robustness of changes in extreme precipitation over Europe from two high resolution climate change simulations. *Quarterly Journal of the Royal Meteorological Society*, **133**, 65–81.
- Busuioc, A., Von Storch, H. and Schnur, R. (1998): Verification of GCM-generated regional seasonal precipitation for current climate and of statistical downscaling estimates under changing climate conditions, *Journal of Climate*, **12**, 258-272.
- Chandler, R. E. (2006): *Generalized Linear Modelling for Daily Climate Time Series (GLIMCLIM)*. London England, University College of London.
- Chandler, R. E. & Wheeler, H. S. (2002): Analysis of rainfall variability using generalized linear models: A case study from the west of Ireland. *Water Resource Research*, **38** (10), 1192.
- Christensen, J. H., Boberg, F., Christensen, O. B. & Lucas-Picher, P. (2008): On the need for biascorrection of regional climate change projections of temperature and precipitation. *Geophysical Research Letters*, **35** (20), L20709.
- Christensen, J. H. & Christensen, O. B. (2007): A summary of the PRUDENCE model projections of changes in European climate by the end of this century. *Climatic Change*, **81**, 7-30.
- Conway,D., Hanson C. E.,Doherty,R and Persechino,A.,(2005): GCM simulations of the Indian Ocean dipole influence on East African rainfall: Present and future .*Geophysical Research Letters*, VOL. **34**, L03705, doi:10.1029/2006GL027597, 2007
- Cravatte S, Madec G, Izumo T, Menkes C, Bozec A (2007) Progress in the 3-D circulation of the eastern equatorial Pacific in a climate ocean model. *Ocean Mod* **17**(1):28–48

- Del Genio AD, Yao M-S (1993): Efficient cumulus parameterization for long-term climate studies: the GISS scheme. The representation of cumulus convection in numerical models. *Meteor Monogr* **46**:181–184
- Durman, C. F., Gregory, J. M., Hassell, D. C., Jones, R. G. & Murphy, J. M. (2004) A comparison of extreme European daily precipitation simulated by a global and a regional climate model for present and future climates. *Quarterly J. Royal Meteorological Society*, **127** (573).
- East African Secretariat Report (2006): A project to prepare investment plans for 15 secondary urban centres under the Lake Victoria basin water and sanitation initiative in Kenya, Tanzania, Uganda, Burundi and Rwanda Lake Victoria Basin Commission LVWATSAN Phase II 1-23 pp
- Findlater, J (1969): A major low level air current near western Indian Ocean during the northern summer. *Q. J. Roy. Met. Soc.*, **95**, 362–380.
- Findlater, J (1971): The low-level cross equatorial air current of western Indian Ocean during Northern Summer. *Mon. Wea. Rev.*, **29**, 411-416.
- Fowler, H. J. & Ekstrom, M. (2009): Multi-model ensemble estimates of climate change impacts on UK seasonal precipitation extremes. *Int. J. Climatology*, **29** (3), 385-416.
- Frei, C., Scholl, R., Fukutome, S., Schmidli, J. & Vidale, P. L. (2006): Future change of precipitation extremes in Europe: Intercomparison of scenarios from regional climate models. *Journal of Geophysical Research*, **111** (6), D06105.
- Giorgi, F., and T. Bates (1990): The climatological skill of a regional climate model over complex terrain. *Mon. Wea. Rev.*, **117**, 2325-2347.
- Giorgi, F. & Mearns, L. (1991) Approaches to the simulation of regional climate change: A review. *Reviews of Geophysics*, **29** (2), 191-216.
- Giorgi, F. & Mearns, L. (1999): Introduction to special section: Regional climate modelling revisited. *Journal of Geophysical Research*, **104** (D6), 6335-6352.
- Griffith, J.F (1972): Climates of Africa survey of climatology. Vol. 10. *Edited by Landberg, H.E. Else Publishing Co. Amsterdam-London-New York.*
- Hagedorn, R., Palmer, T. N., Shutts, G. J., Doblas-Reyes, F.J., Jung T., and Leutbecher, M., (2005): Representing model uncertainty in weather and climate prediction. *Annual Review of Earth and Planetary Sciences*, **33**, 163-193.
- Ininda, J.M, (2008): Towards Improvement of seasonal rainfall forecasting through model output statistics (MOS) and downscaling of ECHAM Forecasts over Tanzania. *J. Kenya Meteorol. Soc.*, **2** (2), 96-104.

- Ininda J.M (1998): Simulation of the impact of sea surface temperature anomalies on the short rains over East Africa. *J. African Met Soc.*, **3**, 127-138.
- Ininda, J. M (1995a): Simulation of the impact of sea surface temperature anomalies on the short rains over East Africa. *J. African Met. Soc.*, **3**, 1, 127-140.
- Ininda, J.M (1995b): Numerical simulation of the influence of sea surface temperature anomalies on the East African seasonal rainfall. *PhD. Thesis*, Department of Meteorology, University of Nairobi, Kenya.
- IPCC (2001): *Climate Change 2001*, The Scientific Basis, Contribution of Working Group I to the Third Assessment Report of the Intergovernmental Panel on Climate Change, Cambridge University Press, Cambridge, UK.
- IPCC (2007): *Climate Change 2007*, The Scientific Basis, Contribution of Working Group I to the Fourth Assessment Report of the Intergovernmental Panel on Climate Change, Cambridge University Press, Cambridge, UK and New York, USA.
- Jenkins, G., Murphy, J., Sexton, D., Lowe, J., Jones, P. & Kilsbu, C. (2009): *UKCP09 Briefing report. UK Climate projections*. Exeter, UK, Met Office Hadley Centre.
- Jolley, T. J. and Wheeler, H. S. (1996): A large-scale grid-based hydrological model of the Severn and Thames catchments. *Water and Environment Journal*, **10** (4), 253-262.
- Jones, R. G., Murphy, J. M., Noguer, M. & Keen, A. B. (1997): Simulation of climate change over Europe using a nested regional-climate model. II: Comparison of driving and regional model responses to a doubling of carbon dioxide. *Quarterly Journal of the Royal Meteorological Society*, **123** (538), 265- 292.
- K-1 model developers: K-1 Coupled GCM (MIROC) Description, K-1 Technical Report No.1, Center for Climate System Research (Univ. of Tokyo), National Institute for Environmental Studies, and Frontier Research Center for Global Change, available at: <http://www.ccsr.u-tokyo.ac.jp/kyosei/hasumi/MIROC/> tech-repo.pdf (last access: 30 September 2011), 2004.
- Kabanda T.A and Jury M.R, (1999):“Interannual Variability of Short Rains over Northern Tanzania,” *Climate Research*, **13**, (3), pp. 231-241. doi:10.3354/cr013231
- Kiangi, P. M. R., M. M. Kavishe, and J. K. Patnaik, (1981): Some aspects of the mean tropospheric motion field in East Africa during the long rains season. *Kenya J. of Sci. and Tech. (A)*, **2**, 91-103.
- Kilsby, C. G., Jones, P. D., Burton, A., Ford, A. C., Fowler, H. J., Harpham, C., James, P., Smith, A. & Wilby, R. L. (2007): A daily weather generator for use in climate change studies. *Environmental Modelling and Software*, **22** (12), 1705-1719.

- Kinuthia, J. H. and G. C. Asnani, (1982): A newly found jet in North Kenya (Turkana Channel). *Mon. Wea. Rev.*, **110**, 1722 – 1728.
- Kizza, M, Rodhe, A, Ntake, K.H and Halldin, S. (2009): Temporal Variability in the Lake Victoria Basin in East Africa During the Twentieth Century. *Journal of Climatology*, **98**, 119-135.
- Krishnamurti, T. N., and H. N. Bhalme (1976): Oscillations of a monsoon system, Part I. Observational aspects. *J. Atmos. Sci.*, **33**, 1937-1954.
- Krishnamurti, T. N., Kishtawal, C. M., Zhang, Z., LaRow, T. E., Bachiochi, D. R., Williford, C.E., Gadgil, S. and Surendran, S., (2000): Improving tropical precipitation forecasts from a multi analysis super ensemble; *J. Climate*, **13**, 4217-4227.
- Krishnamurti, T.N., Basu, S., Sanjay, J. and Gnanaseelan, C., (2008); Evaluation of several different planetary boundary layer schemes within a single model, a unified model and a multimodel superensemble. *Tellus*, **60A**, 42-61
- Leggett J, Pepper W, Swart RJ (1992): Emissions Scenarios for the IPCC: an Update. In: Houghton JT, Callander BA, Varney SK (eds) Climate change 1992. The Supplementary Report to the IPCC Scientific Assessment. Cambridge University Press, Cambridge, pp 71–95
- Levy M, Estubier A, Madec G (2001) Choice of an advection scheme for biogeochemical models. *Geophys Res Lett* **28**(19):3725–3728
- LVEMP (2003) (Lake Victoria Environmental Management Project) Phase 1, Revised Draft Scientific Stocking Report-Progress During LVEMP1 and Challenges for the Future. World Bank; Washington DC.
- Maraun, D., Wetterhall, F., Ireson, A. M., Chandler, R. E., Kendon, E. J., Widmann, M., Brienen, S., Rust, H. W., Sauter, T., Themesl, M., Venema, V., Chun, K. P., Goodess, C. M., Jones, R. G., Onof, C., Vrac, M. & Thiele-Eich, I. (2010) Precipitation downscaling under climate change. Recent Developments to bridge the gap between dynamical models and the end user. *Reviews of Geophysics*
- Moss R, Babiker M, Brinkman S, Calvo E, Carter T, Edmonds J, Elgizouli I, Emori S, Erda L, Hibbard KA et al (2008): Towards new scenarios for analysis of emissions, climate change, impacts, and response strategies. IPCC Expert Meeting Report on New Scenarios. Intergovernmental Panel on Climate Change, Noordwijkerhout.

- Muhati, F., Opijah, F. J. and Ininda, J., 2007: Relationship between ENSO Parameters and the Trends and Periodic Fluctuations in East African Rainfall. *J. Kenya Meteorol. Soc.* **1** (1), 20-43.
- Mukabana, J. R (1992): Numerical simulation of the influence of large-scale monsoon flow on weather patterns over Kenya using a three-dimensional limited area model. *PhD. Thesis*, Department of Meteorology, University of Nairobi.
- Mukabana, J.R., and R.A. Pielke (1996): Investigating the influence of synoptic scale winds and meso-scale circulations and diurnal weather patterns over Kenya using a mesoscale numerical model. *Mon Wea Rev.*, **124**, 224-243.
- Mutai, C (2000): Diagnosis and prediction of East African rainfall on intraseasonal to interannual time scales. *PhD. Thesis*, Department of Meteorology, University of Nairobi.
- Mutai, Charles C., M. Neil Ward, (2000): East African Rainfall and the Tropical Circulation/Convection on Intraseasonal to Interannual Timescales. *J. Climate*, **13**, 3915–3939. doi:[http://dx.doi.org/10.1175/1520-0442\(2000\)013<3915:EARATT>2.0.CO;2](http://dx.doi.org/10.1175/1520-0442(2000)013<3915:EARATT>2.0.CO;2)
- Mutai C.C, Ward M.N, Colman A.W. (1998): Towards the prediction of the East Africa Short Rains based on sea-surface temperature–atmosphere coupling. *International Journal of Climatology* **18**: 975–997.
- Mutemi J.N. (2003): Climate anomalies over East Africa associated with various ENSO evolution phases. *PhD. Thesis*, Department of Meteorology, University of Nairobi, 187pp.
- Mutua, F. M; Mutemi J. N and Oludhe, C (1999): Homogeneous Climatological Zoning. DMC, Lecture Notes, Chapter 3, p29–43.
- Murphy, J. M., Sexton, D. M. H., Jenkins, G. J., Booth, B. B. B., Brown, C. C., Clark, R. T., Collins, M., Harris, G. R., Kendon, E. J., Betts, R. A., Brown, S. J., Boorman, P., Howard, T. P., Humphrey, K. A., McCarthy, M. P., McDonald, R. E., Stephens, A., Wallace, C., Warren, R., Wilby, R. & Wood, R. A. (2009) *Climate change projections. UK Climate projections 2009*. Exeter, UK.
- Nakicenovic, M., Riahi, K., and Grubler, A (2000) Special Report on Emissions Scenarios (SRES). Cambridge University Press, Cambridge
- Nicholson, S.E (1996): A review of Climate Dynamics and Climate Variability in Eastern Africa: The Limnology, Climatology and Paleoclimatology of the East Africa Lakes. Gordon and Breach, New York, 25-56.

- Nicholson, E.S., (2013): A Review of Recent Studies on the Rainfall Regime and Its Inter-annual Variability. *Earth, Ocean, and Atmospheric Sciences Department, Florida State University, Tallahassee, FL 32306*. doi.org/10.1155/2013/453521.
- Nordeng TE (1994) Extended versions of the convective parameter- ization scheme at ECMWF and their impact on the mean and transient activity of the model in the tropics. Tech. Rep. 206, ECMWF, Reading
- Nozawa, T., Nagashima, T., Ogura, T., Yokohata, T., Okada, N., and Shiogama, H.(2007): Climate change simulations with a coupled ocean-atmosphere GCM called the Model for Interdisciplinary Research on Climate: MIROC, CGER Supercomput. Monogr. Rep., 12, Cent. For Global Environ. Res., Natl. Inst. for Environ. Stud., Tsukuba, Japan.
- Nyenzi, S.E (1988): A Review of Climate Dynamics and Climate Variability in Eastern Africa. Department of Meteorology, Florida State University, Tallahassee, Florida, United States.
- Ochumba, P.B.O., (1996). Measurement of water currents, temperature, dissolved oxygen and winds on the Kenyan Lake Victoria. In *The Limnology, Climatology and Paleoclimatology of the East African Lakes* (T.C. Johnson and E.O. Odada, eds.). Gordon and Breach Publ, p. 155-168
- Odada E. O., Olago D.O. & Ochola W. (2006) Environment for Development: An Ecosystems Assessment of Lake Victoria Basin, UNEP/PASS
- Ogalo, L.A.J., I. R. Nassib (1984): Drought patterns and famines in East Africa during 1922-1983: The second WMO symposium on meteorological aspects of Tropical droughts. *Fu. 1984*, 41-44.
- Ogalo L.A.J (1988): Relationship between seasonal rainfall in East Africa and Southern Oscillation *J. Clim* 8, 34-43.
- Ogalo L.A.J (1989): The spatial and temporal pattern of the East African seasonal rainfall derived from principal component analysis. *Int. J. Climatology*, 9, 145-167.
- Ogalo L.A.J (1981): Dynamics of East Africa climate In Proc. Indian Academy Sci. (Earth planet Sc) *Vol 102, No. 1 March*, 1193, 203-217.
- Ogalo L.A.J (1993b): Climate change signals over eastern and southern Africa. (*Presented at 3rd Technical cont. on met. Research in eastern and southern Africa Feb. 1993*).
- Okoola, R.E (1996): Space-Time characteristics of the ITCZ over equatorial eastern Africa during Anomalous Years. *PhD. Thesis*, Department of Meteorology, University of Nairobi.

- Omeny, P., Ogallo, L. and Okoola, R., (2008): East Africa rainfall variability associated with the MJO, *J.Meteorol. Rel. Sci.*, **2**, 105–114.
- Omondi, P., Ogallo L. and Okoola, R., (2009): Decadal Rainfall Variability Modes in observed Rainfall Records over East Africa and their Predictability using Sea Surface Temperature *J.Meteorol. Rel. Sci.*, **3**, 37–54.
- Otieno, G., (2013): Assessing The Skill Of The Seasonal Rainfall Prediction Over The Greater Horn Of Africa Using Global Models As Multimodel Ensemble. *Msc. Thesis*, Department of Meteorology, University of Nairobi.
- Owiti, Z., Ogallo, L. and Mutemi, J., 2008: Linkages between the Indian Ocean Dipole and East African Seasonal Rainfall Anomalies, *J.Kenya Meteorol. Soc.*, **2**(1), 3–17.
- Owiti, Z., and Weijun, Z., 2012; Spatial distribution of rainfall seasonality over East Africa *Journal of Geography and Regional Planning*. **5** (15), pp. 409-421, DOI: 10.5897/JGRP12.02
- Palmer, T. N., Alessandri, A., Andersen, U., Cantelaube, P., Davey, M., Alessandri, A., Gualdi, S., Andersen, U., Feddersen, H., Cantelaube, P., Terres, J-M., Davey, M., Graham, R., Délecluse, P., Lazar, A., Déqué, M., Guérémy, J-F., Díez, E., Orfila, B., Hoshen, M., Morse, A. P., Keenlyside, N., Latif, M., Maisonave, E., Rogel, P., Marletto, V. and Thomson, M. C., (2004): Development of a European multi-model ensemble system for seasonal to interannual prediction (DEMETER). *Bull. Amer. Meteor. Soc.*, **85**, 853-872.
- Palmer T.N., Brankovic C. and Richardson, D.S., (2000): A probability and decision-model analysis of PROVOST seasonal multi-model ensemble integrations, *Q. J. R. Meteorol Soc.*, **126** (567), 2013-2033.
- Philippon, N., Camberlin, P and Fauchereau, N., (2002). Empirical Predictability Study of October–December East African Rainfall. *Quartely J.Meteorol.Soc.* (2002),128.2239–2256 doi:10.1256/qj.01.190.
- Pohl, B., Camberlin, P., (2006). Influence of the Madden–Julian Oscillation on East African rainfall. I: Intraseasonal variability and regional dependency. *Q. J. R. Meteorol. Soc.*(2006),132 . 2521–2539 doi: 10.1256/qj.05.104.
- Penduff T, Le Sommer J, Barnier B, Treguier A-M, Molines J-M, Madec G (2007) Influence of numerical schemes on current topography interactions in 1/4_ global ocean simulations. *Ocean Sci* 3(4):491–528

- Rauscher, S. A., Coppola, E., Piani, C. & Giorgi, F. (2009) Resolution effects on regional climate model simulations of seasonal precipitation over Europe. *Climate Dynamics*, 1-27.
- Roullet G, Madec G (2000) Salt conservation, free surface and varying volume: a new formulation for ocean GCMs. *J Geophys Res* 105:23927–23942
- Rowell, P., 2013: Simulating SST Teleconnections to Africa: What is the State of the Art? *J.climate*, **26**; 5397-5417.
- Rotstayn LD (1998) A physically based scheme for the treatment of stratiform clouds and precipitation in large-scale models. II: comparison of modelled and observed climatological fields. *Q J R Meteorol Soc* 124:389–415.
- Sweeney, J and Fealy, R. (2003) Establishing Reference Climate Scenarios for Ireland” *Climate Change Scenarios and Impacts for Ireland*. Environmental Protection Agency, Johnstown Castle, Wexford.
- Sabiiti, G., (2008) Simulation of Climate Scenarios over the Lake Victoria Basin using the PRECIS Regional Climate Model, MSc. Thesis, Department of Meteorology, University of Nairobi.
- Tabor, K and J.W. Williams (2010) Globally downscaled climate projections for assessing the conservation impacts of climate change, *Ecological Applications*, 20(2): 554-565.
- Tiedtke M (1989) A comprehensive mass flux scheme for cumulus parameterization in large-scale models. *Mon Weather Rev* 117(8):1779–1800
- Tomsett, J.E (1961): Average monthly and annual rainfall maps of East Africa. *Techn. Memo No. 14*, Kenya Meteorological Department, Nairobi, Kenya.
- Von Storch, H., Langenberg, H. & Feser, F. (2000) A spectral nudging technique for dynamical downscaling purposes. *Monthly Weather Review*, 128 (10), 3664-3673.
- Water Resources Management Department, WRMD (2005): Dropping water levels of Lake Victoria: Causes, effects and solution. Technical note, SWRMD, Uganda.
- Wilby, R. L., Charles, S. P., Zorita, E., Timbal, B., Whetton, P., and Mearns, L. O.: Guidelines for use of climate scenarios developed from statistical downscaling methods, Supporting material of the Intergovernmental Panel on Climate Change, available from the DDC of IPCC TGCIA, 27, 2004.

- Wilby, R. L., Dawson, C. W., and Barrow, E. M.: SDSM-a decision support tool for the assessment of regional climate change impacts, *Environ. Modell. Softw.*, **17**, 145–157, 2002.
- Wilby, R. L. & Wigley, T. M. L. (1997) Downscaling general circulation model output: a review of methods and limitations. *Progress in Physical Geography*, 21 (4), 530.
- Wilks, D., (2006): Statistical Methods in the Atmospheric Sciences, *Academic Press*, 592.
- World Meteorological Organisation, WMO (1986): Guidelines on the Quality control of Surface Climatological Data. *WCP-85 WMO/TD*, 111, 56.
- Zhang, G. J., McFarlane N. A., (1995): Sensitivity of climate simulations to the parameterization of cumulus convection in the Canadian climate centre general circulation model. *Atmos Ocean* 33:407–446